NASA CR-72507
BOEING D2-121002-1

SIMULATED SPACE ENVIRONMENTAL TESTS ON CADMIUM SULFIDE SOLAR CELLS

by

K. L. Kennerud

THE BOEING COMPANY

prepared for

NATIONAL AERONAUTICS AND SPACE ADMINISTRATION

NASA Lewis Research Center
Contract NAS 3-6008
John J. Smithrick, Project Manager

NASA CR-72507
BOEING D2-121002-1

FINAL REPORT

SIMULATED SPACE ENVIRONMENTAL TESTS ON CADMIUM SULFIDE SOLAR CELLS

by

K. L. Kennerud

THE BOEING COMPANY
Aerospace Group
P. O. Box 3868 Seattle, Washington 98124

prepared for

NATIONAL AERONAUTICS AND SPACE ADMINISTRATION

February 28, 1969

CONTRACT NAS3-6008

NASA-Lewis Research Center
Cleveland, Ohio
John J. Smithrick, Project Manager
Direct Energy Conversion Division

PRECEDING PAGE BLANK NOT FILMED.

TABLE OF CONTENTS

LIST OF ILLUSTRATIONS

LIST OF ILLUSTRATIONS - Cont.

LIST OF TABLES

ABSTRACT

CdS thin-film solar cells, manufactured in 1967 and 1968 were subjected to a simulated space environment, similar to that encountered by a satellite in Earth orbit. The environment included a pressure less than 10^{-6} torr, simulated space ultraviolet radiation, and thermal cycles in which cell temperature varied between $-100^{\circ}C$ and $+60^{\circ}C$. Most cells exhibited a significant loss in power within 500 cycles, but one cell withstood over 2000 cycles without appreciable degradation. The degradation was characterized by: (1) increasing internal series resistance, (2) occasional internal shorting and (3) an unexplained loss in light generated current.

1.0 SUMMARY

This final report contains the results of cadmium-sulfide (CdS) solar-cell tests conducted from March, 1967 to November, 1968 under Phase III of Contract NAS3-6008.

The primary objective of this test program was to evaluate the latest CdS thin-film solar cells for use in a space environment, particularly for supplying power to a satellite in Earth orbit where the cells are exposed to illumination and darkness. A secondary objective of this program was to use the test results to indicate possible causes of cell degradation.

The tests were conducted in a clean vacuum chamber where the pressure was below 10^{-6} torr at all times. The black walls of the chamber were cooled by liquid nitrogen. During a "thermal cycle", consisting of a 60-minute exposure to simulated sunlight followed by 30 minutes of darkness, nominal cell temperature varied from +60°C to -100°C. Cell performance was measured using a light source whose spectrum closely matched that of space sunlight.

Three separate tests involving 300, 506, and 2031 thermal cycles were conducted on selected CdS cells manufactured in April, 1967, November, 1967, and March, 1968, respectively. The March, 1968 cells were the most stable in thermal cycling, as indicated below:

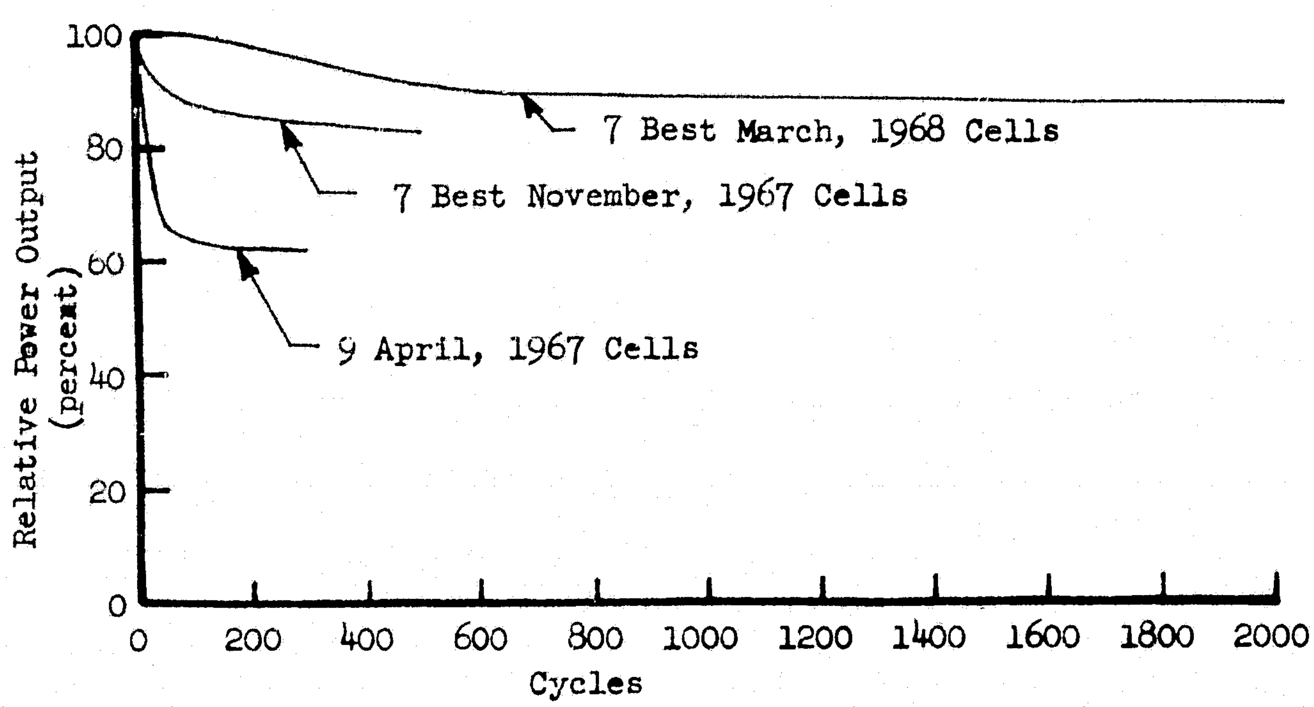

CdS SOLAR CELL POWER OUTPUT VS. CYCLES

Six cell constructions were tested. Cell constructions differed in (1) method of attaching a current collecting grid to the cell (2) cover material and (3) process used in manufacture. The performance of these six groups before, during, and after thermal cyling is summarized in Table 1.

Most of the March, 1968 cells lost less than 15 percent in power output after 2031 thermal cycles. One cell degraded by only four percent, a value almost within experimental error. This cell had a current-collecting grid that had been evaporated on the cell surface. Power losses in other March, 1968 cells are attributed to an increase in series resistance and a decrease in light generated current. The cause of these changes could not be identified. A few cells exhibited erratic decreases in shunt resistance. These decreases are attributed to internal short circuits.

CELL DESCRIPTION: MANUFACTURE DATE	CELL TYPE	NUMBER OF CELLS	CONVERSION EFFICIENCY η at 25° C (1) (%)	SUBSTRATE MATERIAL	FRONT COVER MATERIAL	GRID ATTACHMENT	REMARKS	CELL PERFORMANCE: BEFORE CYCLING CONVERSION EFFICIENCY η (1) at 60° C (%)	AFTER CYCLING CONVERSION EFFICIENCY η (1) at 60° C (%)	DURING CYCLING: LENGTH OF TEST (CYCLES)	OPERATING LOAD VOLTAGE (% OF VOLTAGE OF MAX. POWER)	PERFORMANCE PARAMETERS (2)	AVERAGE VALUES OF PERFORMANCE PARAMETERS AT 60°C (3): ACTUAL VALUES CYCLE-1	(PERCENT OF CYCLE-1 VALUE) CYCLE 300	CYCLE 506	CYCLE 2031
APRIL 1967	1	9	3.7	KAPTON	MYLAR COATED WITH CLEAR PYRE ML VARNISH	BONDED WITH EPOXY		NOT MEASURED	NOT MEASURED	300	140	η (%) = P_M (mW) = V_{oc} (V) = I_{sc} (mA) = FF (%) =	(4)	60 60 96 78 82		
NOVEMBER, 1967	2	1	4.89	COPPER	MYLAR	BONDED WITH EPOXY		4.56	4.06	506	118	η (%) = P_M (mW) = V_{oc} (V) = I_{sc} (mA) = FF (%) =	4.29 330 0.443 1095 68.0	79 79 101 84 94	77 77 102 81 93	
	2	1	5.04	COPPER	MYLAR	BONDED WITH EPOXY		4.55	0.85	506	120	η (%) = P_M (mW) = V_{oc} (V) = I_{sc} (mA) = FF (%) =	4.28 329 0.453 1075 67.6	21 21 41 82 60	25 25 60 81 51	
	3	6	3.54	KAPTON	KAPTON	BONDED WITH EPOXY		2.97	2.73	506	99	η (%) = P_M (mW) = V_{oc} (V) = I_{sc} (mA) = FF (%) =	2.96 228 0.420 835 65.0	86 86 100 93 92	83 83 101 93 89	
	3	1	3.21	KAPTON	KAPTON	BONDED WITH EPOXY		2.68	2.13	506	80	η (%) = P_M (mW) = V_{oc} (V) = I_{sc} (mA) = FF (%) =	2.28 175 0.424 760 54.3	83 83 97 92 91	78 78 97 91 89	
MARCH, 1968	4	4	3.57	KAPTON	KAPTON	BONDED WITH EPOXY		2.99	2.66	2031	93	η (%) = P_M (mW) = V_{oc} (V) = I_{sc} (mA) = FF (%) =	2.87 221 0.414 813 66.0	93 93 102 98 93	89 89 103 93 93	87 87 103 95 89
	5	3	3.40	KAPTON	KAPTON	BONDED WITH EPOXY	LOW LAMINATION PRESSURE ON FRONT COVER	2.88	2.53	2031	94	η (%) = P_M (mW) = V_{oc} (V) = I_{sc} (mA) = FF (%) =	2.73 210 0.418 789 64.0	93 93 102 97 94	92 92 102 95 94	87 87 104 93 89
	6	1	3.21	KAPTON	KAPTON	BONDED WITH EPOXY	EVAPORATED GRID BENEATH STANDARD GRID	2.67	1.96	2031	92	η (%) = P_M (MW) = V_{oc} (V) = I_{sc} (mA) = FF (%) =	2.47 190 0.406 727 64.4	97 97 102 99 97	93 93 103 96 95	49 49 97 91 55
	6	1	2.50	KAPTON	KAPTON	BONDED WITH EPOXY	EVAPORATED GRID BENEATH STANDARD GRID	2.16	2.11	2031	88	η (%) = P_M (mW) = V_{oc} (V) = I_{sc} (mA) = FF (%) =	2.03 156 0.420 549 67.7	103 103 101 101 100	99 99 101 99 99	96 96 102 100 94

THE LIGHT INTENSITY DURING ALL PERFORMANCE MEASUREMENTS WAS 140 mW/cm^2, AMO.

(1) AS MEASURED, IN AIR, WITH THE CELL MOUNTED ON A TEMPERATURE-CONTROLLED BLOCK.

(2) η = CONVERSION EFFICIENCY; P_M = MAXIMUM POWER; V_{oc} = OPEN CIRCUIT VOLTAGE; I_{sc} = SHORT CIRCUIT CURRENT; FF = FILL FACTOR

(3) AS MEASURED, IN SITU, WITH THE CELLS UNDER VACUUM.

(4) THE ACTUAL VALVES OBTAINED FOR THE APRIL, 1967 CELLS ARE INCORRECT BECAUSE OF A FAULT IN THE MEASURING CIRCUIT.

TABLE 1: SUMMARY OF CONSTRUCTION AND PERFORMANCE CHARACTERISTICS OF CdS SOLAR CELLS TESTED IN PHASE III

2.0 INTRODUCTION

Development of cadmium sulfide (CdS) thin-film solar cells started in 1954 (ref. 1). By 1960 conversion efficiencies as high as $3\frac{1}{2}$ percent had been achieved (ref. 1), and CdS solar cells began to look promising as sources of power for spacecraft. In 1963 the NASA-Lewis Research Center (NASA-Lewis) began to evaluate new CdS solar cell designs in the vacuum and thermal environment of space (ref. 2 and 3). These tests soon showed that CdS solar cells subjected to thermal cycling in vacuum, as would be encountered by an Earth satellite, degraded very quickly. Thus, thermal cycling became established as an important test for evaluating new cell designs.

In 1964 NASA-Lewis awarded a two-phase contract (NAS3-6008) to The Boeing Company (Boeing) for conducting thermal cycling tests on promising new CdS solar cell designs, after the new designs had been screened in similar tests at NASA-Lewis. In these thermal cycling tests the cells were subjected to alternating periods of sunlight and darkness with temperatures varying from approximately -100°C to +60°C.

The thermal cycling tests at NASA-Lewis and Boeing uncovered weaknesses in the cell design and gave direction to the design and construction of more stable cells. Concurrently the cell manufacturer increased significantly the conversion efficiency of CdS solar cells. In 1967 NASA-Lewis awarded Boeing an extension (Phase III) to the original contract for evaluating newer cell designs. NASA-Lewis also continued their own thermal cycling program.

This document reports in detail the results of work done by Boeing for NASA-Lewis on Phase III of Contract NAS3-6008. Detailed results of the Phase I and Phase II work have been presented in a Topical Report (ref. 4). Many of the cell designs tested in Phase I and Phase II were shown to be unstable in a space environment involving thermal cycling, and are no longer manufactured. Phase III testing involved newer cells of the type that are presently being manufactured.

The Phase III cells incorporate many variations in design, with conversion efficiencies ranging from 2½ to 5 percent at 25°C in simulated air mass zero (AMO) sunlight having 140 milliwatts per sq. cm. (mW/cm^2) intensity. Appropriate precaution should be applied to any extrapolation of the test results presented herein to production cells not manufactured in the same manner as the ones tested in this program.

The tests described in this report were conducted with CdS solar cells, mounted nine at a time in a vacuum chamber maintained at a pressure of less than 10^{-6} torr. A quartz window allowed the cells to be illuminated by a light source that closely simulated the solar spectrum in space. The black walls of the chamber were cooled with liquid nitrogen so that the cell temperature dropped to lower than -100°C during the dark portion of each cycle and came to an equilibrium of about +60°C during the illuminated portion of each cycle. A complete thermal cycle consisted of 30 minutes of darkness followed by 60 minutes of illumination. Performance of the cells was usually measured about once every 100 cycles, but more frequently whenever cycling of the new cells was started. A matching set of CdS solar cells was kept in double-desiccated storage throughout the test and their performance was also measured every 100 cycles. In this report, the CdS solar cells exposed to the space environment are referred to as "test cells". Those kept in double desiccated storage are referred to as "control cells".

3.0 TEST SPECIMENS

The CdS thin-film solar cells tested in this program were approximately 3 by 3 inches (7.62 by 7.62 cm), with an overall thickness of about 4 mils (100 μm). Although the cells differed in many respects, they all shared the same basic construction illustrated below:

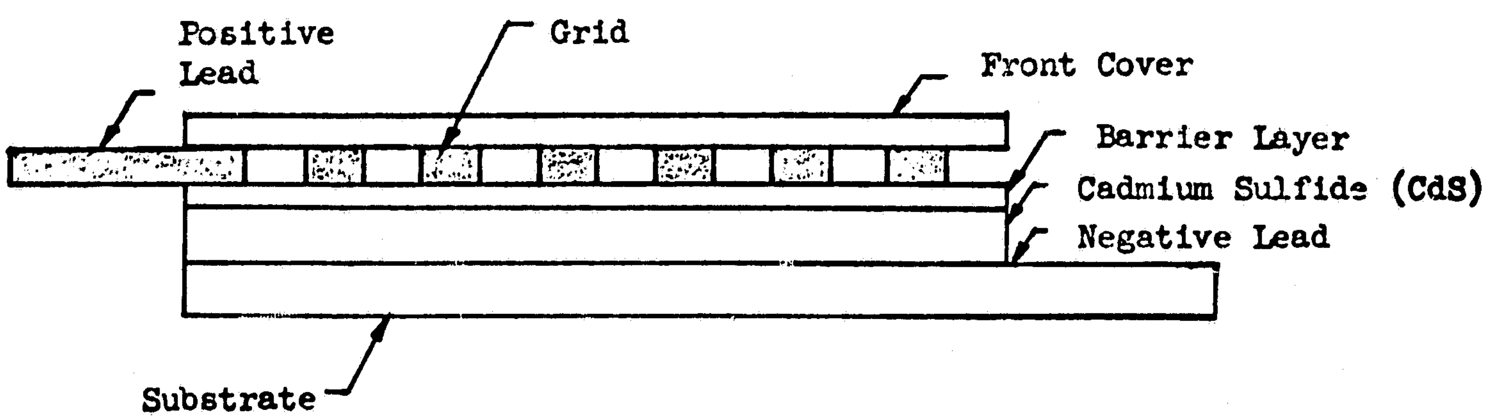

FIG. 1: BASIC CONSTRUCTION OF CdS THIN-FILM SOLAR CELLS

The cells were made by evaporating a layer of CdS on a thin sheet of metal or metalized plastic, called the substrate. A thin layer of copper sulfide called the barrier layer was then formed on the exposed CdS. A metal current-collecting grid with a high transmittance was later put on this barrier layer. Laminating a thin, transparent sheet of plastic over the grid completed the cell. The negative electrode of the cell is simply an extension of the substrate. The positive electrode is either an extension of the grid or a piece of metal foil attached to the grid.

3.1 CdS Cells Tested in Phases I and II

Characteristics of the CdS solar cells tested in Phases I and II are summarized in the following table:

MANUFACTURE DATE	SUBSTRATE MATERIAL	GRID	ATTACHMENT OF ELECTRODES	LAMINATION ADHESIVE
1964	MOLYBDENUM	ELECTRO-PLATED	PRESSURE	CAPRAN
1964	MOLYBDENUM	ELECTRO-PLATED	SPOT WELDED	CAPRAN
1965	KAPTON	PREFORMED, HELD BY PRESSURE	PRESSURE	CAPRAN
1966	KAPTON	PREFORMED, HELD BY PRESSURE	INTEGRAL	CAPRAN

CHARACTERISTICS OF CdS SOLAR CELLS
TESTED IN PHASES I AND II

TABLE II

The earliest cells had molybdenum substrates, but later cells had plastic substrates. Plastic replaced molybdenum as a substrate material because it resulted in a lighter, more flexible solar cell. In some cells, the grid was formed by electroplating gold directly on the barrier layer. In other cells, preformed grids, held in contact with the barrier layer solely by pressure from the plastic cover, were used. The positive electrode on one type of cell was an integral extension of the grid, but in all other cells the positive electrode, distinct from the grid, was either spot welded to the grid or held against the grid by pressure from the plastic cover. Capran, a nylon adhesive, was used to bond the plastic cover in all the cells.

Testing at Boeing and NASA-Lewis revealed some undesirable aspects of these cell designs. In the Phase I and II thermal cycling tests conducted at Boeing (ref. 4), some cells in each of the four different groups eventually exhibited large decreases in both maximum power output and shunt resistance. These failures are believed to be the result of an increase in the number of shorting paths through the barrier layer (ref. 5).

In cells with either electrodes or grids held in place solely by pressure from the plastic cover, movements of the electrode or grid could have worn holes in the barrier layer, producing the undesired shorts. In cells with the electrodes spot welded to the grid, the welded joint may have eventually broken and allowed the electrode to move. Analyses conducted by the cell manufacturer on a few of the cells after thermal cycling revealed that the cause of the short circuits in the CdS film in those particular cells were pinholes which resulted from splattering of CdS particles onto the substrates during CdS film evaporation (ref. 6). Tests conducted at NASA-Lewis (ref. 7) also revealed that CdS cells using Capran to bond the plastic cover degraded when exposed to water vapor.

3.2 CdS cells Tested in Phase III

Characteristics of the CdS solar cells tested in Phase III are summarized in Table 1. Most of the new cells had Kapton substrates; however two copper-substrate cells were tested also. The undesirable features of the CdS cells tested in Phases I and II had been eliminated in these new cell designs; for example a conductive epoxy held the grids in contact with the barrier layer, rather than pressure from the plastic cover. This reduced the shorting-type failures which plagued earlier cell designs during thermal cycling. Also in the new cell designs an integral extension of the grid formed the positive electrode. Better control of the evaporation process, and better inspection techniques eliminated pinholes in the CdS layer, reducing cell shorting. A clear epoxy replaced Capran as the lamination adhesive, preventing degradation from water vapor.

Three different types of plastic covers were used: (1) Mylar, (2) Mylar, coated with a 0.2 mil ($5 \mu m$) layer of Pyre-ML (a polyimide varnish) and (3) Kapton. Mylar transmits light better than the other two types, but is known to degrade under exposure to ultraviolet (UV) radiation (ref. 8). The Pyre-ML layer decreased the initial transmission of the Mylar by about five percent, but it may partially protect the Mylar from UV radiation. Kapton transmits about 20 percent less light than Mylar, but it is resistant to UV radiation (ref. 8). Since the conversion efficiency of CdS solar cells is proportional to the light transmitted by the front cover, the pre-cycling conversion efficiencies varied considerably, depending primarily upon the type of plastic cover used:

(1) Cells with plain Mylar covers have the highest efficiencies (4.9 to 5.0 percent at 140 mW/cm^2, 25°C).

(2) Cells with Pyre-ML-coated-Mylar covers have the next higher efficiencies (3.5 to 4.1 percent at 140 mW/cm^2, AMO, 25°C).

(3) Cells with Kapton covers have the lowest efficiencies (2.5 to 3.9 percent at 140 mW/cm^2, 25°C).

Several minor variations in the processing of the new cells are worth mentioning. The April, 1967 cells were manufactured with minimal quality control. As a result, many of these cells exhibited unstable performance even before thermal cycling was started. In three of the March, 1968 cells, the plastic cover was purposely laminated on with a below-normal pressure. It had been suggested that the normal lamination pressure could have cracked the CdS layer and produced a potentially unstable cell. Two of the March, 1968 cells have an additional evaporated gold grid beneath the standard preformed grid. The objective of this technique was to improve the current collection.

The cell designs tested in Phase III are currently available (December, 1968). However, it should be noted that many of the cells which Boeing tested were the most promising cells selected from screening tests conducted by the cell manufacturer and NASA-Lewis, and therefore they may not represent typical production cells.

4.0 TEST APPARATUS

In this section is discussed the apparatus used to provide the test environment and the data acquisition equipment.

4.1 Test Environment Apparatus

The test environment apparatus includes a vacuum chamber, a light source, a test-cell supporting frame, and a control-cell mounting block. The test-cell supporting frame, used to hold the test-cells during thermal cycling, was located inside the vacuum chamber. The control-cell mounting block, used to hold control-cells when their performance was being measured, was located outside the vacuum chamber. The light source could be rotated to illuminate either the test-cells or the control cells. The test setup is shown schematically in Figure 2. A photograph appears in Figure 3. The apparatus used is discribed in detail in the following paragraphs.

4.1.1 Vacuum Chamber

The vacuum chamber (Figure 2) is composed of a shell, a cold shroud, an end plate, an access door, a quartz window, a shutter, a mounting bracket for the test cell supporting frame, and a vacuum pump. The shell of the chamber is built from two stainless steel cylinders, one 15 inches in diameter and 41 inches long, and the other 34 inches in diameter and 30 inches long. The smaller-diameter end has a sealed quartz window through which the CdS cells are illuminated. The other end has an access door. Vacuum is maintained by an ion pump under the shell.

The shell always remains near room temperature. The heat sink simulating a true space environment within the chamber is provided by a cold shroud, composed of two aluminum cylinders of different diameters joined end-to-end. The cold shroud fits inside the shell with a two-inch concentric gap between the shroud and the shell.

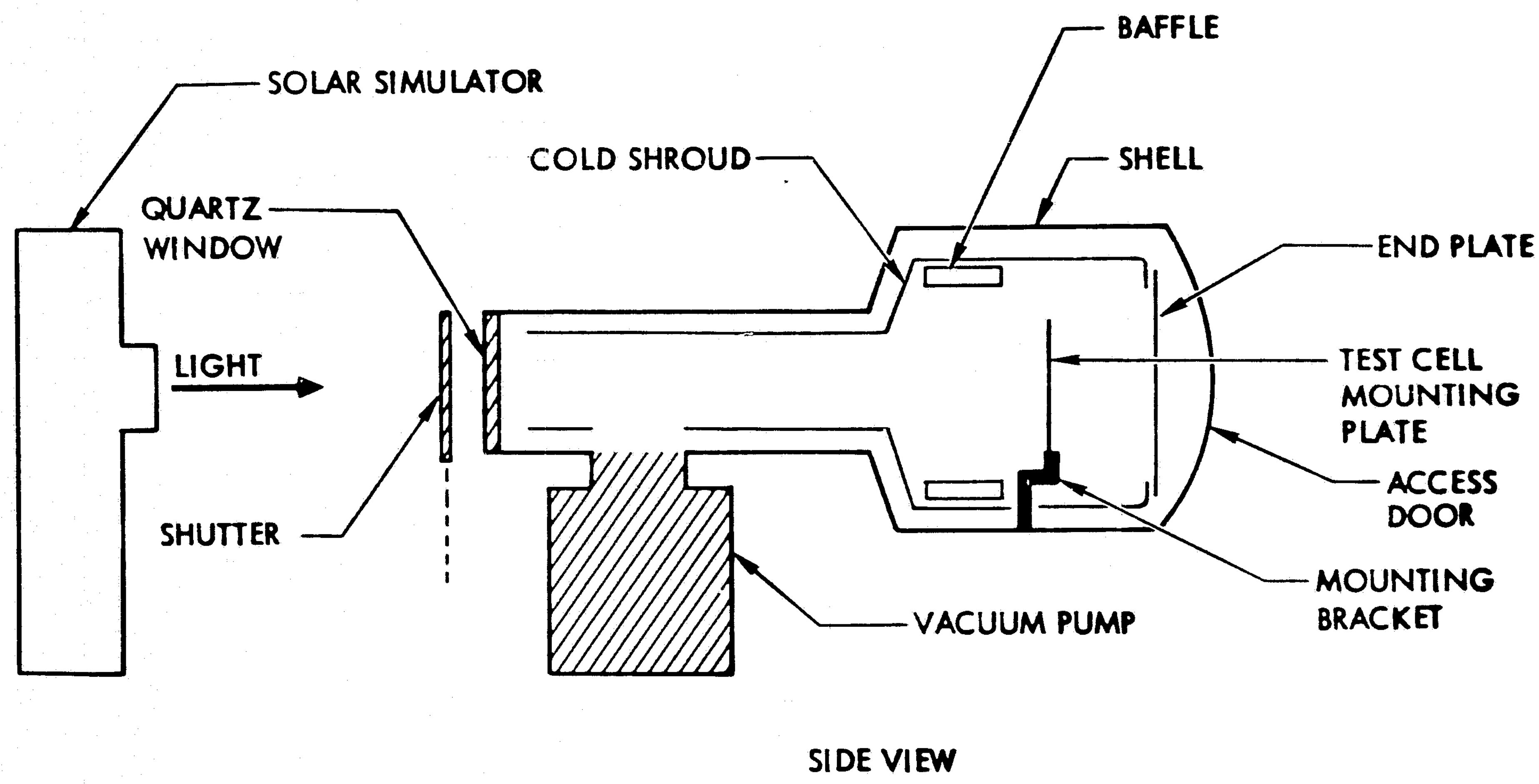

Figure 2: SCHEMATIC OF TEST CHAMBER

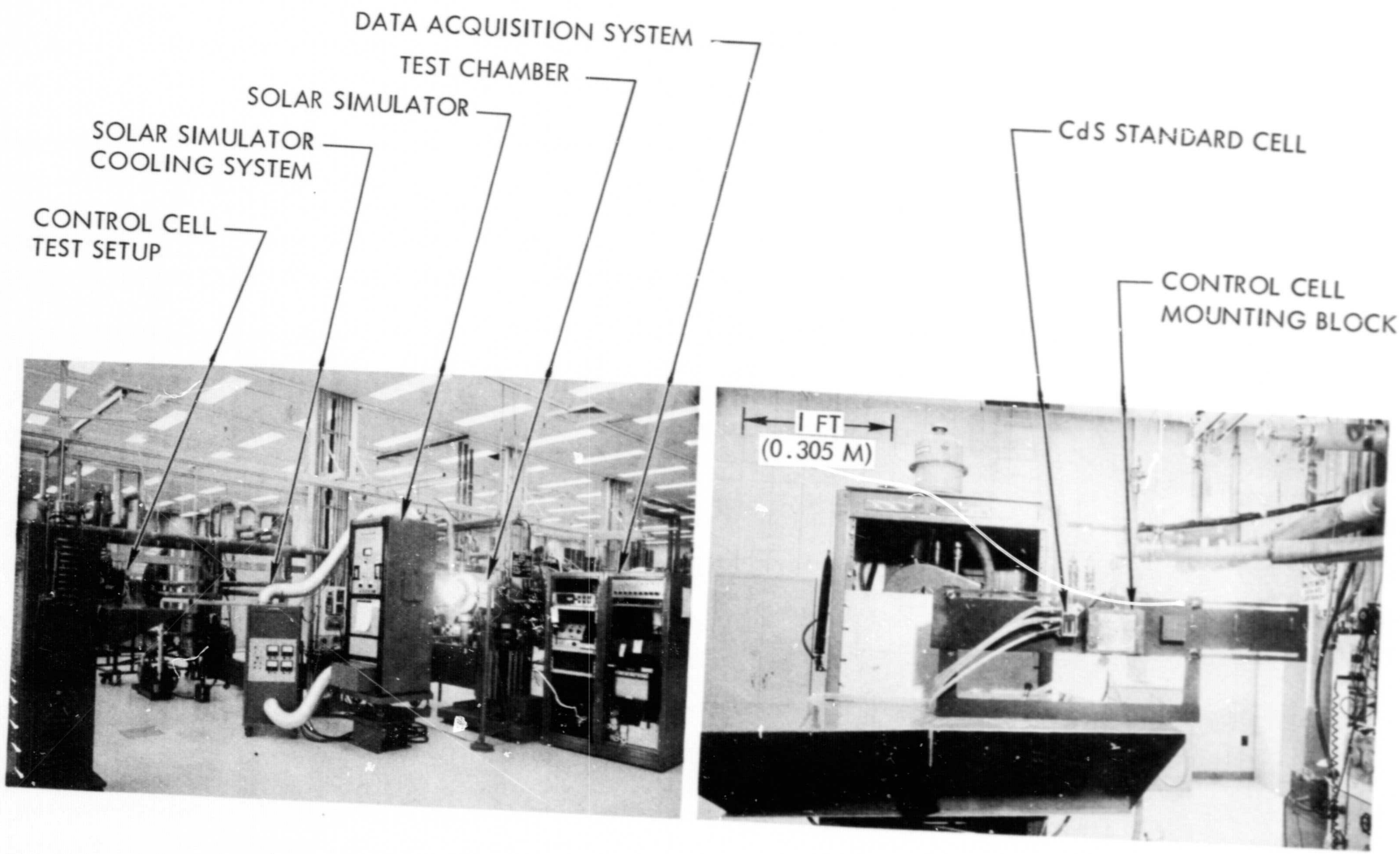

Figure 3: TEST SETUP

The shroud is essentially isolated thermally from the shell, being supported at only 5 points with low-thermal-conductivity stainless steel. The shroud is cooled to -196°C during testing by pumping liquid nitrogen through tubes which are integral with the shroud. All inner surfaces of the shroud are painted black to reduce reflection of thermal radiation. Liquid-nitrogen cooled baffles inside the shroud further reducing reflections.

A blackened aluminum plate bolted to the end of the cold shroud, cooled to -160°C by conduction to the cold shroud, covers the cell-access opening during testing. The chamber is sealed, at the cell-access end, with a stainless steel door which is bolted against a copper gasket that is replaced whenever the door is opened.

The quartz window which admits simulated sunlight into the chamber transmits 94 percent of the ultraviolet energy in the wavelength band 0.25 to 0.35 μm. Transmission in other wavelengths ranges from 88.3 percent to 96.7 percent, as shown in Table 3.

A shutter between the solar simulator and the quartz window interrupts the light beam when the test cells in the chamber are to receive no light from the solar simulator. The shutter is painted black to reduce reflection of room light from the shutter into the chamber. The shutter is water-cooled to reduce the infrared energy radiated by the shutter into the chamber. During cycling the shutter is automatically closed for 30 minutes and opened for 60 minutes.

A mounting bracket supports the test-cell frame in the chamber. The mounting bracket is fastened only to the shell, making no contact with the cold shroud. It is made of low-thermal-conductivity stainless steel, to restrict heat conduction to the shell.

A mechanical roughing pump and an ion pump are used to provide vacuum. The roughing pump brings the chamber pressure down to

Wavelength Band (μm)	Fraction of Incident Light Energy Transmitted Through Quartz Window (percent)
0.25 - 0.35	93.9
0.35 - 0.40	95.2
0.40 - 0.45	92.5
0.45 - 0.50	96.4
0.50 - 0.60	94.8
0.60 - 0.70	92.8
0.70 - 0.80	95.2
0.80 - 0.90	92.3
0.90 - 1.00	96.7
1.00 - 1.20	95.7
1.20 - 1.50	93.0
1.50 - 1.80	91.1
1.80 - 2.20	88.3
2.20 - 2.50	90.5

TABLE 3: TRANSMISSION OF QUARTZ WINDOW

10^{-4} torr, after which the ion pump is started and the roughing pump is removed. The ion pump maintains a pressure of 10^{-8} torr during cycling when there is liquid nitrogen in the shroud, and 10^{-6} torr during test interruptions when the shroud is at room temperature. The pressure increases to 10^{-6} torr during test interruptions because of gas released from the shroud surface when the shroud is allowed to warm up.

4.1.2 Light Source

The light source is a Spectrolab X25L xenon solar simulator, equipped with lenticular optics for high uniformity of intensity, and special filters to provide a spectrum close to that of space sunlight. It is located outside the vacuum chamber (Figure 2) providing a 13¼-inch diameter light beam to illuminate simultaneously nine test-cells in the vacuum chamber. The spectrum of the beam matched Johnson's space spectrum (ref. 9) very closely, as shown by the typical spectrum in Table 4. The intensity at any place in the beam did not deviate from that in the center by more than three percent as shown in the typical uniformity plot in Figure 4. An intensity equivalent to 140 milliwatts per sq. cm (mw/cm^2) of space sunlight was maintained throughout the test by periodically checking with an airplane-flown CdS standard cell provided by NASA-Lewis. A rapid intensity flicker of about 1½ percent, presumably caused by the xenon lamp, made precise intensity and uniformity measurements difficult as well as producing undesirable wiggles in the current-voltage curves of the CdS solar cells.

4.1.3 Test-Cell Supporting Frame

Two different types of supporting frames were used in this program to hold the test-cells. The April, 1967 and November, 1967 cells were held in a aluminum supporting frame composed of two thin aluminum discs bolted together with cutouts to expose the fronts and back of the cells. Both electrodes of the April, 1967 cells were

Band Number	Wavelength Interval (microns)		Spectral Intensity Outside Vacuum Chamber when Control Cell Performance is Measured			Spectral Intensity Inside Vacuum Chamber When Test Cell Performance is Measured			Spectral Intensity Inside Vacuum Chamber When Test Cells are Being Cycled		
	— to —		Actual	Deviation from Johnson's*		Actual	Deviation from Johnson's*		Actual	Deviation from Johnson's	
			(mw/cm^2)	(mw/cm^2)	(%)	(mw/cm^2)	(mw/cm^2)	(%)	(mw/cm^2)	(mw/cm^2)	(%)
1	0.25	0.35	5.45	-0.85	-13.49	5.46	-0.84	-13.33	5.46	-0.84	-13.33
2	0.35	0.40	7.46	+1.30	+21.10	7.57	+1.41	+22.89	7.57	+1.41	+22.89
3	0.40	0.45	7.58	-2.04	-21.21	7.48	-2.14	-22.25	7.48	-2.14	-22.25
4	0.45	0.50	8.75	-1.89	-17.76	9.00	-1.64	-15.41	9.00	-1.64	-15.41
5	0.50	0.60	15.83	-3.35	-17.47	16.01	-3.17	-16.53	16.01	-3.17	-16.53
6	0.60	0.70	14.17	-2.07	-12.75	14.03	-2.21	-13.61	14.03	-2.21	-13.61
7	0.70	0.80	12.35	-0.39	- 3.06	12.55	-0.19	- 1.49	12.55	-0.19	- 1.49
8	0.80	0.90	9.27	-0.81	- 8.04	9.13	-0.95	- 9.42	9.13	-0.95	- 9.42
9	0.90	1.00	8.91	+0.79	+ 9.73	9.20	+1.08	+13.30	9.20	+1.08	+13.30
10	1.00	1.20	15.67	+3.49	+28.65	16.00	+3.82	+31.36	16.00	+3.82	+31.36
11	1.20	1.50	11.04	-0.16	- 1.43	10.96	-0.24	- 2.14	10.96	-0.24	- 2.14
12	1.50	1.80	9.03	+2.83	+45.65	8.78	+2.58	+41.61	8.78	+2.58	+41.61
13	1.80	2.20	5.99	+1.55	+34.91	5.64	+1.20	+27.03	5.64	+1.20	+27.03
14	2.20	2.50	3.44	+1.52	+79.17	3.32	+1.40	+72.92	3.32	+1.40	+72.92
Total Intensity	0	∞	140.0			140.2			140.2		

*NASA SP-8005, Solar Electromagnetic Radiation, June, 1965

Contract: NAS 3-6008
Phase: III
Test: 2 (November, 1967 Cells)
Cycles 143 to 506

Date Measured: 3/11/68
Solar Simulator Model No. Spectrolab X25L
Lamp Number Hanovai #731002

TABLE 4. SPECTRAL INTENSITY OF SOLAR SIMULATOR

Readings: Relative short circuit current (percent of value at center of beam) of a 2 X 2 cm silicon solar cell centered on the points shown below. The circles are on one-inch radii.

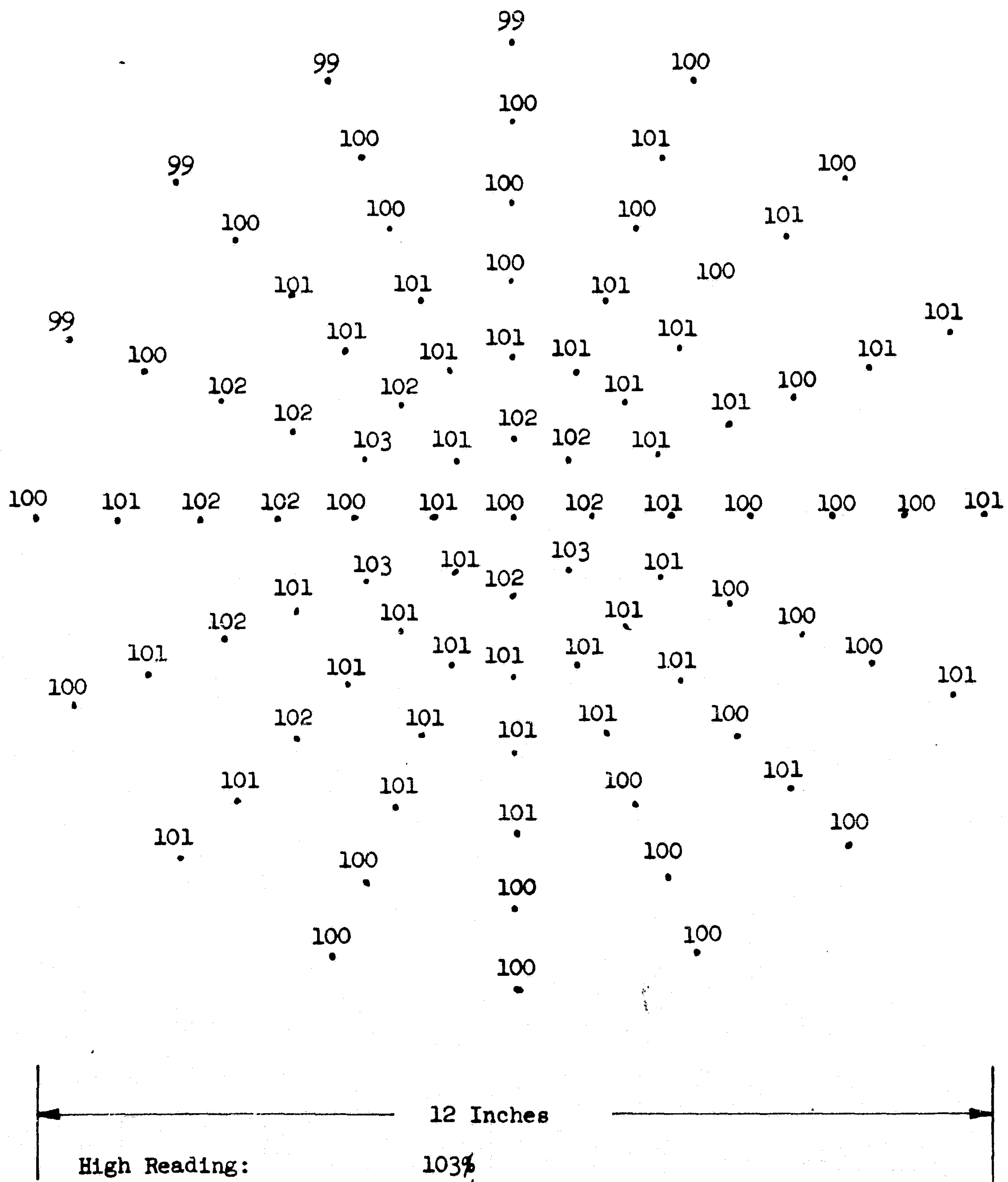

High Reading:	103%
Low Reading:	99%
Reading at Center:	100%
Statement of Uniformity:	Intensity at any place in the beam does not deviate from that in the center by more than 3%

FIGURE 4: INTENSITY UNIFORMITY OF SPECTROLAB X25-L SOLAR SIMULATOR

firmly sandwiched between the two plates. Only one electrode on the November, 1967 cells were constrained. A glass-epoxy board was used to hold the March, 1968 cells. This frame was essentially a disc with a rectangular cutout in its middle (Figure 5). The substrate electrode of each cell was attached with double-back tape to cross bars which spanned the cutout. Each cell was allowed to hang freely, with its positive electrode constrained within a 1/16-inch slot in a cross bar beneath it. Both types of frames were painted black and had silicon solar cells (reference cells) mounted on their front surfaces.

During testing, the test-cell supporting frame was held by the stainless-steel mounting bracket in the vacuum chamber.

4.1.4 Control Cell Mounting Block

Whenever the electrical performance of a control-cell was to be measured, the cell was mounted on the control-cell mounting block (Figure 3) and illuminated with the light source. The temperature of the metal mounting block is controlled by a recirculating water supply. Good thermal contact between the block and the control cell is assured by applying vacuum to grooves in the front of the block. Electrical contact to the cell is made with gold-plated copper strips held by pressure against the cell electrodes: (1) two large-area strips, one on each electrode, make contact for the current-carrying leads, and (2) two small area strips, one on each electrode, make contact for the voltage measuring leads. The mounting block and the airplane-flown CdS standard cell were both mounted on the same sliding plate so that either one could be centered in the light beam.

4.2 Data Acquisition Equipment

The data are acquired with (1) instruments for measuring the

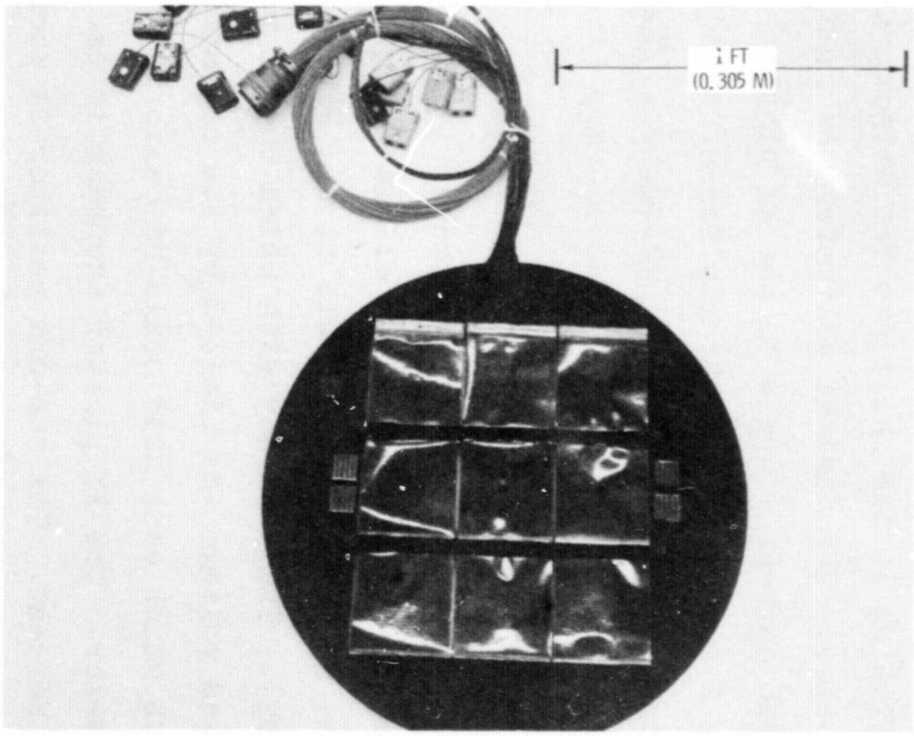

(a) FRONT VIEW

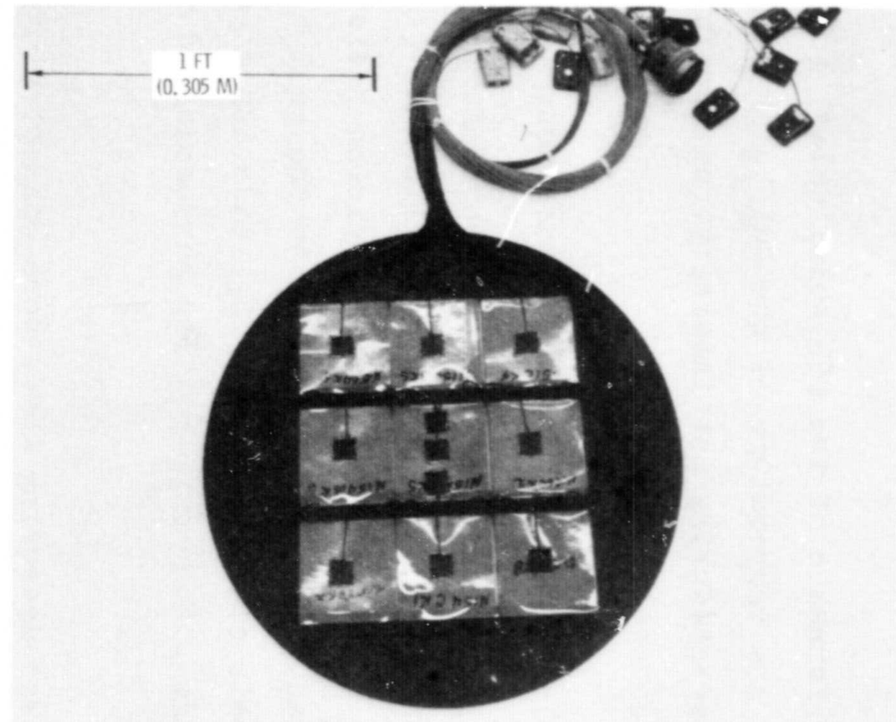

(b) REAR VIEW

Figure 5: TEST CELL SUPPORTING FRAME

electrical performance of the CdS solar cells, (2) instruments for measuring the temperature of the CdS solar cells, and (3) instruments for measuring the intensity, uniformity, and spectrum of the light source.

4.2.1 CdS Solar Cell Performance Measurement

The important equipment used to record current-voltage (I-V) curves of the test-cells and control cells are: (1) a digital voltmeter (2) an XY recorder (3) a precision resistor and (4) an electronic load. Electrical contact to the cell electrodes is made with a pair of current-carrying leads and a pair of voltage-measuring leads. Four copper wires were soldered to the test-cell electrodes.

The voltage measuring leads were connected directly into the X-axis of the XY plotter. The current carrying leads contained two elements in series; a precision one-ohm resistor and an electronic load. The voltage drop across the one-ohm resistor, representing the current flowing in the cell, was fed directly into the Y-axis of the XY plotter. The digital voltmeter was used to calibrate the voltage and current signals to the XY plotter. The variable scales of the X and Y axes of the plotter were adjusted to correspond to the readings of the digital voltmeter. The electronic load, designed and built at Boeing, was used to vary the current by means of a manually-operated dial.

The accuracy of the digital voltmeter is $\pm$ 0.1 percent. The digital voltmeter was periodically calibrated against a secondary standard whose accuracy is traceable to the National Bureau of Standards (NBS). The accuracy with which the XY plotter recorded the current and voltage was limited by its repeatability and the precision with which each axis could be calibrated against the digital voltmeter. The XY plotter accuracy is estimated on this basis at 0.5 percent. The one-ohm resistor is accurate to $\pm$ 0.1 percent.

The smoothness of the recorded I-V curve is directly related to the stability of the light source used to illuminate the cell whose I-V curve is being recorded. An I-V curve traced when a stable tungsten light source was used is very smooth (Figure 6) whereas a wiggly curve is obtained when a xenon solar simulator is used (Figure 7). Flicker in the light produced by the solar simulator is responsible for these wiggles. The effect of light flicker was further demonstrated when the intensity of the tungsten light source was purposely varied a few percent while an I-V curve was being traced (Figure 8).

The effect of the intensity variation on the I-V curve is a drastic change in voltage at currents near short-circuit current. This is because the electronic load maintains a constant current at any setting of the load dial regardless of fluctuatings in intensity; consequently the voltage of the cell must change drastically as the intensity changes to maintain constant current.

During the periods between performance measurements, a load resistor was placed across the current leads of the test cells. The load resistors were selected so that the cells would operate near their maximum power point. However, in testing of the April, 1967 cells, the effect of lead resistance was overlooked and the combined load resistance values were too high. As a result these cells operated near their open circuit voltages during cycling.

4.2.2 CdS Solar Cell Temperature Measurement

The sensor used for all temperature measurements was a thermocouple formed by soldering a copper wire and a constantan wire together. The thermocouple was coated with heat-sink compound to insure good thermal contact prior to bonding to the back of the CdS cell (Figure 5) with aluminum tape. A narrow bead of low-temperature polyurethane adhesive was applied along the four edges of the tape as a precaution against peeling. The tape was then painted with a black paint whose emittance approximated that of the cell back.

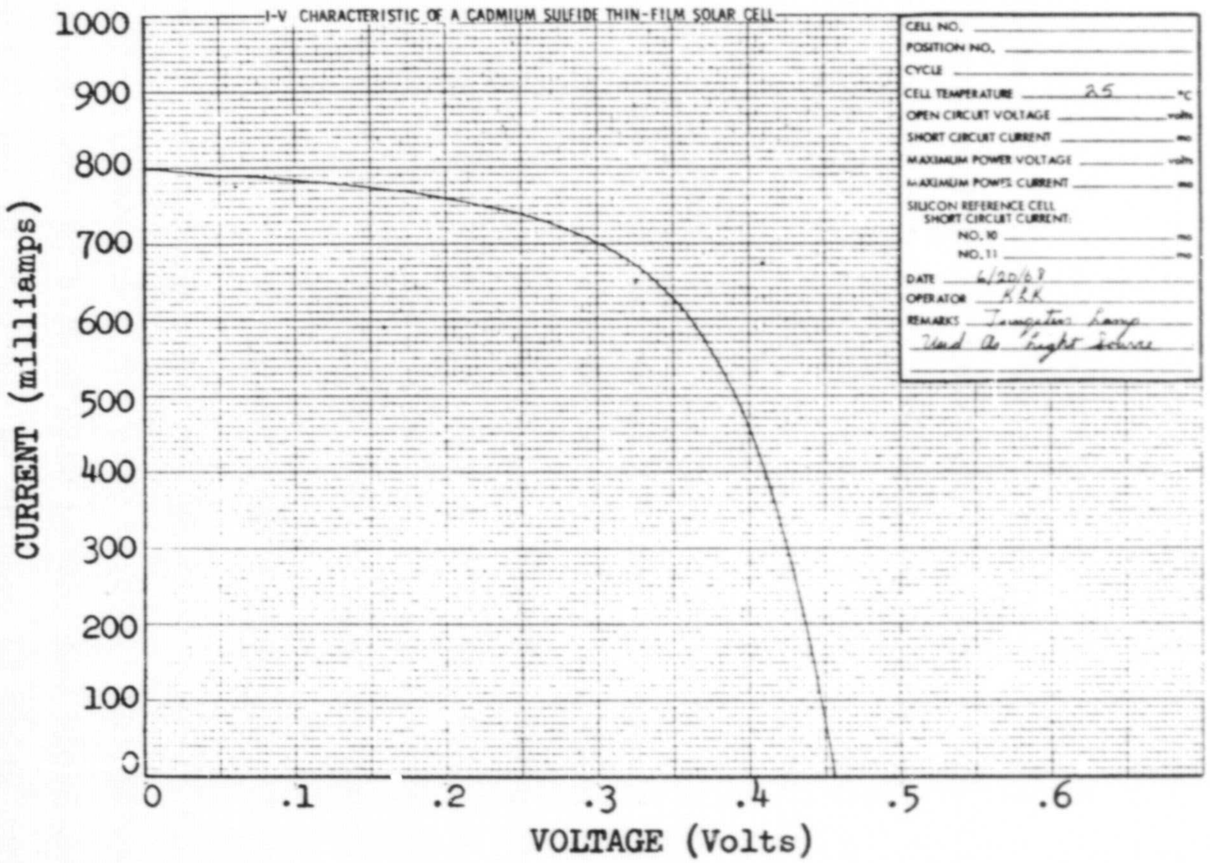

FIGURE 6: I-V CURVE OF A CdS SOLAR CELL USING TUNGSTEN LIGHT SOURCE

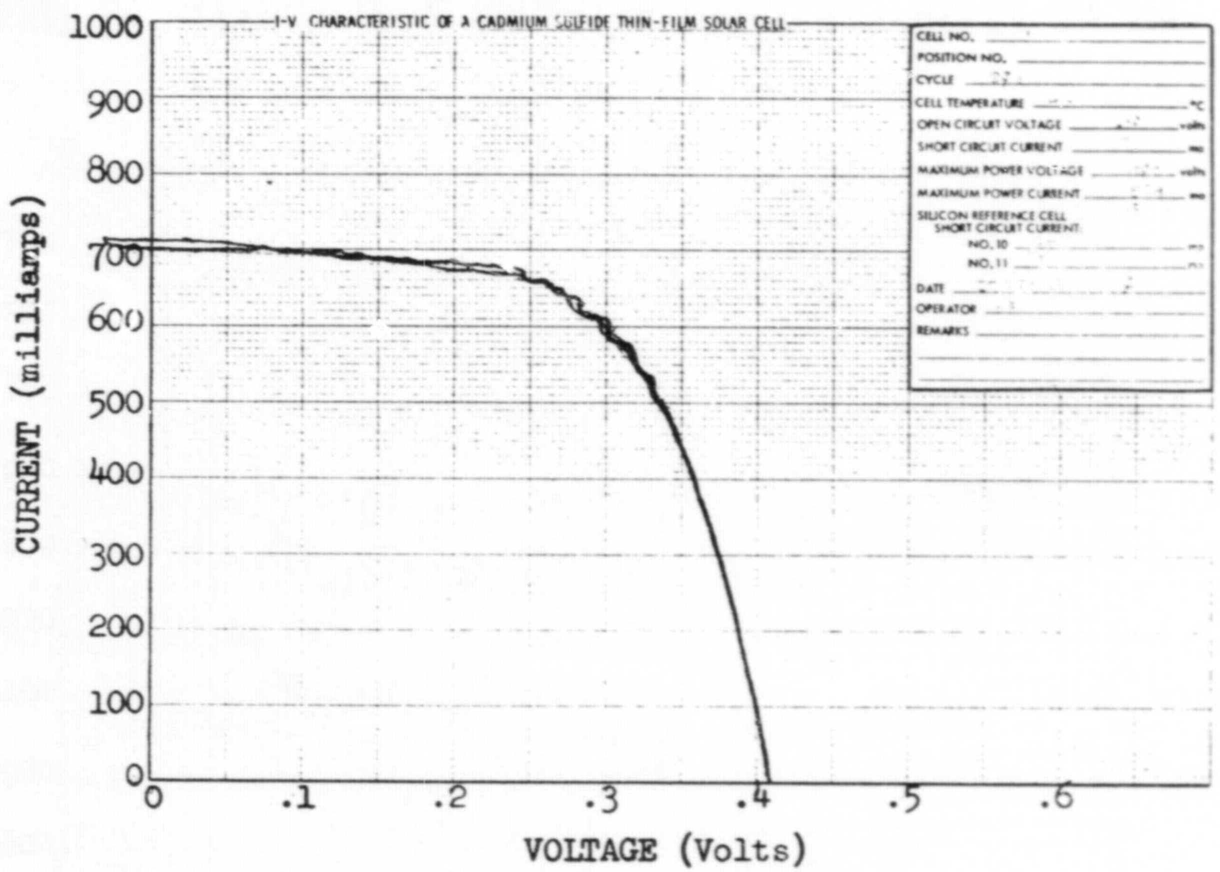

FIGURE 7: I-V CURVE OF A CdS SOLAR CELL USING XENON SOLAR SIMULATOR LIGHT SOURCE

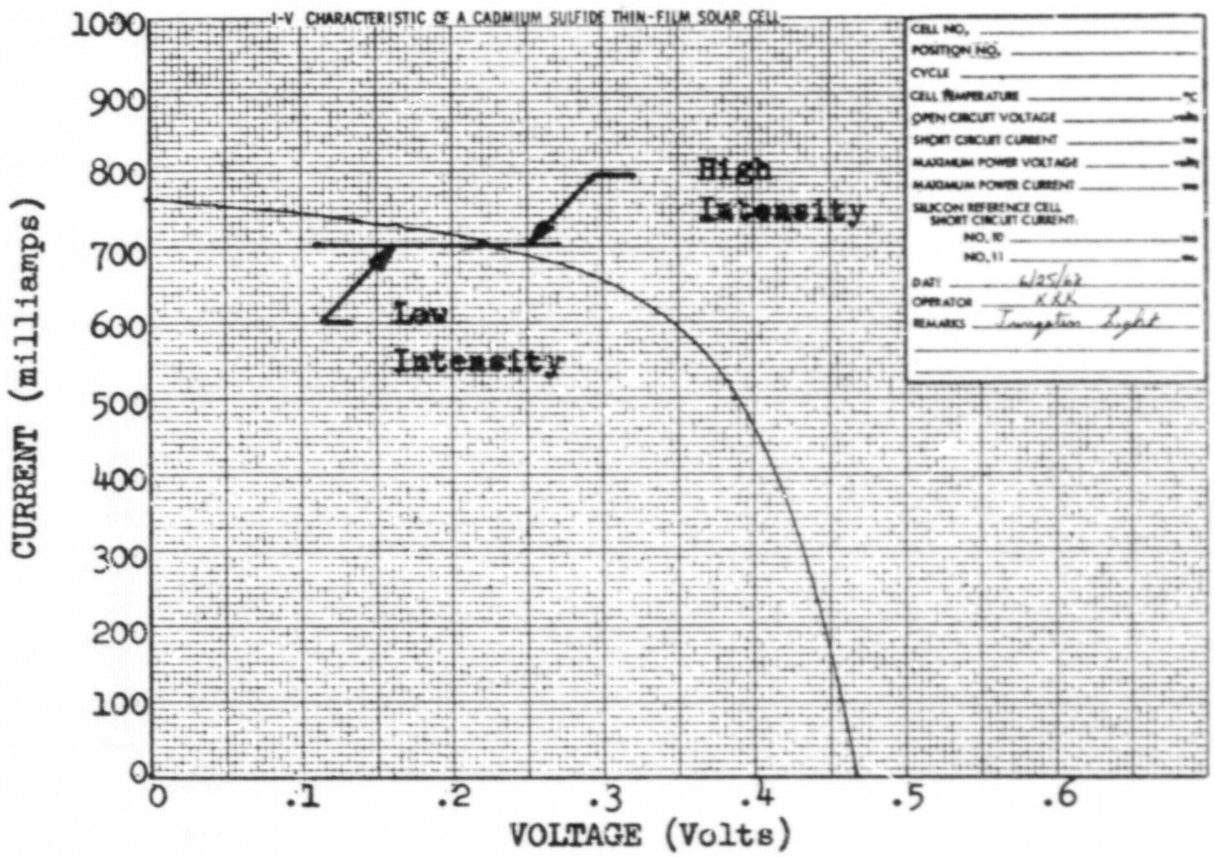

FIGURE 8: EFFECT OF A CHANGING LIGHT INTENSITY ON THE I-V CURVE OF A CdS SOLAR CELL

A thermocouple was soldered to the back of each silicon reference cell and thermocouples were bonded to the front and back of the test cell supporting frame as well as to the end plate of the cold shroud in the vacuum chamber. Copper-constantan feed-through connectors were used to route the thermocouple leads out of the vacuum chamber. The temperature of the control-cell mounting block was measured with a thermocouple imbedded in the side of the block. All thermocouples were connected to a temperature recorder which printed the output of each thermocouple once every 2½ minutes. The recorder could also display continuously the output of any one thermocouple. A reference junction compensator in the recorder facilitated display of the thermocouple outputs directly in $^{\circ}$C.

Temperatures between -150°C and +100°C could be recorded with an accuracy of ± 2°C and a reproducibility of ± 1°C. The temperature recorder was periodically calibrated against a secondary standard whose accuracy is traceable to the NBS.

4.2.3 Solar Simulator Light-Intensity Measurement

The true intensity of the light beam in the test plane was measured with a radiometer whose response to radiation is essentially independent of wavelength. Its range of response was .25μm to 2.7μm. Its estimated accuracy in sunlight is ± 3.5 percent. The radiometer was periodically checked against a secondary standard radiometer which had been calibrated at Table Mountain, California.

The equivalent space sunlight intensity, as seen by a CdS solar cell, was determined with an encapsulated CdS standard cell which had been calibrated in an airplane at high altitudes and whose output was extrapolated to air-mass zero conditions.

4.2.4 Solar Simulator Light-Spectrum Measurement

Because the spectrum of the solar simulator is not identical to that of space sunlight, the true intensity measured with the radiometer was slightly different from the equivalent space sunlight (AMO) intensity measured with the CdS standard cell. However the two measurements always agreed within 2 percent. The equivalent space sunlight (AMO) intensity was used throughout this report for calculating the conversion efficiency of CdS solar cells. The true intensity was used only in processing the spectrum data.

The relative spectrum of the light beam was determined with a prism-type spectroradiometer which recorded the relative energy contained within a .05 μm bandwidth, scanning the wavelength region from .25 μm to 2.5 μm. The accuracy of the relative energy recorded by the spectrophotometer was ± 10 percent. The spectroradiometer was calibrated periodically with a NBS 1000-watt standard of irradiance and a magnesium diffusing block.

4.2.5 Solar Simulator Light-Uniformity Measurement

The uniformity of the light beam was determined by recording the short circuit current of a 2 x 2 cm silicon solar cell mounted on a rotary scanner. The output of this cell was recorded at the center of the beam and then continuously while roated at radii of 1, 2, 3, 4, 5, and 6 inches about the center. The output of this silicon cell vs. angle at each circle for a typical uniformity scan is shown in Figure 9.

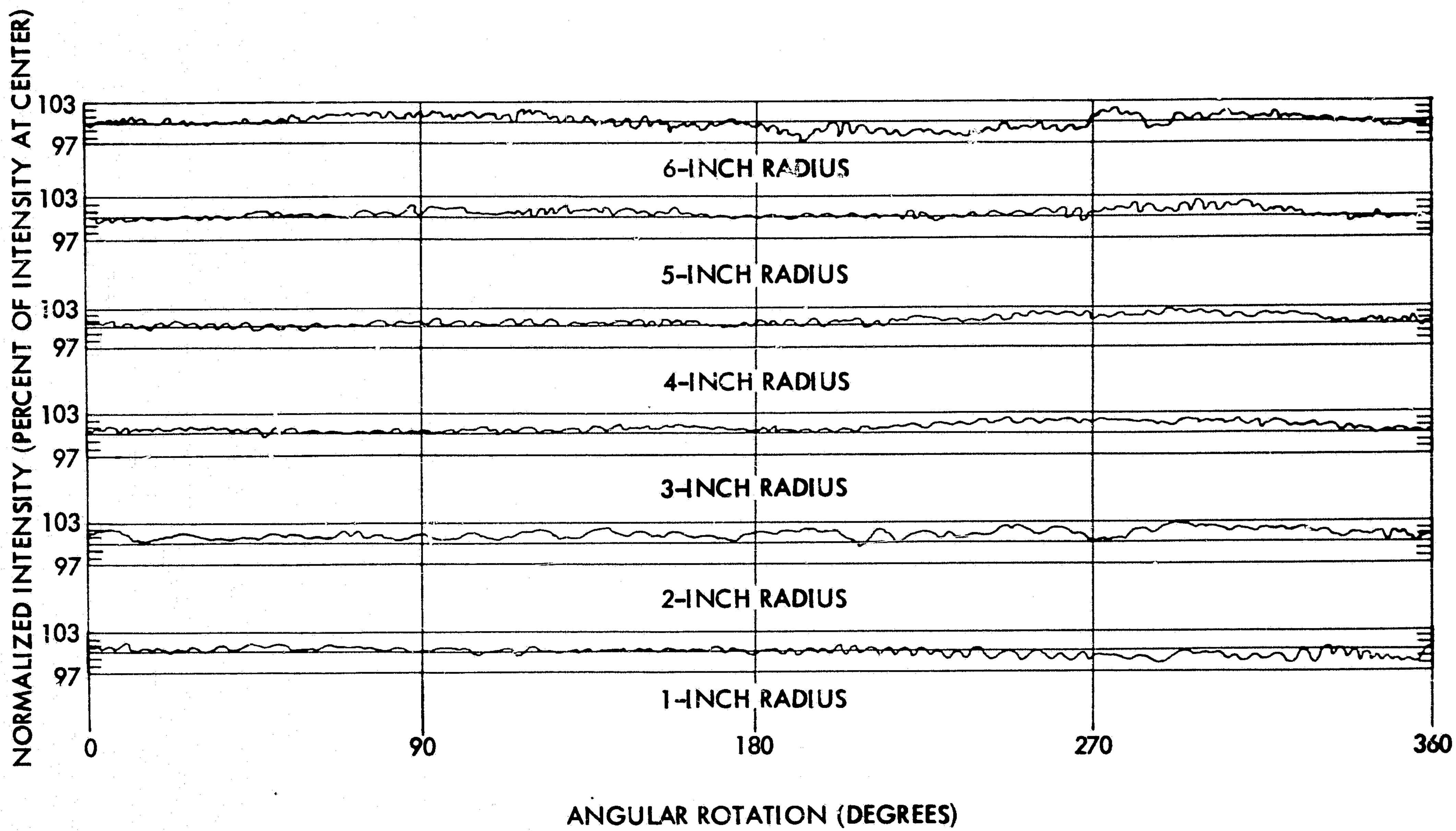

Figure 9: SOLAR SIMULATOR UNIFORMITY SCANS

5.0 TEST PROCEDURES

During Phase III of this program, three consecutive thermal cycling tests were conducted on CdS solar cells manufactured in April, 1967, November, 1967, and March, 1968. Each test had nine CdS solar cells (test cells) mounted in the vacuum chamber at a pressure less than 10^{-6} torr. Thermal cycling was produced by exposing the cells to 30 minutes of darkness followed by 60 minutes of illumination; the cell temperatures dropped to less than -100°C during the dark portion of each cycle and came to an equilibrium of about +60°C during the illuminated portion of each cycle. Control cells were kept in double-desicated storage.

The first test, involving the April, 1967 cells, ran for 368 thermal cycles. The second test, involving November, 1967 cells, ran for 533 thermal cycles. The third test, involving March, 1967 cells, ran for 2031 thermal cycles. In all of these tests, the electrical performance of both the test-cells and control cells was measured at least once every 100 cycles. During the first 300 cycles of each test, the performance of the test-cells was measured more often: once every ten cycles for the first 100 cycles and once every 30 cycles for the next 200 cycles. In addition to the performance measurements made during cycling, performance measurements were also made before and after cycling - some in situ and others not. The performance measurements consisted primarily of tracing the current-voltage (I-V) curve of the cells under known conditions of light intensity and temperature.

Initially, cycling was conducted continuously five days a week, although occasionally solar simulator lamp failures and laboratory power failures required additional suspension of cycling. When other tests were being conducted in the laboratory on weekends, cycling was continued 7-days-a-week. Installation of automatic monitoring and safety controls was completed in August, 1968, permitting cycling on a 24-hour-per-day, 7-day-per-week basis.

5.1 Startup of Cycling

After the test-cell supporting frame containing the test cells was installed in the chamber, a mechanical roughing pump was used to evacuate the chamber to 10^{-4} torr, usually within two hours. Then the ion pump was turned on to reduce the chamber pressure to 10^{-6} torr, usually within several hours. Then liquid nitrogen was fed to the cold shroud, reducing the pressure to 10^{-7} torr within a few minutes. Thirty minutes after the admission of liquid nitrogen, the shutter was opened to allow the solar simulator to illuminate the test cells. The admission of the liquid nitrogen and the opening of the shutter are considered the beginnings of the dark and light portions, respectively, of the first cycle.

5.2 Suspension of Cycling

Whenever cycling had to be suspended because of weekends, lamp failures, or other causes, the shutter was first closed and then the liquid nitrogen was blown out of the shroud with forced air.

As the shroud warmed to room temperature, molecules once trapped on the cold shroud were released, increasing the chamber pressure from 10^{-8} to 10^{-6} torr. Startup of cycling after a shutdown followed the procedure described in the preceding section.

Cycling was also suspended for short periods (e.g. five hours) when maintenance of the solar simulator was required, for example, replacement of a lamp. In these cases the shutter was closed, but liquid nitrogen was not blown from the shroud.

5.3 Measurement of Test-Cell Performance

Measurements of test-cell performance were started at the end of the illuminated portion of a cycle and took about thirty minutes to complete, thus requiring a 30-minute extension of the illuminated portion of that cycle. The performance test was not started until the end of the illuminated portion of the cycle to insure that the cells were near thermal equilibrium.

The first step in a performance test was to adjust the light intensity in the center of the beam to be equivalent to space sunlight having an intensity of 140 mw/cm^2, AMO, as indicated by the outputs of the silicon reference cells on the test-cell supporting frame. Calibration of the silicon reference cells against the CdS standard cell had been accomplished during the preceding cycle. The load resistor on the first cell was then removed and the voltage and current leads of that cell were switched into the I-V curve measuring circuit in a open-circuited condition. Calibration of both axes of the XY plotter against the digital voltmeter at two points on the I-V curve then followed. The I-V curve of the first cell was then traced from open circuit to short circuit, and back again. Immediately upon completing the I-V trace, the operator recorded the output of the two reference cells and the test-cell temperature, and then replaced the load resistor.

This procedure was repeated for the remaining eight cells, except calibration of the XY recorder was not repeated. After completing all nine I-V traces, the operator recorded the load voltage of each cell to insure that its load resistor was replaced. He then recorded the temperatures of the silicon reference cells and the test-cell supporting frame. Upon completion of the performance test, the shutter was closed, the solar simulator was rotated, and the output of the CdS standard cell was recorded after being located in the center of the light beam.

5.4 Measurement of Control-Cell Performance

Measurements of control-cell performance, obtained during the dark portion of a cycle, took about forty minutes to complete, thus requiring that the dark portion of that cycle be extended by ten minutes. The first step in this performance test was to adjust the intensity in the center of the beam to equal space sunlight intensity of 140 mw/cm^2, as indicated directly by the CdS standard cell. The first control cell was then placed on the control-cell mounting block, whose temperature had previously been adjusted to 25°C. The block was then moved to the center of the beam and the I-V curve of the cell was traced from open circuit to short circuit, and back again. Immediately after the I-V curve was traced, the block temperature was recorded, the CdS standard cell was again placed in the center of the beam, and its output was recorded. This procedure was repeated for the remaining eight control cells.

5.5 Determination of Intensity Loss in Quartz Window

The light intensity in the vacuum chamber could not be measured directly with the CdS standard cell during thermal cycling. Therefore, before the chamber was closed at the beginning of each test, the loss in intensity due to the light passing through the quartz window was determined. This was done by measuring the output of the CdS standard cell while located outside the vacuum chamber after the intensity had already been increased so that the equivalent space sunlight intensity at the test-plane inside the vacuum chamber was 140 mW/cm^2 as measured directly by the CdS standard cell placed in the chamber.

5.6 Adjustment of Light Intensity

Equivalent space sunlight intensity of the illumination at the control-cell block was easily obtained by directly monitoring the output of the CdS standard cell.

Adjustment of the intensity at the test plane in the vacuum chamber was more difficult, involving the silicon reference cells and absorption losses in the quartz window. At the end of the light cycle preceding the one in which the performance of the test-cells were to be measured, the outputs of both silicon-reference cells were recorded, the solar simulator was rotated, and the output of the CdS standard cell at the center of the beam was measured. The recorded silicon reference cell readings were then adjusted to correspond to the proper CdS standard cell reading. This periodic calibration of the reference cells was necessary because some of the reference cells degraded over long periods of time.

5.7 Measurement of Light Uniformity

The uniformity of the light intensity of the solar simulator was measured whenever the lamp or optics were changed, and at the beginning and end of the test. The procedure used is described in section 4.2.5.

5.8 Measurement of Light Spectrum

The spectrum of the solar simulator was measured whenever the lamp or optics were changed and at the beginning and end of the test. This was done by rotating the solar simulator away from the vacuum chamber and centering the beam on the entrance slit of the spectroradiometer described in section 4.2.4. The wavelength region between 25 and 2.5 microns was scanned and plotted automatically by the spectroradiometer. This plot represented the relative spectrum of the light beam. Before the plot was made, the equivalent space sunlight intensity at the entrance slit was adjusted to 140 mW per sq. cm as indicated by the CdS standard cell. The true intensity at the entrance slit was then measured with the radiometer.

The relative spectrum was determined by integrating the area under curve produced by the spectroradiometer in each of the six wavelength bands of interest. These areas were converted to intensities by normalizing the total area under the curve to the total intensity as measured by the radiometer. The resulting intensities represent the absolute spectrum of the solar simulator outside the test chamber.

The absolute spectrum at the test-cell plane inside the vacuum chamber was determined from the CdS standard cell setting used during test-cell performance measurements, the spectral transmission of the quartz window, and the absolute spectrum of the solar simulator outside the vacuum chamber. This absolute spectrum was calculated by modifying the outside spectrum by (1) multiplying all the values by the ratio of the CdS standard cell setting used during test-cell performance measurements to the setting used during control-cell performance measurements, and (2) reducing all the spectrum values by the corresponding absorptions in the quartz window.

5.9 Monitoring Test Environment Conditions

During thermal cyling, the chamber pressure, the light intensity, and the test-cell temperatures were periodically monitored between performance tests to insure that the cells were being exposed to the desired space environment. The chamber pressure and the light intensity were read and recorded by laboratory personnel two or three times during each laboratory shift. In addition, an alarm would sound if the vacuum were lost, if the illumination were lost, or if the shutter opened or closed improperly. The temperatures of the test-cells, the supporting frame, and the silicon reference cells were recorded every 2½ minutes during a complete thermal cycle at least once during each eight hour shift. A plot of CdS cell temperature for a typical cycle is shown in Figure 10.

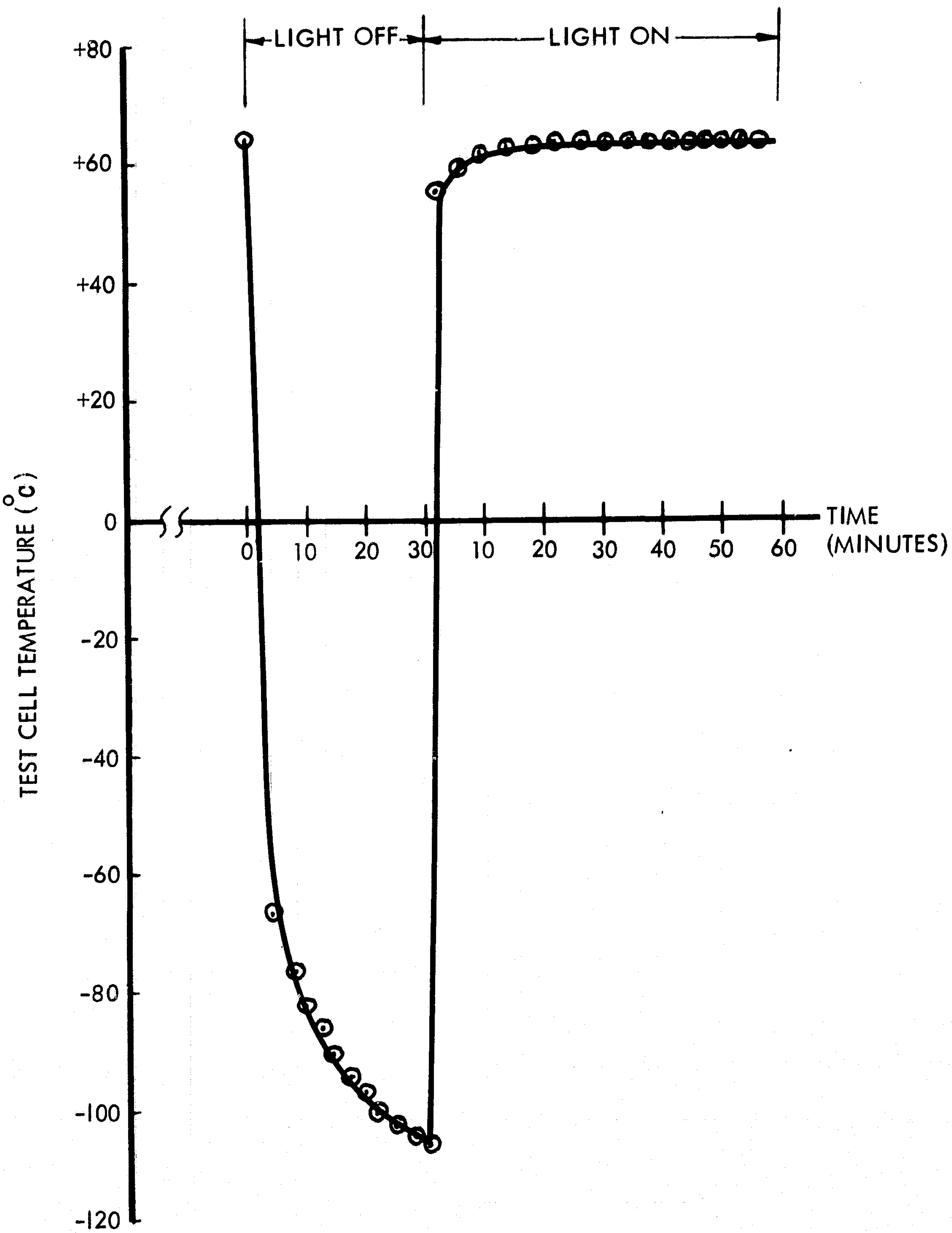

Figure 10—TEST CELL TEMPERATURE CYCLE

6.0 DISCUSSION AND RESULTS

One objective of this contract was to determine experimentally how the power output of CdS solar cells is affected by prolonged exposure to a simulated space environment, including thermal cycling. Second objective was to determine what physical or chemical changes in the cells were responsible for any losses in power resulting from such an exposure. In this work the physical and chemical changes were postulated from an analysis of the illuminated current-voltage (I-V) curves obtained before, during, and after thermal cycling tests. This analysis is based on a mathematical model which relates the I-V curves to physically meaningful parameters in the cells.

This section begins with a description of the mathematical model, and the changes in cell performance it predicts when postulated physical and chemical changes occur in the cell. Then the results of each of the three thermal cycling tests conducted during Phase III are presented and discussed.

6.1 Changes in Cell Performance Predicted by a Mathematical Model

The I-V curve of a CdS solar cell can be represented by the equation (ref. 7):

$$I = I_o\left\{ \exp\left[\frac{q}{AkT}\,(V-IR_s)\right] - 1\right\} - I_g + \frac{V-IR_s}{R_{sh}} \qquad (1)$$

where the symbols are defined as follows:

I = current output of the cell

I_g = light-generated current

I_o = reverse saturation current

q = electronic charge

A = empirical fitting constant equal to 1 for an ideal junction

k = Boltzmann constant

T = absolute temperature, ^oK

V = the voltage appearing at the cell terminals

R_s = series resistance

R_{sh} = shunt resistance

The values of I_g, R_s, R_{sh}, I_o, and A in a given cell may change as a result of physical and/or chemical changes in the cell. Assuming that the intensity and spectrum of the light at the front surface of the cell is constant, I_g may decrease because -

(1) The transmission of the front cover and/or the laminating epoxy is reduced at wavelengths to which the cell responds.

(2) The barrier layer is changed chemically or physically in such a manner that fewer of the photons reaching the barrier layer produce electron-hole pairs (e.g. its spectral response is changed).

(3) The active area is reduced.

R_s, the series resitance may increase because -

(1) The conductive substrate is delaminated from the CdS layer

(2) The grid is separated from the barrier layer or the conductive epoxy

(3) The photoconductive layer increased in resistivity in the depletion region formed at the barrier layer-CdS interface. The cause can be less green light being transmitted by the front cover-laminating epoxy combination

(4) The conductive epoxy changed chemically, increasing in resistivity

(5) The CdS or barrier layers cracked, increasing the average distance traveled by an electron from the depletion region to the cell electrode.

(6) The substrate metal layer changed, chemically increasing its resistivity.

More shorting paths between the barrier layer and the CdS layer will decrease R_{sh}, the shunt resistance. Shorting paths may be caused by movements of the grid wearing holes in the barrier layer or by pinholes in the CdS layer (and hence the barrier layer) filling with conductive epoxy during attachment of the grid. Chemical reactions or diffusion processes in the barrier layer - CdS layer interface can change A and I_o.

The effects of changes in I_g, R_s, R_{sh}, I_o and A on the I-V curve of a cell are shown in Figures 11 to 15. These curves were obtained by repeatedly solving equation 1 for I at various values of V, using different values of the above parameters. The equation was solved by the Newton-Raphson technique with a digital computer (ref. 10), since the equation cannot be solved in closed form. The undegraded I-V curve in Figures 11 to 15 is identical to the pre-test I-V curve obtained for one of the CdS test cells at an intensity of 140 mW/cm^2 and a temperature of 60^oC.

The effects of I_g, R_s, R_{sh}, I_o and A on the maximum power (P_M), short-circuit current (I_{sc}), open-circuit voltage (V_{oc}) and fill factor ($FF = P_M (V_{oc} \times I_{sc})$) were calculated using the I-V curves in Figures 11 to 15. The results are plotted in Figures 16 to 20.

It will be observed that R_s affects P_M and FF, (Figure 16), and also the slope of the I-V curve at V_{oc} (Figure 11). We define the negative value of this slope as R_{oc}, the equivalent series resistance:

$$R_{oc} = - \left[\frac{\Delta V}{\Delta I}\right]_{I = 0}$$

The effect of R_s on R_{oc}, obtained from the I-V curves in Figure 11, is plotted in Figure 21.

Losses in P_M result from changes in any of the parameters in the CdS solar-cell equation. Significant degradation in P_M occurs only when the light generated current, I_g, or the shunt resistance, R_{sh}, changes. Losses in V_{oc} result from deterioration in any

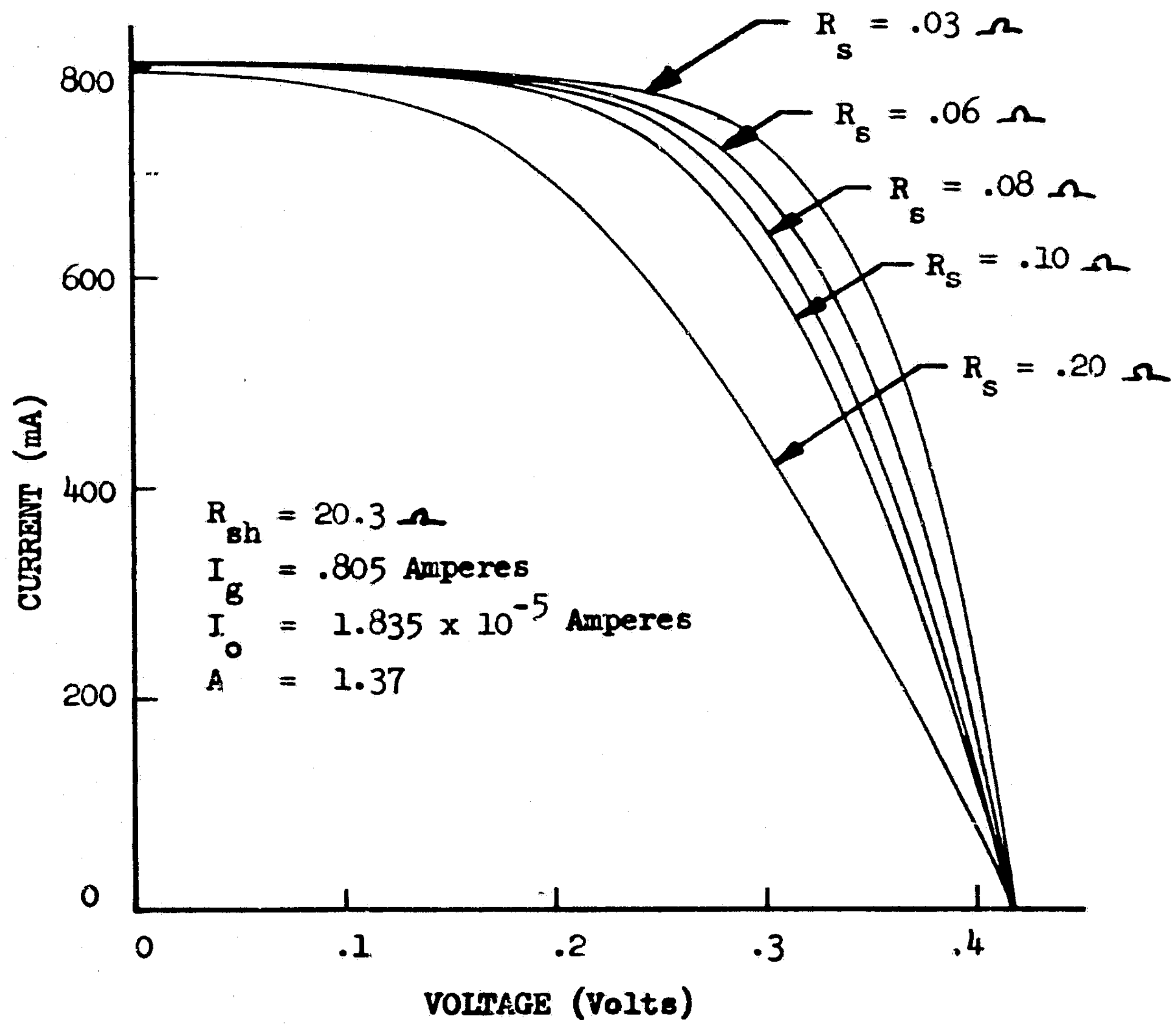

FIGURE 11: Effect of Changes in Series Resistance on the I-V Curve of a CdS Solar Cell

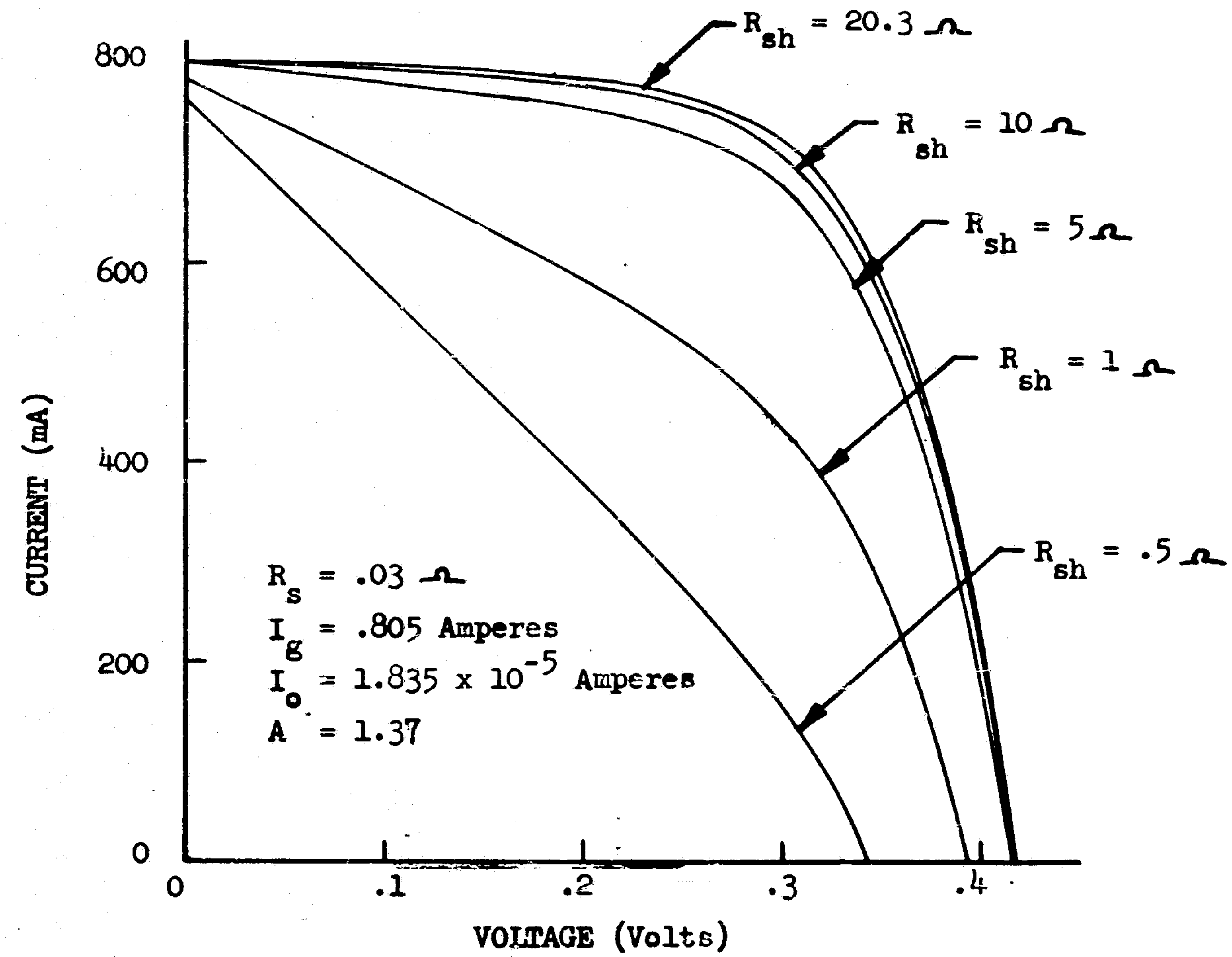

FIGURE 12: Effect of Changes in Shunt Resistance on the I-V Curve of a CdS Solar Cell

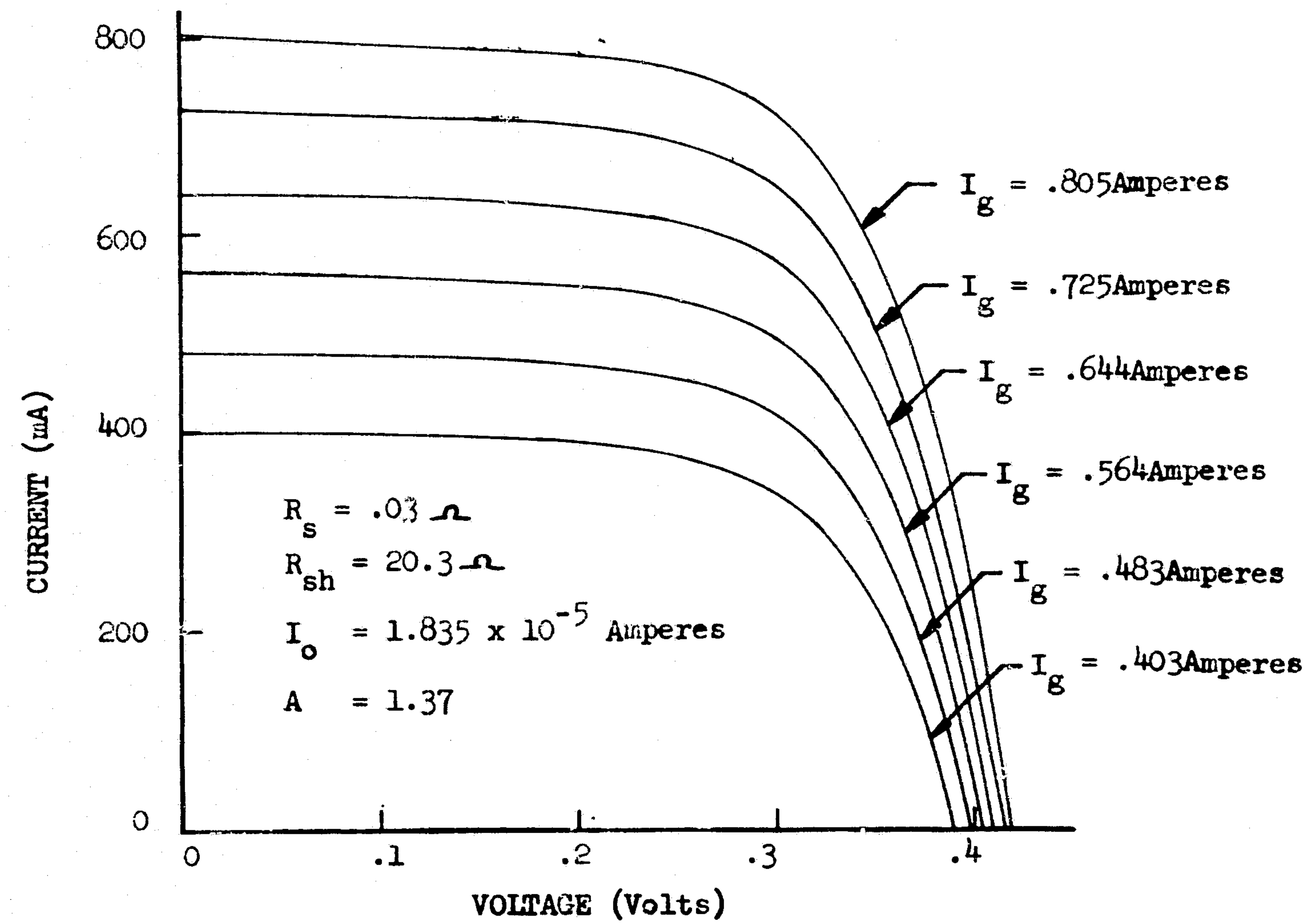

FIGURE 13: Effect of Changes in Light Generated Current on the I-V Curve of a CdS Solar Cell

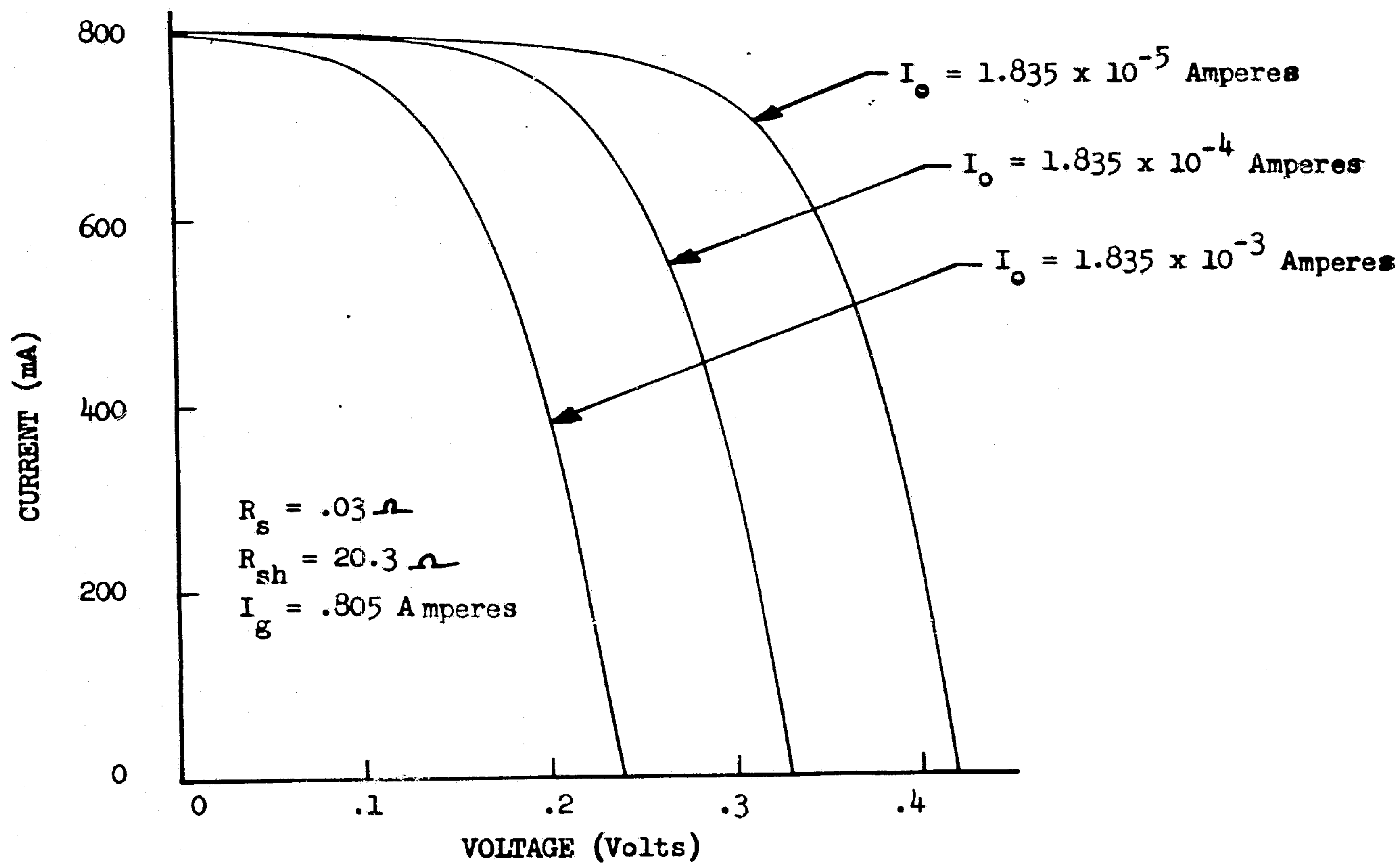

FIGURE 14: Effect of a Change in Reverse Saturation Current on the I-V Curve of a CdS Solar Cell

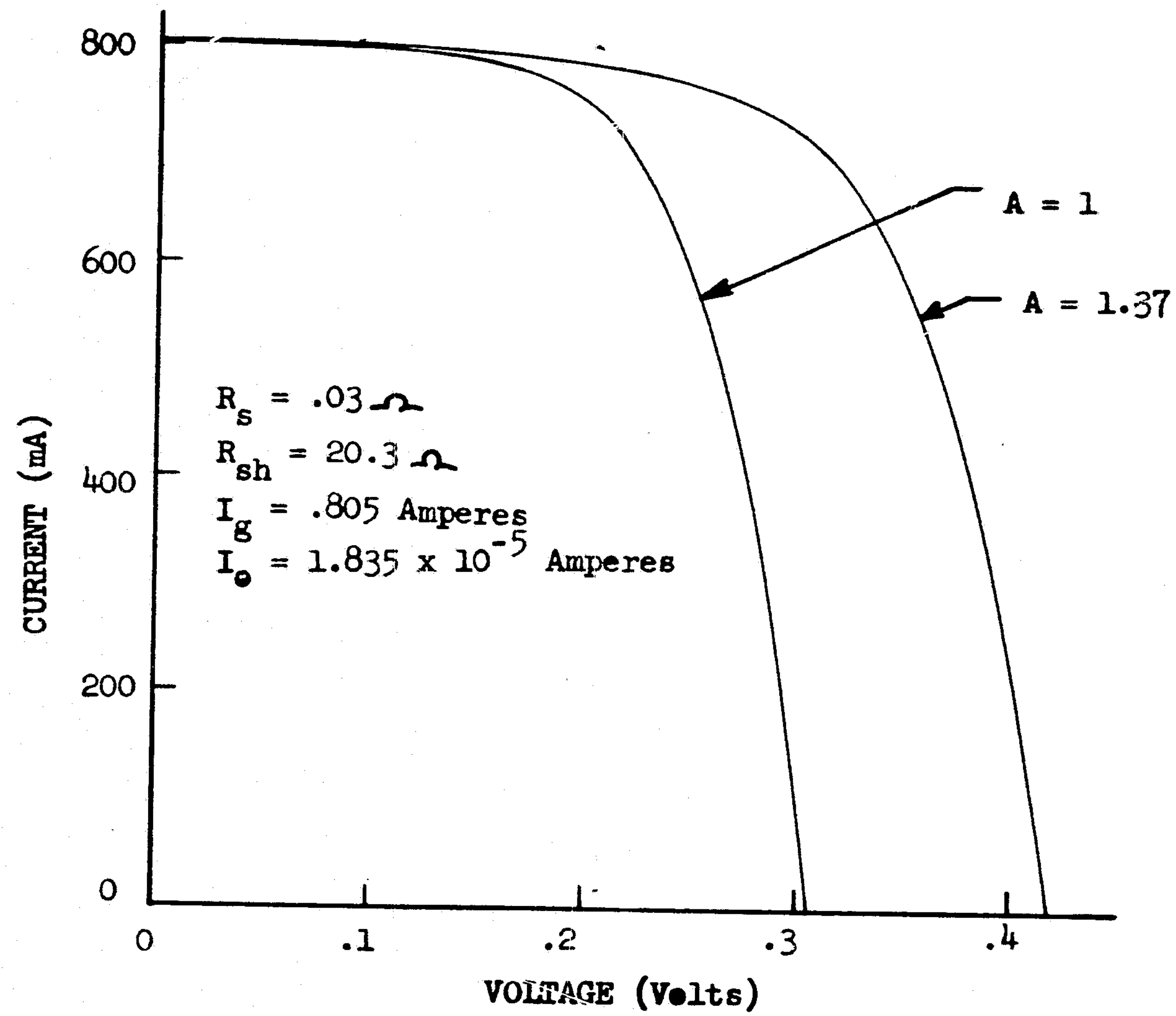

FIGURE 15: Effect of Changes in Empirical Fitting Constant on the I-V Curve of a CdS Solar Cell

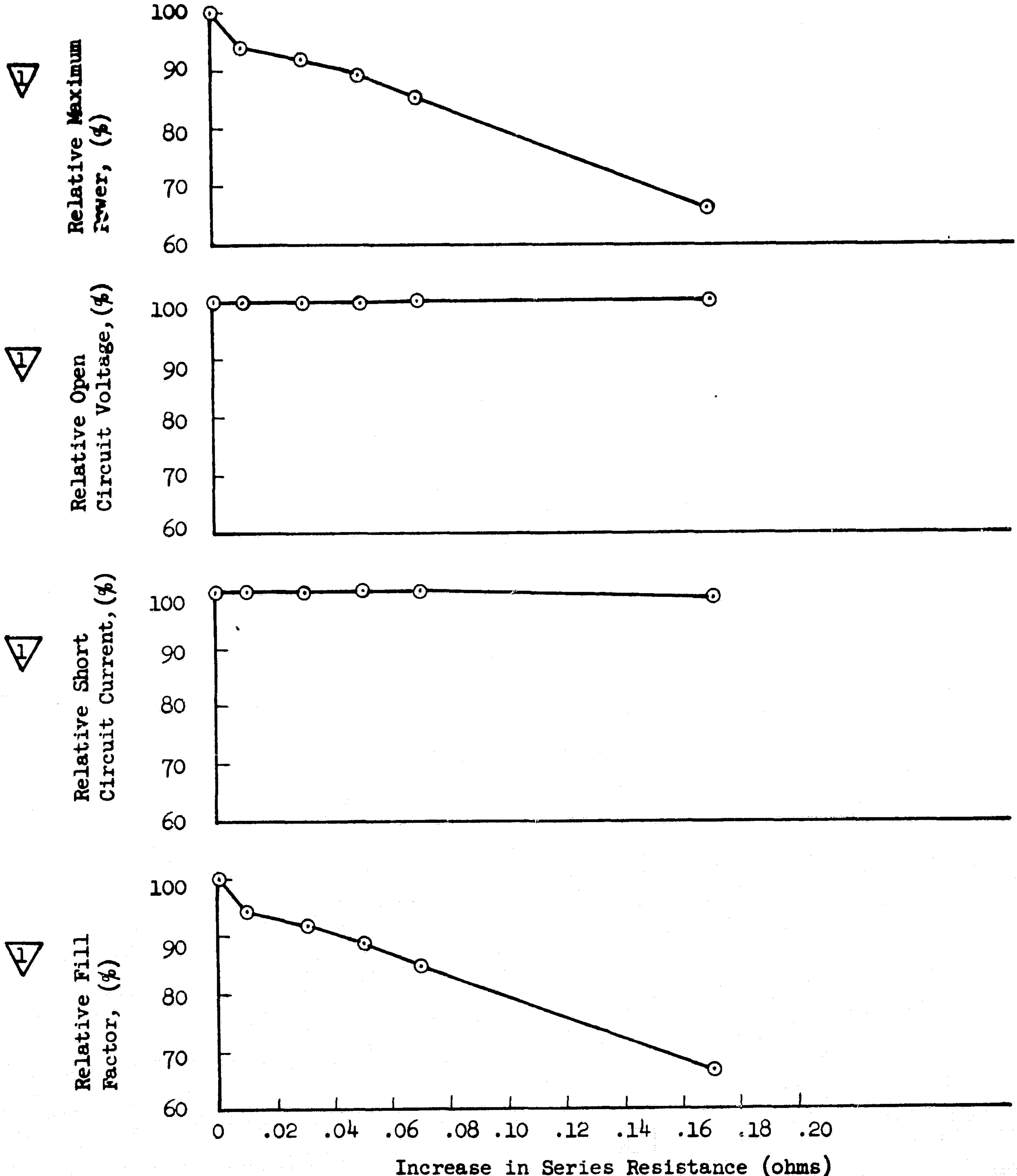

(1) These values were obtained from I-V curves generated by the equation

$$I = I_o \left\{ \exp\left[\frac{q}{AkT}(V-IR_s)\right] -1 \right\} - I_g + \frac{V-IR_s}{R_{sh}}$$

for various values of R_s, series resistance. Other parameters were not changed. Initially, R_s = .03 ohms.

FIGURE 16: PERFORMANCE CHARACTERISTICS OF A CdS SOLAR CELL vs CHANGING SERIES RESISTANCE

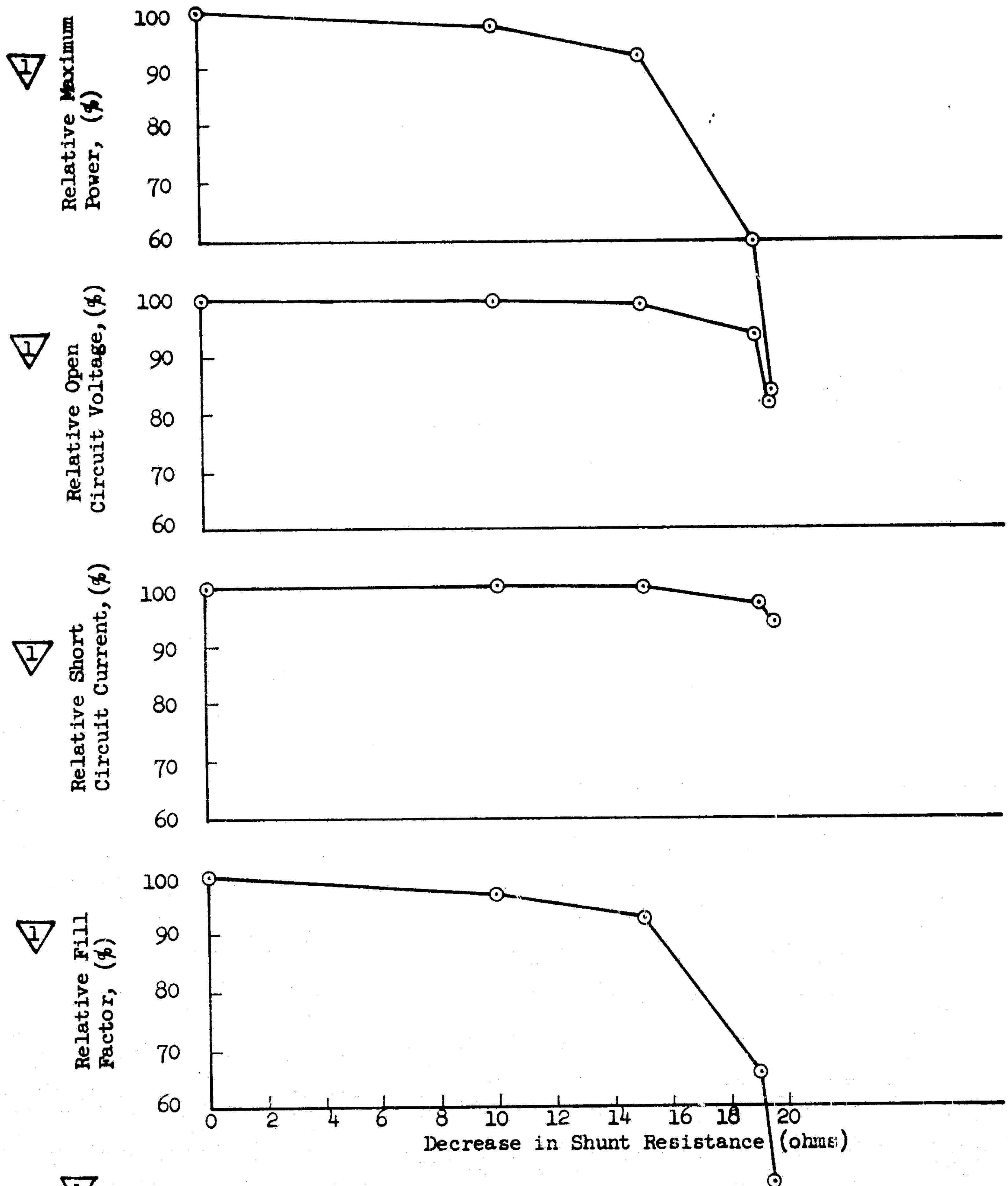

(1) These values were obtained from I-V curves generated by the equation $I = I_o\left\{\exp\left[\frac{q}{AkT}(V-IR_s)\right]-1\right\} - I_g + \frac{V-IR_s}{R_{sh}}$ for various values of R_{sh}, shunt resistance. Other parameters were not changed. Initially, R_{sh} = 20 ohms.

FIGURE 17: PERFORMANCE CHARACTERISTICS OF A CdS SOLAR CELL vs CHANGING SHUNT RESISTANCE

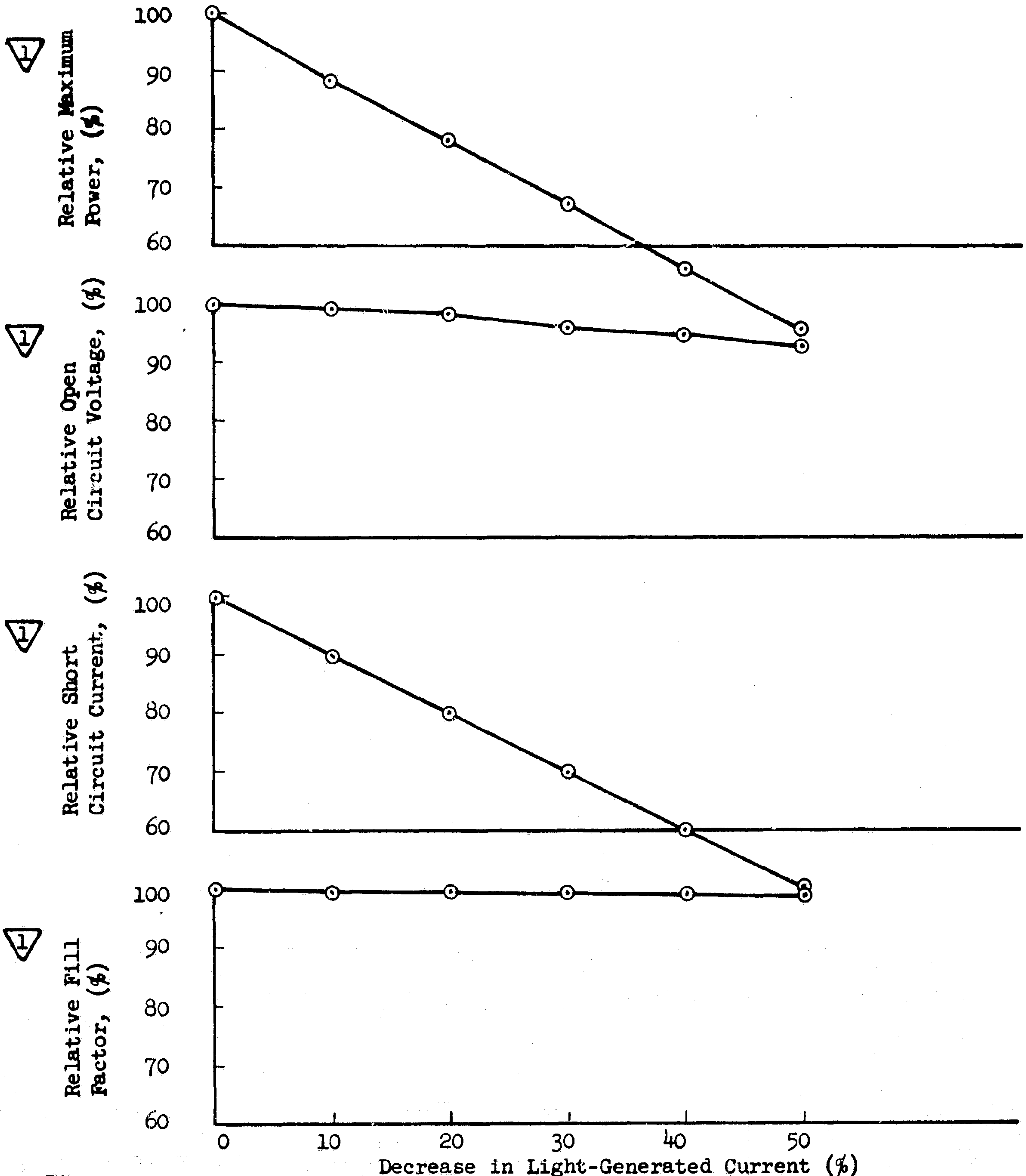

1 These values were obtained from I-V curves generated by the equation $I = I_o\left\{\exp\left[\frac{q}{AkT}(V-IR_s)\right]-1\right\} - I_g + \frac{V-IR_s}{R_{sh}}$ for various values of I_g, light-generated current. Other parameters were not changed. Initially, I_g = .805 amperes.

FIGURE 18: PERFORMANCE CHARACTERISTICS OF A CdS SOLAR CELL vs CHANGING LIGHT GENERATED CURRENT

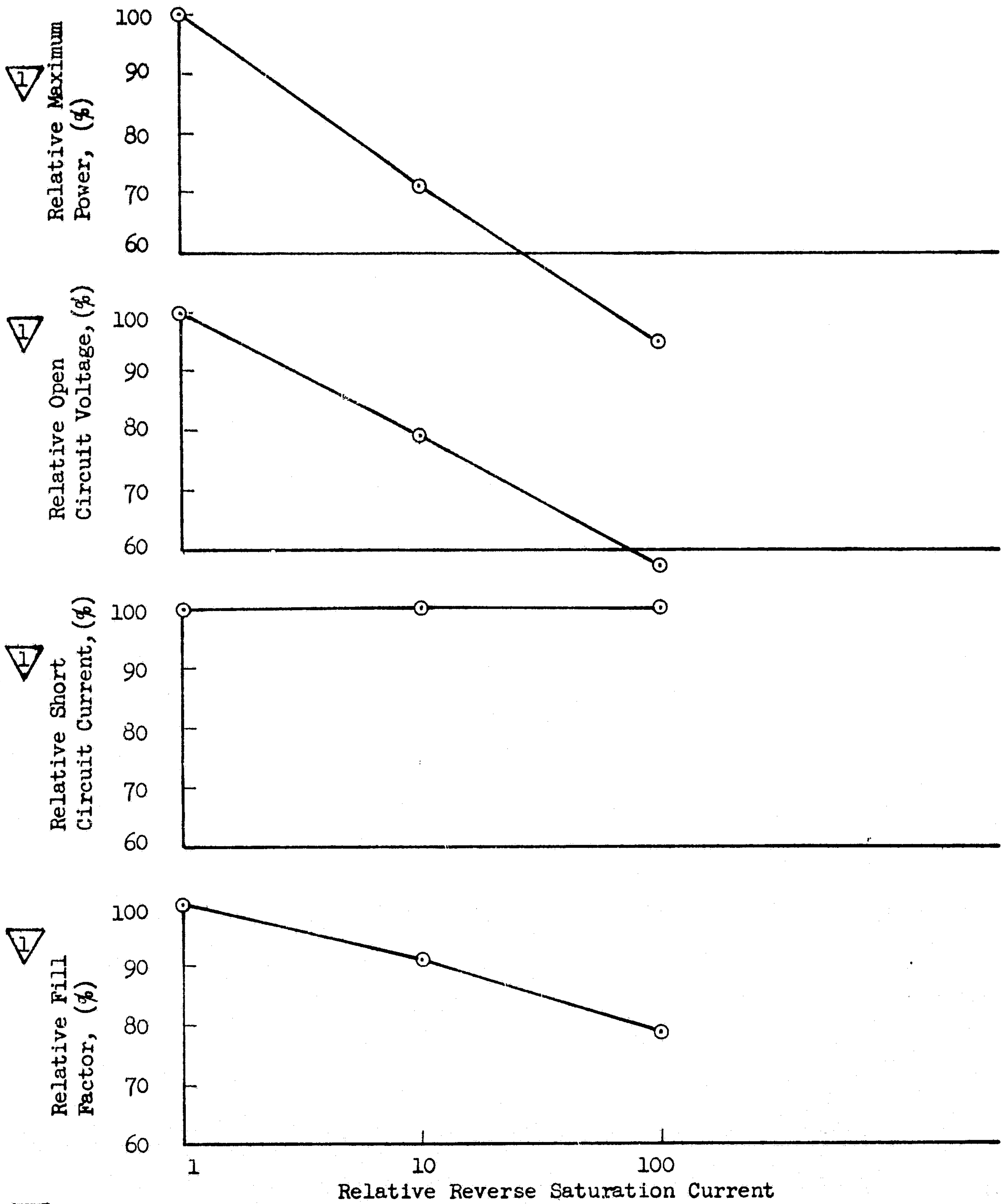

1 These values were obtained from I-V curves generated by the equation $I = I_o\left\{\exp\left[\frac{q}{AkT}(V-IR_s)\right] - 1\right\} - I_g + \frac{V-IR_s}{R_{sh}}$ for various values of I_o, reverse saturation current. Other parameters were not changed. Initially, $I_o = 1.835 \times 10^{-5}$ amperes.

FIGURE 19: PERFORMANCE CHARACTERISTICS OF A CdS SOLAR CELL vs CHANGING REVERSE SATURATION CURRENT

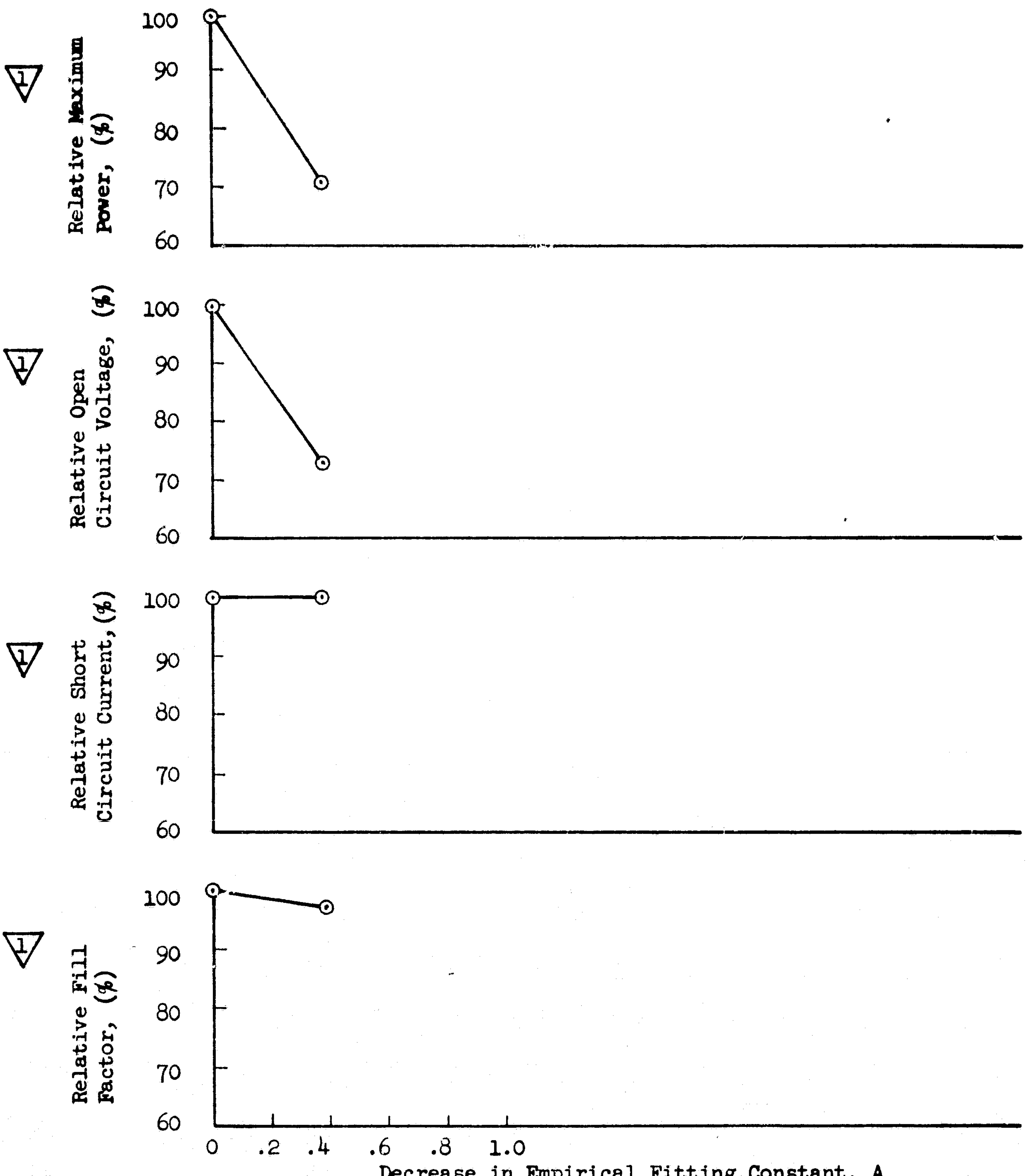

(1) These values were obtained from I-V curves generated by the equation $I = I_o\left\{\exp\left[\frac{q}{AkT}(V-IR_s)\right] -1\right\} - I_g + \frac{V-IR_s}{R_{sh}}$ for various values of A, empirical fitting constant. Other parameters were not changed. Initially, A = 1.37.

FIGURE 20: PERFORMANCE CHARACTERISTICS OF A CdS SOLAR CELL vs CHANGING EMPIRICAL FITTING CONSTANT

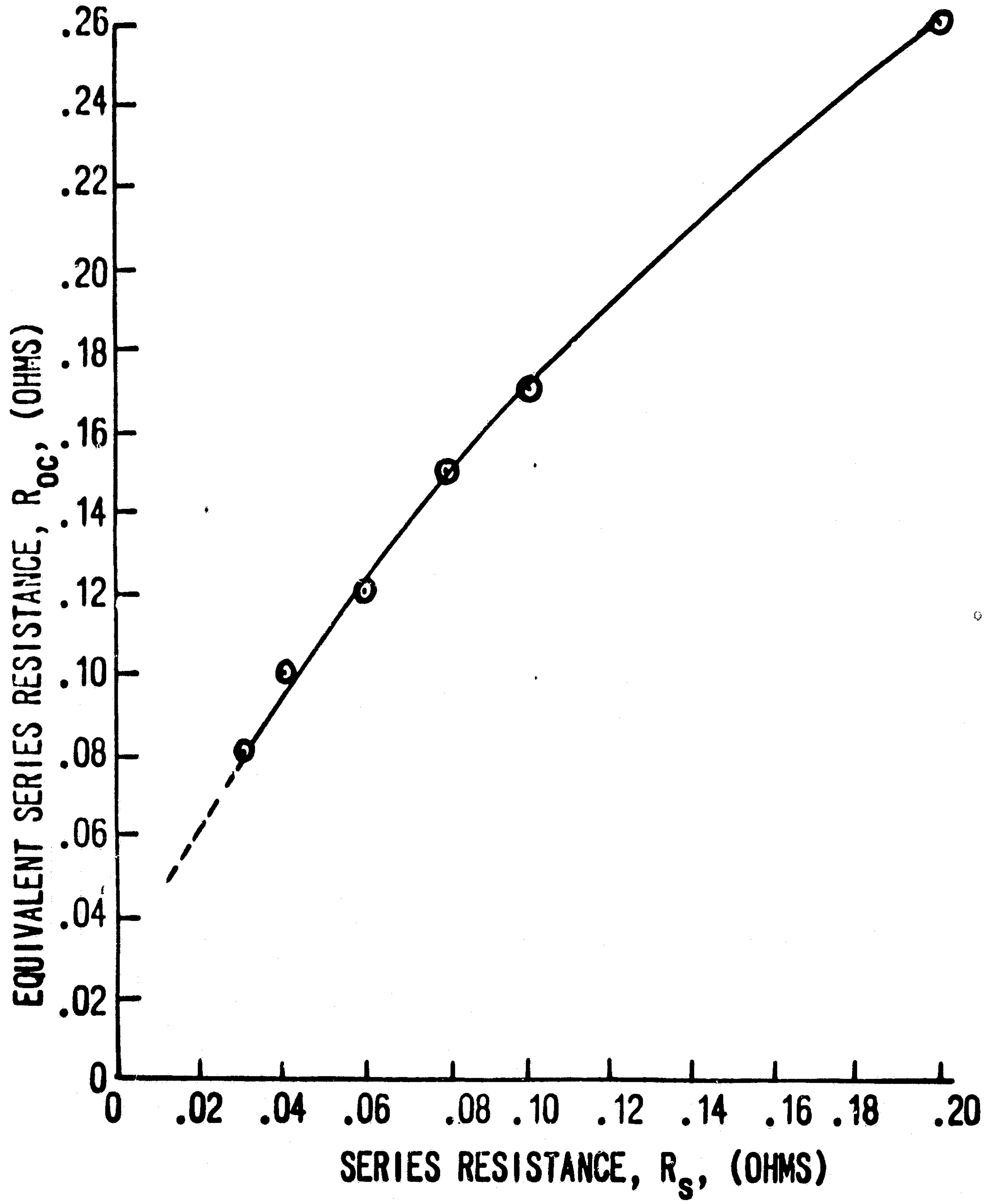

FIGURE 21: EFFECT OF CHANGES OF SERIES RESISTANCE ON EQUIVALENT SERIES RESISTANCE

parameter except the series resistance, R_s, and are always accompanied by losses in FF, except when I_g is responsible for the degradation. A loss in FF due to a change in R_s occurs without measurable losses in V_{oc} or I_{sc}.

It is helpful to keep these observations in mind when studying the experimental results presented later in this report.

6.2 Reproducibility and Accuracy of Experimental Results

The results in this report consist primarily of values of P_M, V_{oc}, I_{sc}, and FF obtained at various stages of the tests. In order to evaluate the reproducibility of these results, 33 sets of data obtained from a stable CdS cell over a period of two months were analyzed. The average values, standard deviations and maximum deviations of P_M, V_{oc}, I_{sc}, and FF were calculated and are presented in Table 5.

Fluctuations in the data were the result of these random experimental errors: (1) variations in light intensity, (2) errors in the measured temperature, and (3) errors in the measured values of current and voltage. Since all cells were subject to the same experimental errors, the standard deviations shown in Table 5 represent the reproducibility of all performance data in this report. The maximum deviations shown are the largest deviations expected from experimental error and are useful in separating changes in performance caused by experimental error from those caused by changes in the cell.

The performance data obtained in the test involving April, 1967 cells were all too low because of a systematic error caused by a circuit fault. However, the precision and reproducibility of the results was not affected, and the measured relative changes in overall performance are still to be trusted. Performance data for the November, 1967 and March, 1968 cells contain no known systematic errors and are therefore believed to be accurate.

	AVERAGE $\bar{X}$	STANDARD DEVIATION σ_s	$\sigma_s/\bar{X}$ (percent)	MAXIMUM DEVIATION σ_M	$\sigma_M/\bar{X}$ (percent)
Maximum Power, P_M, (mW)	157.4	2.6	1.7	4.4	2.8
Open Circuit Voltage, V_{oc}, (V)	0.4239	.0068	1.6	.0071	1.7
Short Circuit Current, I_{sc}, (mA)	548.1	7.6	1.4	16.1	2.9
Fill Factor, FF, (%)	67.73	.96	1.5	2.33	3.4

P_M, V_{oc} and FF corrected to 60°C

Values in table are based on 33 sets of data from one CdS solar cell, (March, 1968 Test Cell No. N150BK6)

TABLE 5: PRECISION OF PERFORMANCE DATA

6.3 Experimental Results

The results of the three thermal cycling tests are discussed separately. For each test, the relative values $P_M' = P_M/P_M(1)$, $V_{oc}' = V_{oc}/V_{oc}(1)$, $I_{sc}' = I_{sc}/I_{sc}(1)$, and $FF' = FF/FF(1)$ are presented where the 1 in parenthesis refers to initial values. Values obtained with the cells in the vacuum chamber, either under vacuum or at ambient pressure, are percentages of the values obtained at the end of cycle-1. Post-test values obtained with the cells outside of the vacuum chamber mounted on a temperature controlled block, are percentages of the values obtained under the same conditions before the test started. Values predicted by the mathematical model are in percentages of the values obtained from the initial undegraded I-V curve.

All measurements have been corrected for temperature variations. The measurements are also corrected for light intensity, when necessary. The effective intensity for all measurements is 140 mW/cm^2, AMO. The equations used to make the corrections are shown in the Appendix (section 9.0).

The April, 1967 cells were cycled at a load voltage considerably higher than their maximum-power voltage (see Table 1). The November, 1967 cells and March, 1968 cells were operated at a load voltage slightly lower than the maximum power voltage. According to ref. 11 the higher load voltages result in unstable performance of CdS solar cells under illumination, even without thermal cycling. Therefore, the high load voltages used in testing the April, 1967 cells may have contributed to the poor observed performance.

6.3.1 April 1967 Cells

The test-cells manufactured in April, 1967 were subjected to 300 thermal cycles during which P_M degraded on the average, to 62 percent of initial, with individual values ranging between 53 and 82 percent.

A graph of the P_M', V_{oc}', I_{sc}' and FF' of each of the nine test cells as a function of cycles is presented in Figures 22 to 30. Each graph also shows the P_M' of a matching control cell. All the test-cell data presented in these graphs is tabulated in Table 6. All data have been corrected for temperature variations to correspond to the temperature recorded for each cell during the first cycle.

Cell Number D537D

There is evidence which suggests that part of the loss in P_M was caused by a loss in the light-generated current (I_g). The strongest evidence comes from the behavior of cell D537D, which after 300 cycles, had a P_M', V_{oc}', I_{sc}', and FF' of 82, 102, 82 and 98 percent, respectively. Based on the calculated effects of R_s, R_{sh}, I_g, I_o, and A on the performance of a CdS solar cell, (Figures 16 to 20), the observed power loss in this cell was most likely caused by a 16 percent loss in I_g. Applying a 16 percent decrease in I_g to the mathematical model resulted in P_M', V_{oc}', I_{sc}', and FF' values of 82, 98, 82, and 98, which are close to the experimental values. Changing R_s, R_{sh}, I_o, and A to create the 82 percent experimental value of P_M' resulted in an I_{sc}' of greater than 99 percent, a value far greater than the 82-percent experimental value.

Low light intensity could explain a low value of I_{sc}', hence this possibility was examined carefully. The I_{sc} of the control cells at cycle 300 indicated that the intensity could not have been less than 96 percent of nominal at this time. Since the same solar simulator setting was used for both control cells and test cells, only a darkening of the quartz window could have reduced the illumination at the test cells. This was not so because measurements made before and after the test with a CdS standard cell indicated that the transmission of the quart window did not change by more than one percent. Also, the I_{sc} of one of the silicon reference cells in the chamber did not drop more than one percent below its cycle-1 value at any time during the test.

CELL NUMBER	CELL TEMPERATURE (°C)	CYCLES 1	10	20	30	41	50	60	70	79	90	100	130	161	190	223	257	287	300
		▽1 ▽2 (mW)	RELATIVE MAXIMUM POWER, $P_M/P_M(1)$, (PERCENT)																
D557A	56	145	80	80	58	56	60	63	63	59	58	56	52	53	61	69	59	60	60
D545A	60	148	91	84	73	65	59	65	63	61	60	61	58	57	63	65	65	59	61
D537E	63	98	67	66	64	58	73	55	52	48	48	53	46	48	51	51	47	49	53
D536C	57	209	98	94	75	69	61	65	62	58	65	62	47	61	64	61	59	51	61
D537D	62	122	96	94	95	92	90	86	86	87	82	79	78	75	82	83	78	83	82
D536A	67	204	94	91	72	67	59	60	63	63	56	61	49	56	61	60	51	53	58
D535D	67	189	95	96	85	78	73	73	70	66	64	63	56	86	62	67	64	61	61
D534B	56	162	91	84	64	73	66	74	70	64	59	65	60	60	67	61	63	62	60
D533E	57	152	86	75	68	64	56	69	67	71	65	67	65	61	61	61	57	56	61
		▽1 (V)	RELATIVE OPEN CIRCUIT VOLTAGE, $V_{OC}/V_{OC}(1)$, (PERCENT)																
D557A	56	0.400	98	98	93	94	92	94	95	95	94	93	91	96	96	96	97	98	98
D545A	60	0.395	98	97	92	93	89	95	94	93	94	93	92	92	95	96	95	94	96
D537E	63	0.330	97	94	78	81	79	93	97	97	92	75	96	78	88	85	88	88	94
D536C	57	0.412	100	99	95	94	94	96	93	92	94	94	86	94	95	94	94	90	95
D537D	62	0.405	101	100	100	101	100	102	102	102	100	100	100	99	99	100	100	103	102
D536A	67	0.402	99	100	98	97	94	95	96	96	94	94	94	94	95	95	94	94	96
D535D	67	0.414	100	97	97	96	95	97	96	93	93	93	92	93	96	93	93	93	93
D534B	56	0.400	96	96	88	94	95	96	95	91	92	92	91	91	94	94	95	94	94
D533E	57	0.390	97	97	95	96	94	98	98	99	97	98	98	96	96	98	97	97	97
		▽1 ▽2 (mA)	RELATIVE SHORT CIRCUIT CURRENT, $I_{SC}/I_{SC}(1)$, (PERCENT)																
D557A	56	830	95	94	93	88	89	88	88	87	85	85	83	79	83	83	81	81	81
D545A	60	875	93	91	90	86	86	85	84	82	93	81	81	77	75	78	75	74	75
D537E	63	780	89	80	79	77	78	78	75	75	73	74	72	70	69	72	70	68	70
D536C	57	860	96	94	91	88	86	87	87	85	85	83	80	80	81	80	79	79	78
D537D	62	720	96	94	95	91	90	89	88	88	84	83	82	80	84	82	82	81	82
D536A	67	870	94	93	89	86	84	84	84	84	81	81	79	79	80	78	77	77	76
D535D	67	785	98	98	96	93	92	91	91	90	88	86	85	83	74	87	84	84	84
D534B	56	890	94	93	92	89	88	90	90	87	86	85	84	83	85	82	71	82	81
D533E	57	815	92	90	88	86	85	86	86	85	83	83	81	80	84	79	77	77	75
		▽1 ▽2 (%)	RELATIVE FILL FACTOR, FF/FF(1), (PERCENT)																
D557A	56	43.7	86	87	67	68	73	76	75	79	73	71	69	70	77	87	75	76	76
D545A	60	42.8	100	95	88	81	77	80	80	80	69	81	78	80	88	87	91	85	85
D537E	63	38.1	78	88	104	93	118	76	71	66	71	95	67	88	84	83	76	82	81
D536C	57	59.0	102	101	87	83	75	78	77	74	81	79	68	81	88	81	79	72	82
D537D	62	41.8	99	100	100	100	100	95	96	97	98	95	95	95	99	101	95	99	98
D536A	67	58.3	101	98	83	80	75	75	78	78	74	80	66	76	80	81	70	73	79
D535D	67	58.2	97	101	91	87	84	83	80	79	78	79	72	111	87	83	82	78	78
D534B	56	45.5	101	94	79	87	79	86	82	81	75	83	79	79	84	79	93	80	79
D533E	57	47.8	96	86	83	78	70	82	79	84	81	82	82	79	76	79	76	75	84

▽1 All Cycle-1 data are actual (not relative) values given in the units indicated.

▽2 The actual values are believed to be slightly low because of a fault in the measuring circuit. Since the same circuit was used throughout the test, the relative values presented in this table are believed to be accurate.

TABLE 6: ELECTRICAL PERFORMANCE VS CYCLES FOR CdS SOLAR CELLS MANUFACTURED DURING APRIL, 1967

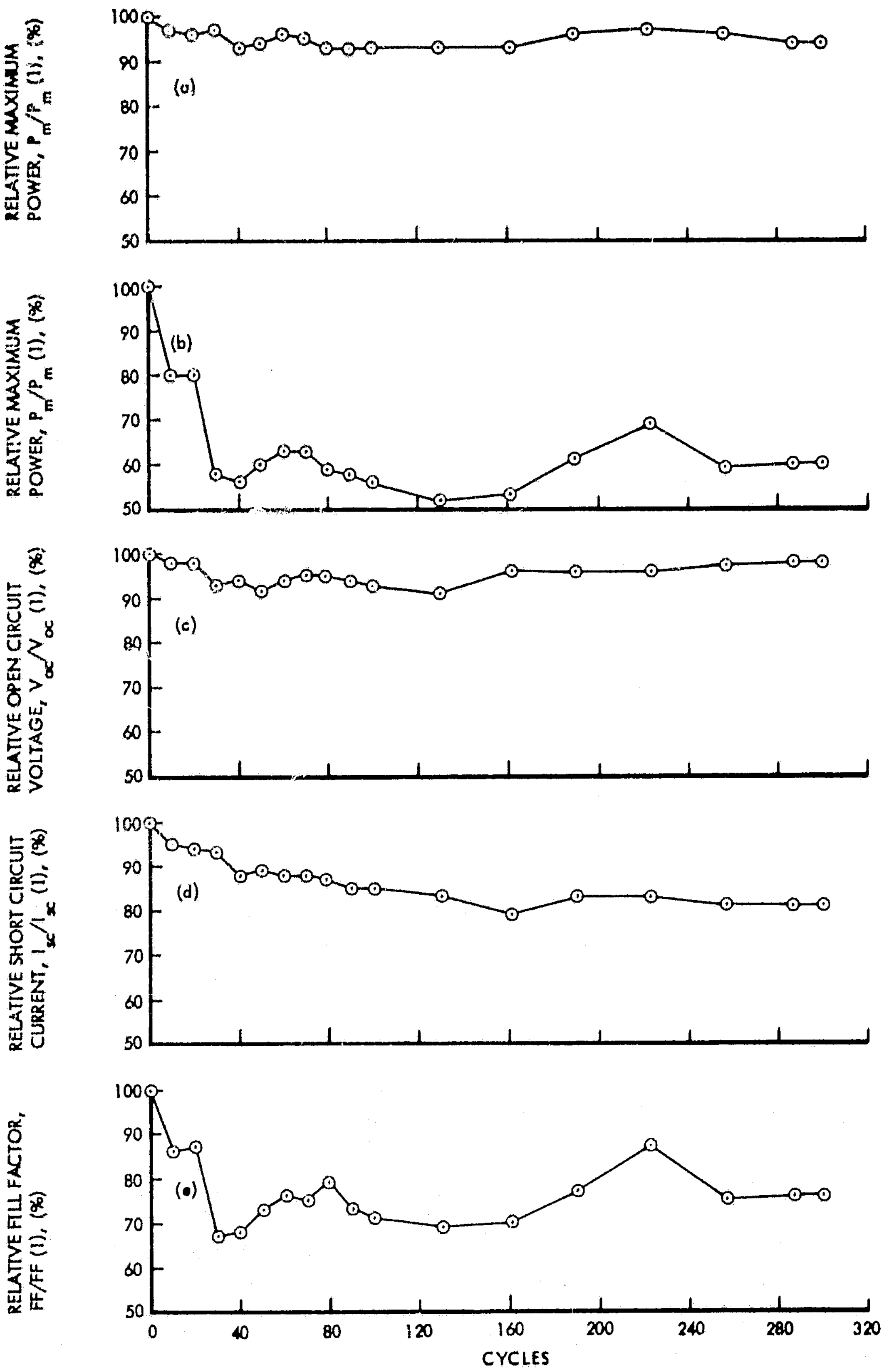

Graph:	(a)	(b), (c), (d), (e)
Test Environment:	Double Desiccated Storage	Space Environment Thermal Cycling
Measurement Condition:	In Air	In Vacuum 6
Cell Temperature:	25°C	56°C
Light Intensity:	140 mW/cm^2	140 mW/cm^2
Cell Number:	D535A	D557A

Figure 22 ELECTRICAL PERFORMANCE VS. CYCLES FOR CdS SOLAR CELLS MANUFACTURED IN APRIL, 1967

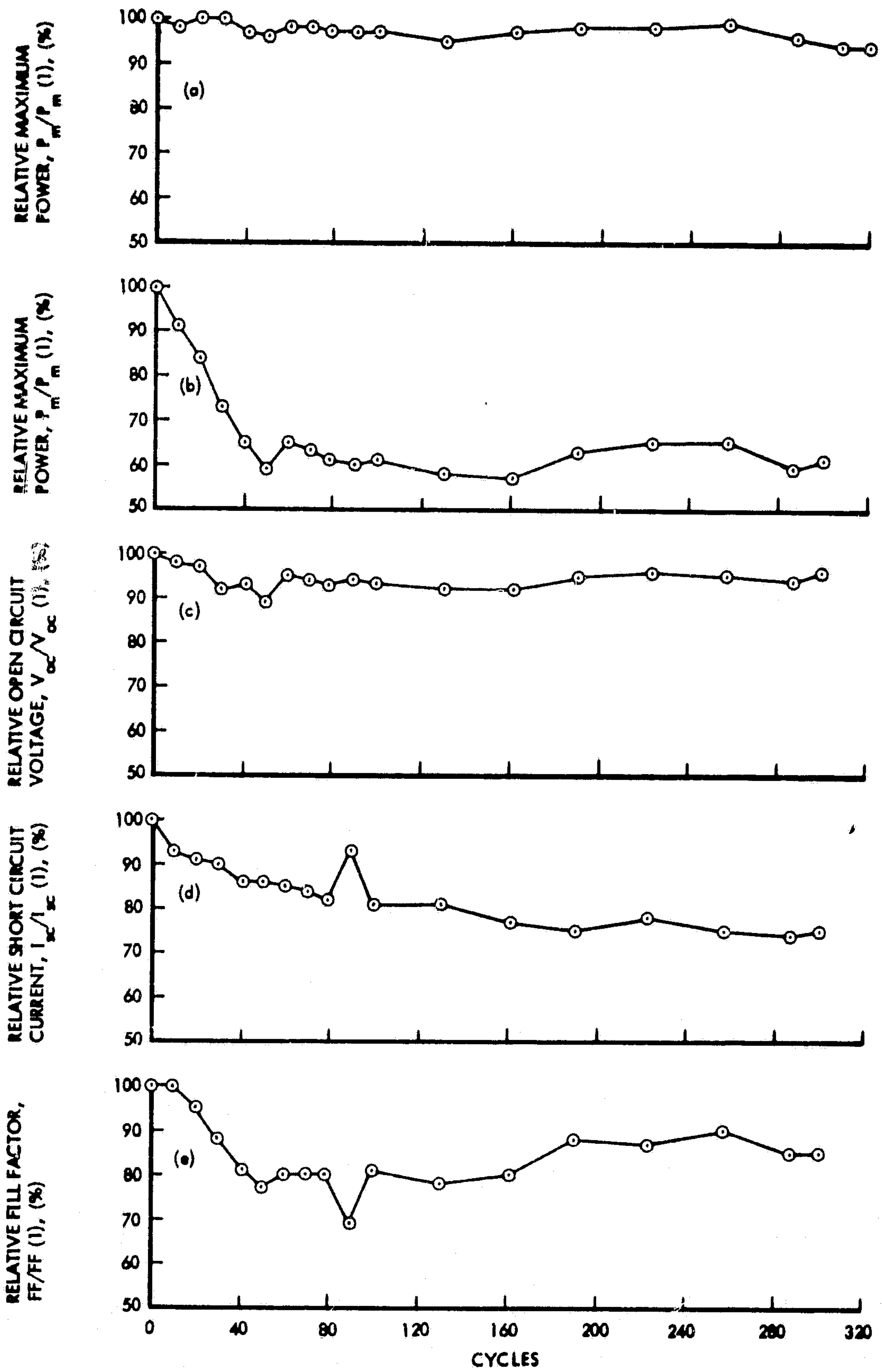

Graph:	(a)	(b), (c), (d), (e)
Test Environment:	Double Desiccated Storage	Space Environment Thermal Cycling
Measurement Condition:	In Air	In Vacuum
Cell Temperature:	25°C	60°C
Light Intensity:	140 mW/cm^2	140 mW/cm^2
Cell Number:	D535E	D545A

Figure 23 ELECTRICAL PERFORMANCE VS. CYCLES FOR CdS SOLAR CELLS MANUFACTURED IN APRIL, 1967

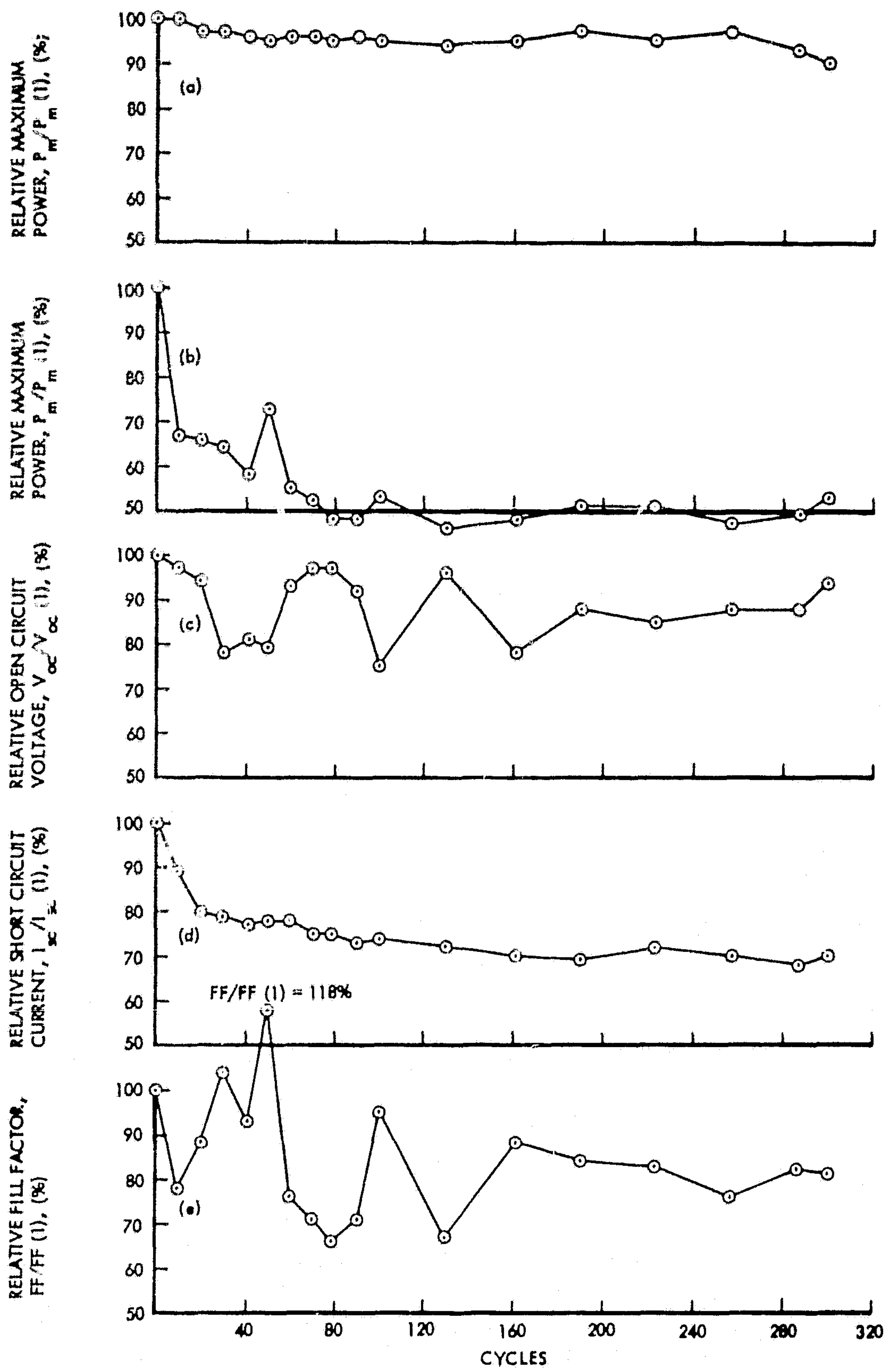

Graph:	(a)	(b), (c), (d), (e)
Test Environment:	Double Desiccated Storage	Space Environment Thermal Cycling
Measurement Condition:	In Air	In Vacuum
Cell Temperature:	25°C	63°C
Light Intensity:	140 mW/cm^2	140 mW/cm^2
Cell Number:	D536D	D537E

Figure 24 ELECTRICAL PERFORMANCE VS. CYCLES FOR CdS SOLAR CELLS MANUFACTURED IN APRIL, 1967

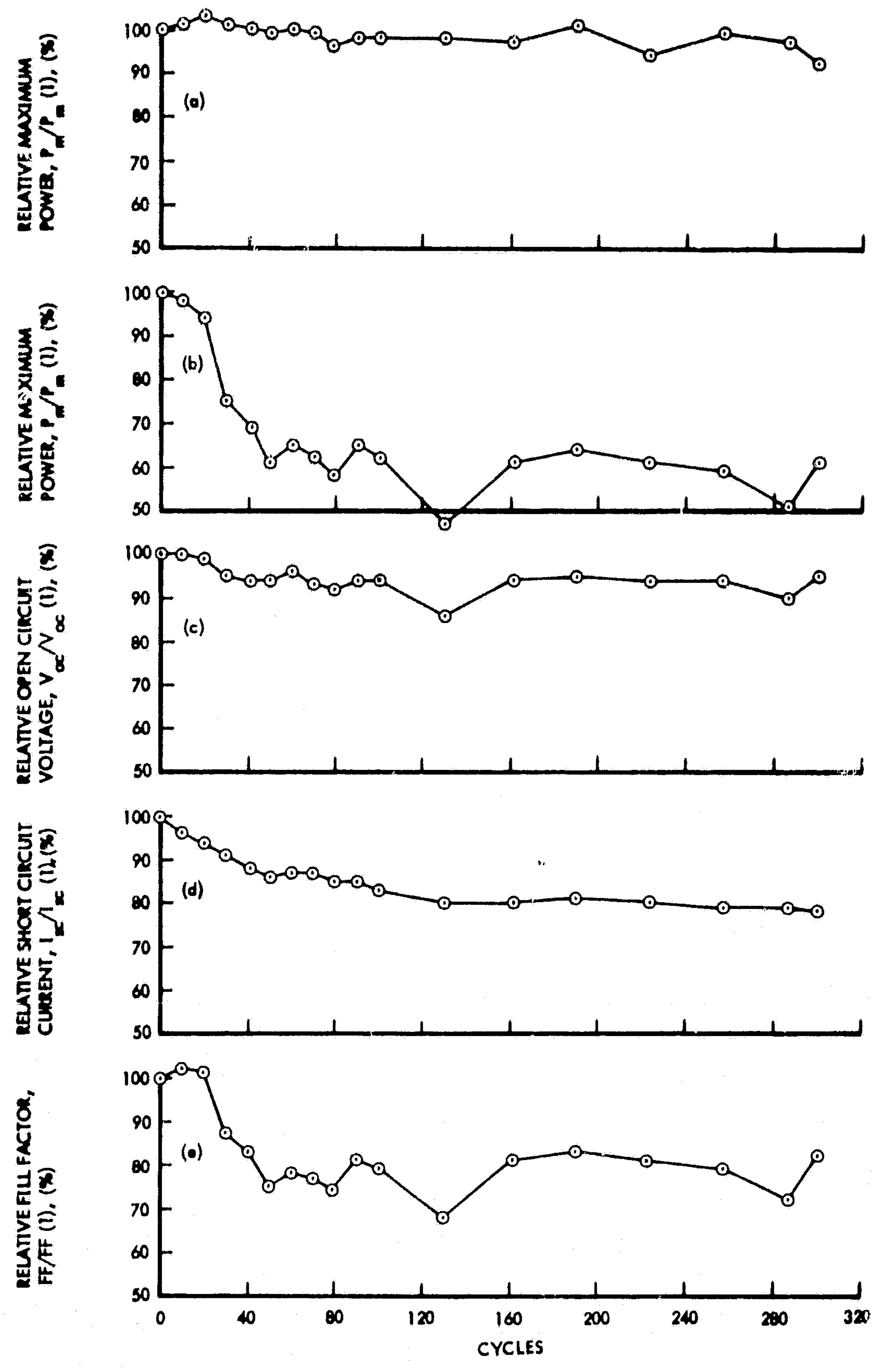

Graph:	(a)	(b), (c), (d), (e)
Test Environment:	Double Desiccated Storage	Space Environment Thermal Cycling
Measurement Condition:	In Air	In Vacuum
Cell Temperature:	25°C	57°C
Light Intensity:	140 mW/cm²	140 mW/cm²
Cell Number:	D536E	D536C

Figure 25 ELECTRICAL PERFORMANCE VS. CYCLES FOR CdS SOLAR CELLS MANUFACTURED IN APRIL, 1967

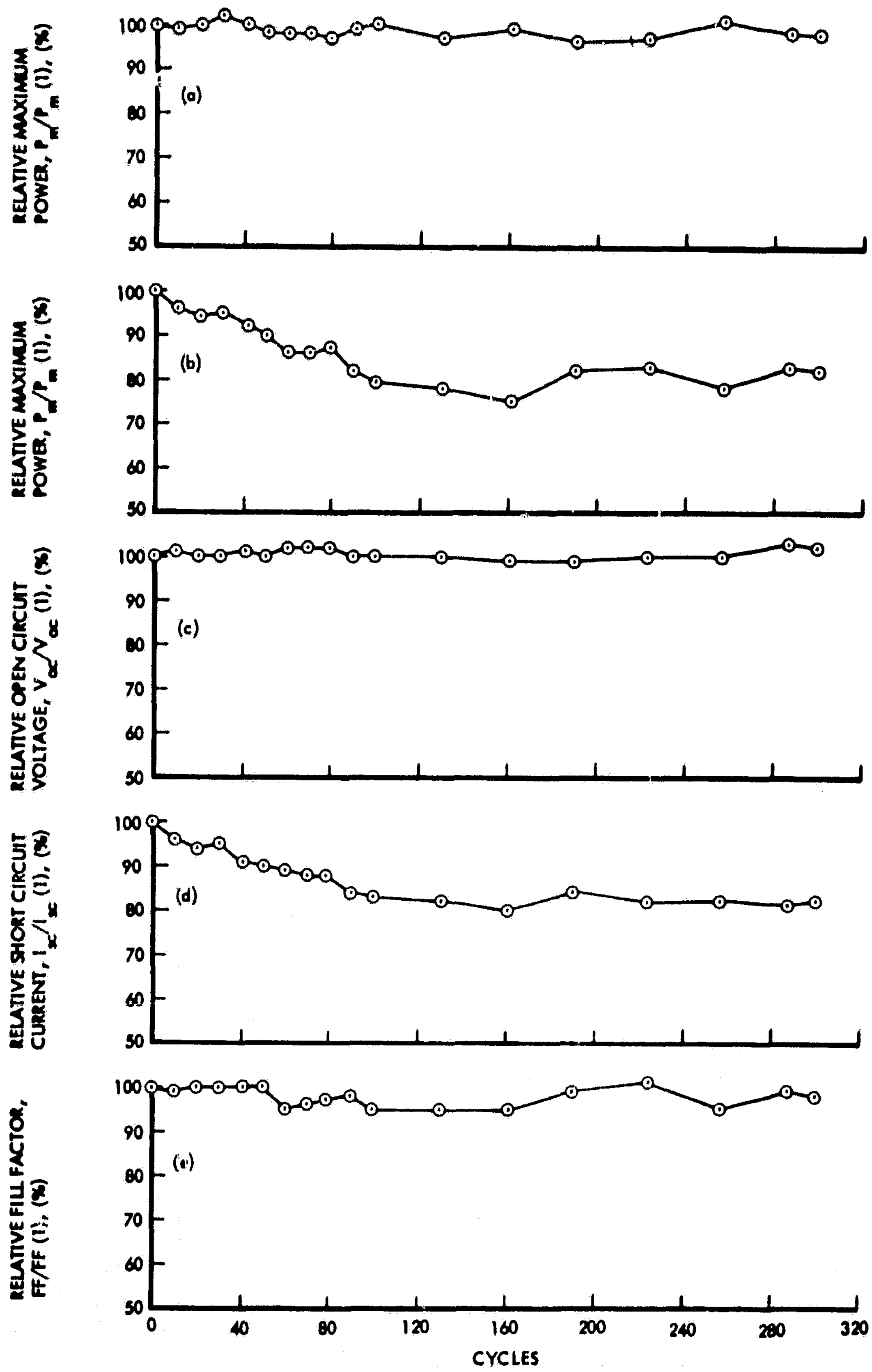

Graph:	(a)	(b), (c), (d), (e)
Test Environment:	Double Desiccated Storage	Space Environment Thermal Cycling
Measurement Condition:	In Air	In Vacuum
Cell Temperature:	25°C	62°C
Light Intensity:	140 mW/cm^2	140 mW/cm^2
Cell Number:	D537E	D537D

Figure 26 ELECTRICAL PERFORMANCE VS. CYCLES FOR CdS SOLAR CELLS MANUFACTURED IN APRIL, 1967

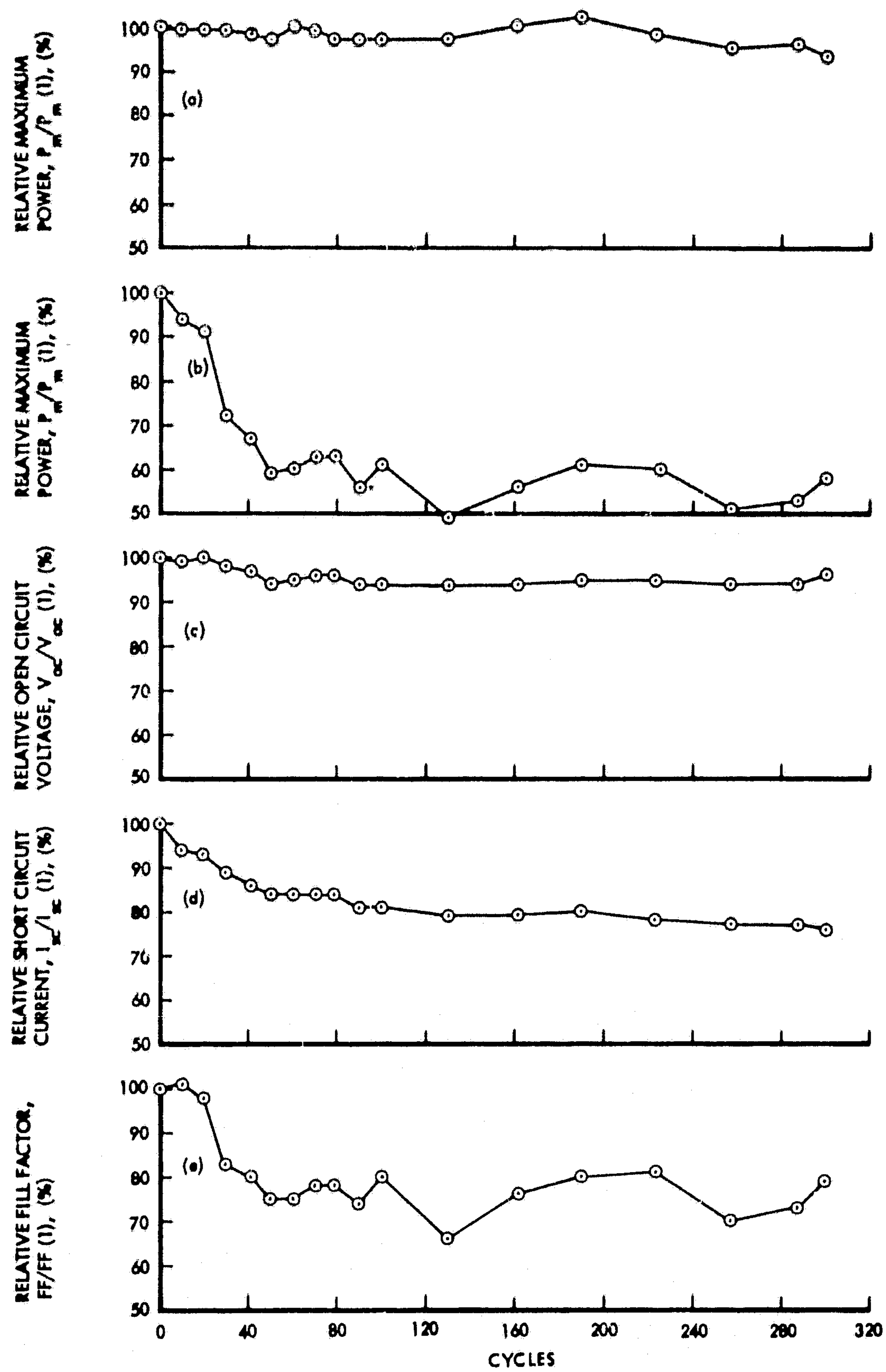

Graph:	(a)	(b), (c), (d), (e)
Test Environment:	Double Desiccated Storage	Space Environment Thermal Cycling
Measurement Condition:	In Air	In Vacuum
Cell Temperature:	25°C	67°C
Light Intensity:	140 mW/cm^2	140 mW/cm^2
Cell Number:	D538D	D536A

Figure 27 ELECTRICAL PERFORMANCE VS. CYCLES FOR CdS SOLAR CELLS MANUFACTURED IN APRIL, 1967

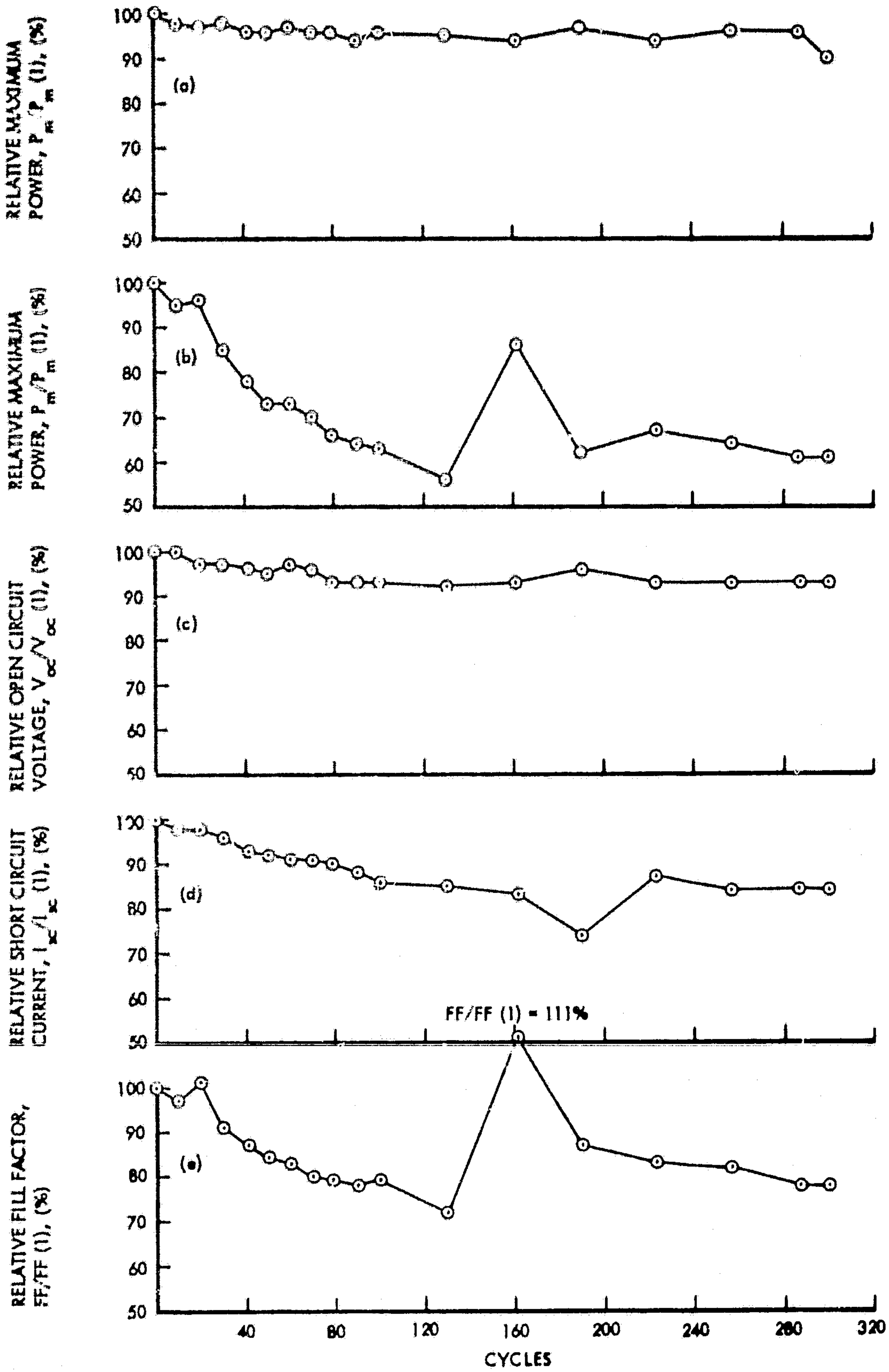

Graph:	(a)	(b), (c), (d), (e)
Test Environment:	Double Desiccated Storage	Space Environment Thermal Cycling
Measurement Condition:	In Air	In Vacuum
Cell Temperature:	25°C	67°C
Light Intensity:	140 mW/cm^2	140 mW/cm^2
Cell Number:	D563E	D535D

Figure 28 ELECTRICAL PERFORMANCE VS. CYCLES FOR CdS SOLAR CELLS MANUFACTURED IN APRIL, 1967

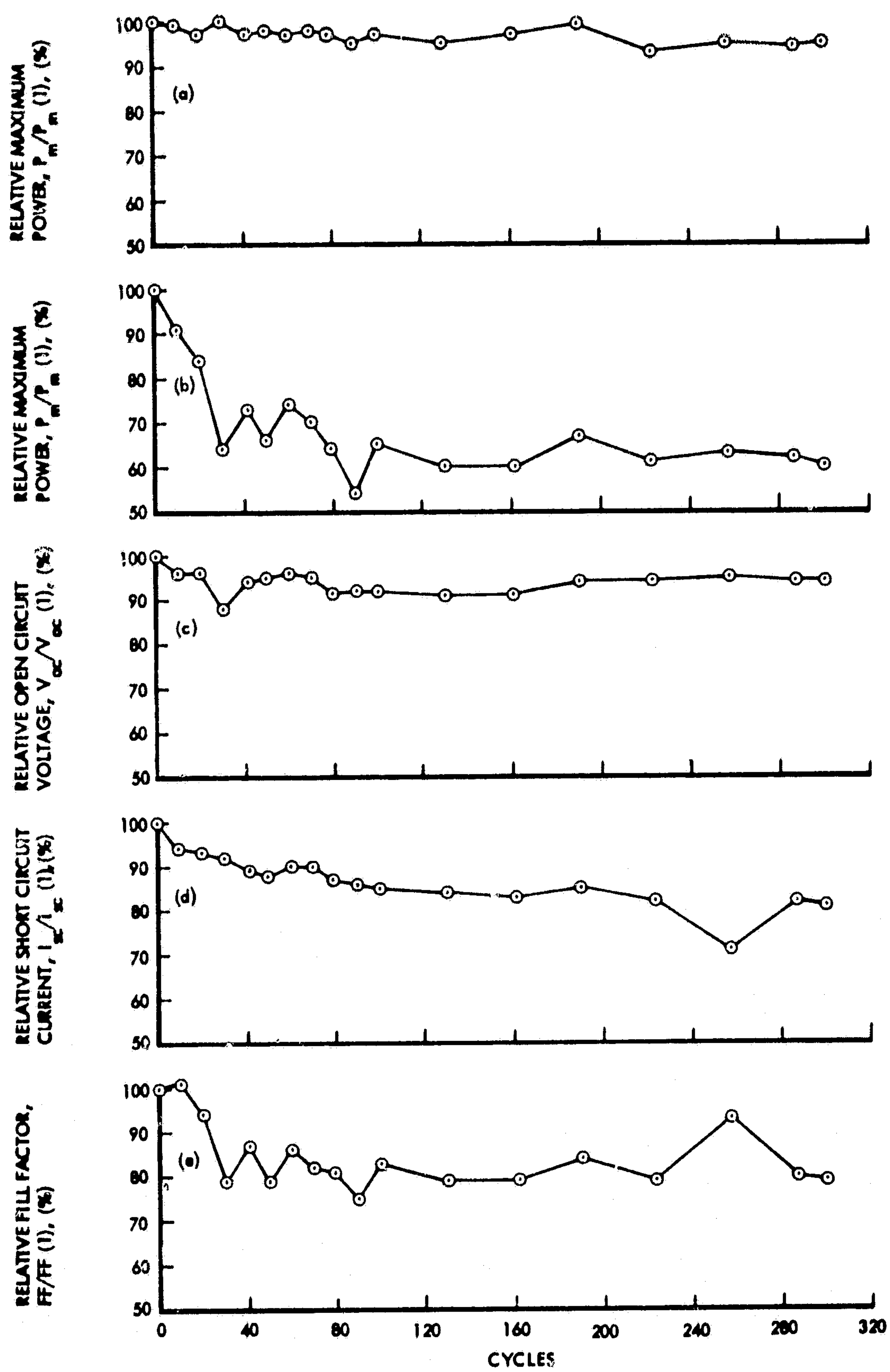

Graph: Test Environment: Measurement Condition: Cell Temperature: Light Intensity: Cell Number:	(a) Double Desiccated Storage In Air 25°C 140 mW/cm^2 D564F	(b), (c), (d), (e) Space Environment Thermal Cycling In Vacuum 56°C 140 mW/cm^2 D534B

Figure 29 ELECTRICAL PERFORMANCE VS. CYCLES FOR CdS SOLAR CELLS MANUFACTURED IN APRIL, 1967

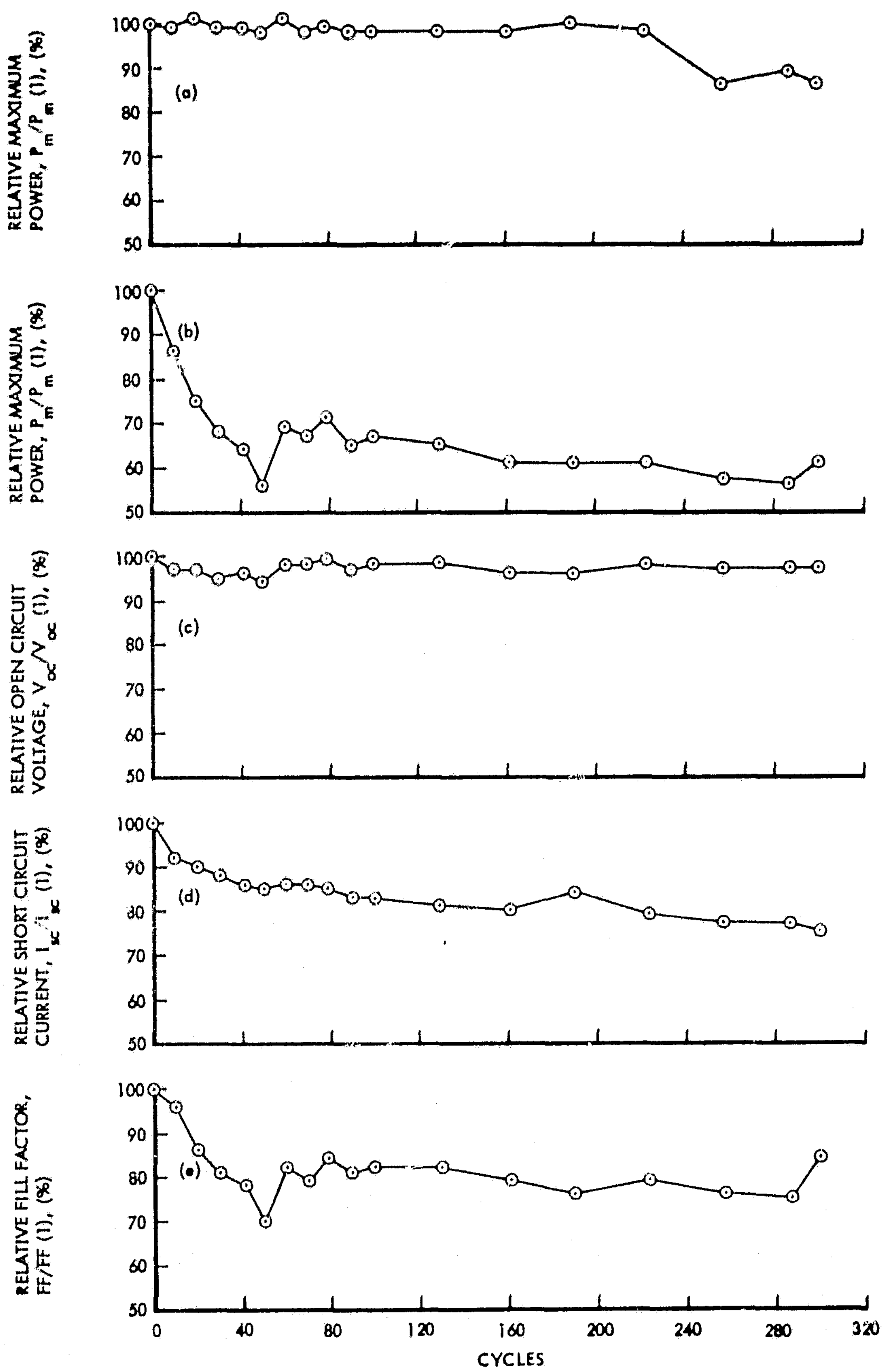

Graph:	(a)	(b), (c), (d), (e)
Test Environment:	Double Desiccated Storage	Space Environment Thermal Cycling
Measurement Condition:	In Air	In Vacuum
Cell Temperature:	25°C	57°C
Light Intensity:	140 mW/cm^2	140 mW/cm^2
Cell Number:	D545E	D533E

Figure 30 ELECTRICAL PERFORMANCE VS. CYCLES FOR CdS SOLAR CELLS MANUFACTURED IN APRIL, 1967

A loss in the I_g of cell D537D may have been caused by a loss in the transmission of its Pyre-ML-coated Mylar cover, especially since it has not been demonstrated conclusively that the Pyre-ML coating protects effectively the Mylar cover from UV radiation. The UV constant of the illumination during the 300 hours of exposure in this test corresponded to about 75 percent of the integrated solar intensity below 0.35 μm. However, other possible causes of the loss in I_g should not be overlooked, since in thermal cycling tests discussed later in this report, where UV-resistant Kapton covers were used, the losses in I_g cannot be readily explained.

Other Cells

After 300 cycles, the average values of P_M', V_{oc}', I_{sc}', and FF' for the remaining eight cells were 59, 95, 78, and 81 percent, respectively. The low average value of I_{sc}' suggests that a decrease in I_g occurred in these cells also. The fact that the FF' was lower than could be explained by a decrease in I_g (see Figure 13) suggests that an additional degrading mechanism was present. Loss in FF' can result from changes in R_s and R_{sh}, but only R_{sh} can explain the low values of V_{oc}' observed in some of the cells. We therefore attribute the power losses in these cells to decreases in both R_{sh} and I_g. Power losses resulting from decreases in R_{sh} probably were caused by internal short circuits in the cell.

In many of the cells, the I-V curve traced in one direction differed from that traced in the other direction (Figures 31a and 31b). This behavior is called hysteresis. Occasionally a cell would exhibit an erratic I-V curve (Figure 31c) which could not be repeated in successive traces. The fact that the hysteresis affected V_{oc}' but not I_{sc}' suggests that the effective shunt resistance varied. Short circuits within a cell are one possible cause of change in effective shunt resistance. The type of hysteresis shown in Figure 31a is roughly what would be expected if a partial short circuit existed in the cell during the

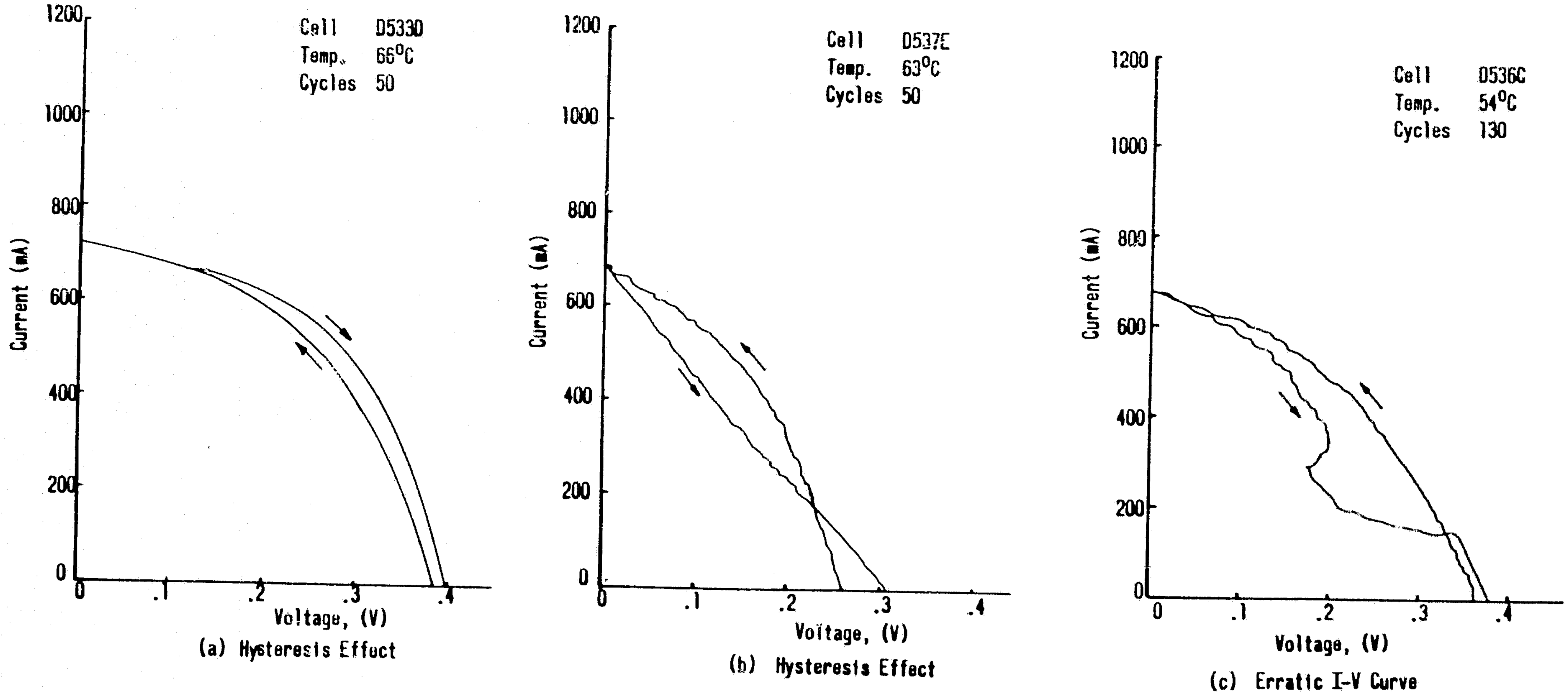

FIGURE 31. DEGRADED I-V CURVES OF APRIL, 1967 CdS SOLAR CELLS

trace from I_{sc} to V_{oc}.

The type of hysteresis shown in Figure 31b is more difficult to interpret. One possibility is that the partial short circuit existing in the cell during the trace from V_{oc} to I_{sc} became even worse when the return trace was started, producing a straight line characteristic. To explain why the return trace ended at a V_{oc} higher than the V_{oc} at the beginning of the first trace, it must be assumed that the short circuit gradually weakened during the latter part of the return trace, completely disappearing by the time the trace was finished. The type of behavior exhibited in Figure 31c can be explained in a similar manner except that perhaps several partial short circuits were involved, one of which did not appear until the latter part of the return trace. The fact that precisely the same curve could not be obtained in successive traces suggests that the shorts appeared intermittently.

Summary of Testing of April, 1967 Cells

The April, 1967 cells degraded quite drastically within 300 cycles. The probable cause of power degradation was a decrease in shunt resistance resulting from internal shorts. A loss in light-generated current, possibly from a degradation of the Pyre-ML-coated Mylar covers, also contributed significantly to the power loss.

6.3.2 November, 1967 Cells

The test-cells manufactured in November, 1967 were subjected to 506 light-dark cycles. The P_M of the two copper-substrate cells had degraded to 77 and 25 percent of initial, respectively, after 506 cycles. During the same time, the P_M' of the seven Kapton-substrate cells had dropped, on the average, to 82 percent, the individual values ranging between 75 and 88 percent.

The P_M', V_{oc}', I_{sc}', and FF' of each of the nine test cells are plotted as a function of cycles in Figures 32 to 40. Each graph also shows the P_M' of a matching control cell. All the test-cell data are also presented in Table 7. These data have been corrected for temperature variations to correspond to 60°C. All test-cell data were obtained with the test-cells mounted in the vacuum chamber, under vacuum, after the cells had been illuminated for about one hour.

Performance data were also obtained for these cells in air, before and after cycling, with the cells mounted on a temperature controlled block maintained at 60°C. These data are presented in Table 8.

6.3.2.1 Kapton Substrate Cells

Cell Number NH200AK3

The most stable cell in the group was number NH200AK3. After 506 cycles, its P_M', V_{oc}', I_{sc}', and FF', were 88, 100, 100, and 88 percent, respectively. Based on the calculated effects of R_s, R_{sh}, I_g, I_o, and A on the performance of a typical cell (Figures 16 to 20), the observed power loss was most likely the result of a 0.054-ohm increase in R_s. These are the reasons:

(1) a 0.054-ohm increase in R_s resulted in calculated P_M' V_{oc}', I_{sc}', and FF' values of 88, 100, 100, and 88 percent which were the same as the experimental values.

(2) Values, R_{sh}, I_g, I_o, or A from which the experimental 88 percent P_M' could be calculated, resulted in a V_{oc}' or an I_{sc}' significantly less than the experimental values.

(3) Furthermore, the R_{oc} obtained from the I-V curves at cycle-1 and cycle 506 was 0.05-ohms and 0.012 ohms respectively. According to Figure 21 this corresponds to a 0.045-ohm increase in R_s, in good agreement with the preceding observations.

Measurements made on this cell in air, before and after cycling, (Table 8), resulted in P_M', V_{oc}', I_{sc}', and FF' values of 94, 101, 100 and 92 percent, indicating that both P_M' and FF' recovered during the period between cycle 506 and removal of the cells from the chamber. Recovery was probably accompanied by a decrease in series resistance.

Table 7: ELECTRICAL PERFORMANCE VS CYCLING FOR CdS SOLAR CELLS MANUFACTURED IN NOVEMBER 1967

CELL NUMBER	CYCLES																									
	1	15	23	32	38	48	62	75	89	99	129	142	157	200	208	221	222	251	286	287	352	397	443	444	505	506
ACTUAL CONVERSION EFFICIENCY, η, (PERCENT)	▽ (%)																									
A970B	4.29	4.10	4.07	3.92	3.98	3.84	3.86	3.78	3.68	3.68	3.51	3.69	3.63	3.01	3.55	3.56	3.51	3.46	3.52	3.41	3.83	3.30	3.39	3.38	3.26	3.29
A969D	4.28	2.76	2.83	2.91	2.95	2.69	2.91	3.23	3.00	3.02	2.94	3.00	2.73	2.44	2.23	0.88	0.87	0.85	0.86	0.88	0.94	1.07	1.08	1.05	1.07	1.07
NH188AK2	2.59	2.46	2.44	2.37	2.31	2.35	2.28	2.21	1.99	2.17	2.19	2.16	2.13	2.13	2.11	2.15	2.13	2.00	2.07	2.08	2.07	2.07	2.02	2.05	1.93	1.94
NH200AK3	2.73	2.52	2.44	2.42	2.38	2.41	2.38	2.41	2.39	2.35	2.31	2.33	2.35	2.42	2.38	2.33	2.37	2.39	2.42	2.38	2.41	2.42	2.42	2.43	2.37	2.41
N89CK7	2.28	1.85	1.39	2.08	2.09	1.99	1.86	1.98	2.05	2.00	1.86	1.95	1.95	1.86	1.87	1.86	1.94	1.90	1.90	1.87	1.87	1.85	1.87	1.74	1.79	1.78
N90AK5	3.26	3.15	3.12	3.06	3.00	3.02	2.94	2.90	2.93	2.87	2.81	2.83	2.90	2.80	2.83	2.76	2.80	2.77	2.72	2.78	2.74	2.70	2.70	2.73	2.67	2.69
N90BK4	3.04	2.86	2.85	2.74	2.76	2.72	2.76	2.74	2.73	2.68	2.70	2.61	2.78	2.65	2.63	2.51	2.55	2.54	2.65	2.63	2.60	2.55	2.57	2.63	2.50	2.56
N90AK1	3.21	3.00	2.99	2.91	2.91	2.93	2.93	2.93	2.93	2.87	2.83	2.85	2.94	2.86	2.82	2.81	2.82	2.78	2.91	2.85	2.80	2.77	2.77	2.80	2.80	2.73
N90AK9	2.91	2.77	2.73	2.70	2.68	2.67	2.61	2.65	2.69	2.61	2.57	2.60	2.64	2.57	2.59	2.57	2.64	2.55	2.56	2.57	2.55	2.50	2.46	2.48	2.43	2.47
RELATIVE MAXIMUM POWER, P_M/P_M (1), (PERCENT)	▽ (mW)																									
A970B	330	95	95	93	93	89	90	88	86	86	82	86	85	84	83	83	82	81	82	79	79	77	79	79	76	77
A969D	329	64	66	68	69	63	68	77	70	71	69	70	64	57	52	21	20	20	20	21	22	25	25	25	25	25
NH188AK2	199	95	94	91	89	91	88	85	77	84	83	83	82	82	81	83	82	77	80	80	80	80	78	79	77	75
NH200AK3	210	92	90	89	87	88	87	88	88	86	85	85	86	89	87	85	87	88	89	87	88	89	89	89	87	88
N89CK7	175	81	90	91	92	87	82	87	90	88	82	86	86	82	83	83	85	83	83	83	83	81	83	77	79	78
N90AK5	251	96	96	94	92	92	90	89	90	88	86	87	89	86	87	84	86	85	83	85	84	83	83	84	82	83
N90BK4	234	94	94	90	91	91	89	91	90	90	88	89	86	91	87	86	82	84	83	87	86	85	84	85	86	82
N90AK1	247	94	93	91	91	91	91	91	91	89	88	89	91	89	88	87	88	87	91	89	87	86	86	87	87	85
N90AK9	224	95	94	93	92	92	90	91	92	90	88	89	91	88	89	88	91	87	88	88	87	86	84	85	83	85
RELATIVE OPEN CIRCUIT VOLTAGE, V_{OC}/V_{OC} (1), (PERCENT)	▽ (V)																									
A970B	.443	102	102	103	103	102	102	102	102	102	101	102	101	102	101	101	101	102	104	101	102	102	103	103	103	102
A969D	.453	96	96	97	98	94	97	98	98	97	97	97	95	95	92	39	39	38	41	41	47	58	62	56	59	60
NH188AK2	.426	101	100	100	100	101	100	100	96	99	100	99	100	101	100	100	101	99	101	101	102	102	102	106	102	101
NH200AK3	.415	99	100	100	99	99	99	98	99	99	98	98	99	101	100	99	99	100	100	99	100	100	100	101	100	100
N89CK7	.424	97	98	99	99	97	97	97	99	98	97	97	95	96	[illegible]	97	97	97	99	97	97	97	99	97	98	97
N90AK5	.416	101	102	101	101	100	100	100	100	100	100	99	99	101	101	101	101	101	102	101	104	103	103	103	103	103
N90BK4	.419	99	99	98	98	98	99	98	98	98	98	97	98	98	98	98	98	98	99	98	99	99	99	100	99	98
N90AK1	.421	100	101	99	100	100	101	101	100	100	101	100	100	102	101	101	100	101	103	102	102	102	102	102	102	102
N90AK9	.420	100	100	101	101	101	101	101	101	100	100	100	100	102	101	101	102	101	102	101	103	102	102	101	102	101
RELATIVE SHORT CIRCUIT CURRENT, I_{SC}/I_{SC} (1), (PERCENT)	▽ (mA)																									
A970B	1005	93	93	91	90	89	88	87	86	87	84	87	87	85	85	85	84	83	82	84	83	81	82	83	81	81
A969D	1075	97	96	93	93	92	91	90	89	90	87	89	89	86	86	83	83	81	81	82	82	81	83	82	81	81
NH188AK2	760	100	100	98	97	96	97	96	95	93	94	93	93	91	93	94	94	92	91	92	92	91	91	91	90	90
NH200AK3	750	101	99	99	99	98	99	99	99	99	98	98	100	98	98	97	99	99	99	99	100	100	101	101	100	100
N89CK7	760	100	99	97	97	97	96	96	97	97	94	94	95	92	92	92	94	92	92	92	92	91	92	92	91	91
N90AK5	945	98	97	96	96	97	95	94	95	95	93	93	92	90	92	91	92	90	89	91	91	90	92	91	80	90
N90BK4	838	98	97	96	97	94	96	96	97	96	95	93	96	94	92	89	91	90	94	93	93	91	92	91	91	93
N90AK1	900	96	95	94	94	94	94	94	95	94	92	93	93	90	93	92	93	92	93	93	92	91	92	93	94	91
N90AK9	817	97	97	95	94	94	93	94	94	94	92	93	94	92	93	92	93	91	91	92	92	91	91	92	90	92
RELATIVE FILL FACTOR, FF/FF(1), (PERCENT)	▽ (%)																									
A970B	68.0	100	100	100	100	99	100	100	98	97	98	98	96	97	96	97	96	94	97	94	94	93	94	93	93	93
A969D	67.5	69	71	75	76	72	76	85	80	80	81	81	75	69	65	63	63	63	60	60	56	53	49	53	51	51
NH188AK2	61.5	95	95	93	93	95	92	90	84	92	89	92	89	90	89	89	87	85	87	87	85	87	85	84	84	84
NH200AK3	67.5	93	91	91	89	91	90	91	90	88	88	90	88	91	90	88	88	90	90	88	88	90	88	88	88	88
N89CK7	54.3	83	93	94	96	93	87	93	94	93	89	94	94	93	91	91	93	93	93	91	91	91	91	85	89	89
N90AK5	63.8	97	97	97	95	94	94	94	94	92	92	94	97	94	94	91	92	92	92	92	89	89	88	89	89	89
N90BK4	66.7	96	97	96	96	96	96	96	94	93	96	94	97	94	96	94	94	94	94	94	93	93	93	94	91	91
N90AK1	65.2	97	97	97	97	97	97	97	95	95	95	95	98	97	94	94	94	94	95	94	92	92	92	92	91	92
N90AK9	65.3	98	97	97	97	95	95	97	97	95	97	97	97	95	95	95	97	95	95	95	94	92	91	92	92	92

All Cycle-1 data are actual (not relative) values given in indicated units.

Test Environment: Space Environment Thermal Cycling
Measurement Condition: In Vacuum
Cell Temperature: 60°C
Light Intensity: 140mw/cm^2, AMO

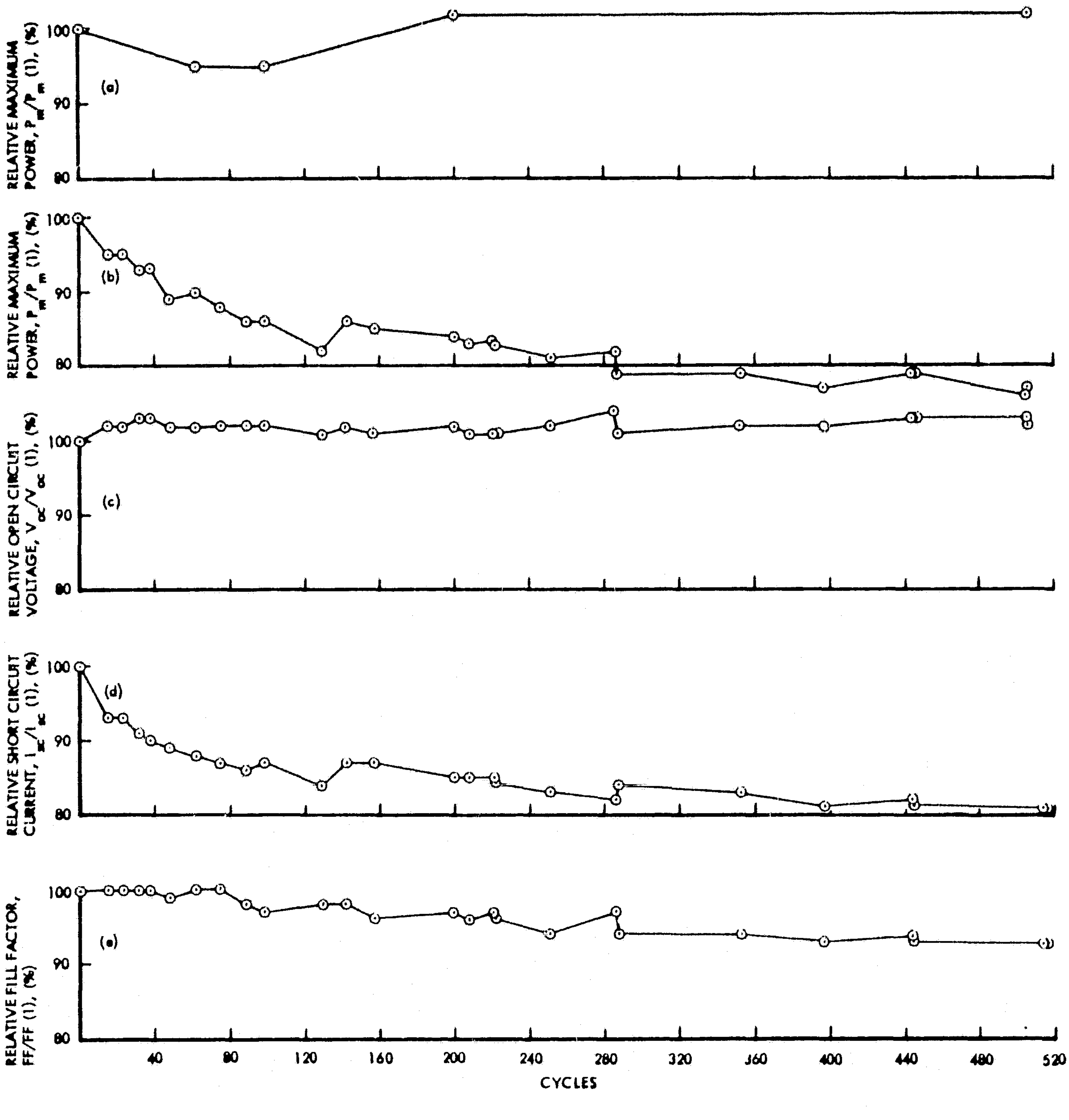

Graph:	(a)	(b), (c), (d), (e)
Test Environment:	Double Desiccated Storage	Space Environment Thermal Cycling
Measurement Condition:	In Air	In Vacuum
Cell Temperature:	25°C	60°C
Light Intensity:	140 mW/cm^2	140 mW/cm^2
Cell Number:	A970C	A970B

Figure 32 ELECTRICAL PERFORMANCE VS CYCLES FOR CdS SOLAR CELLS MANUFACTURED IN NOVEMBER, 1967

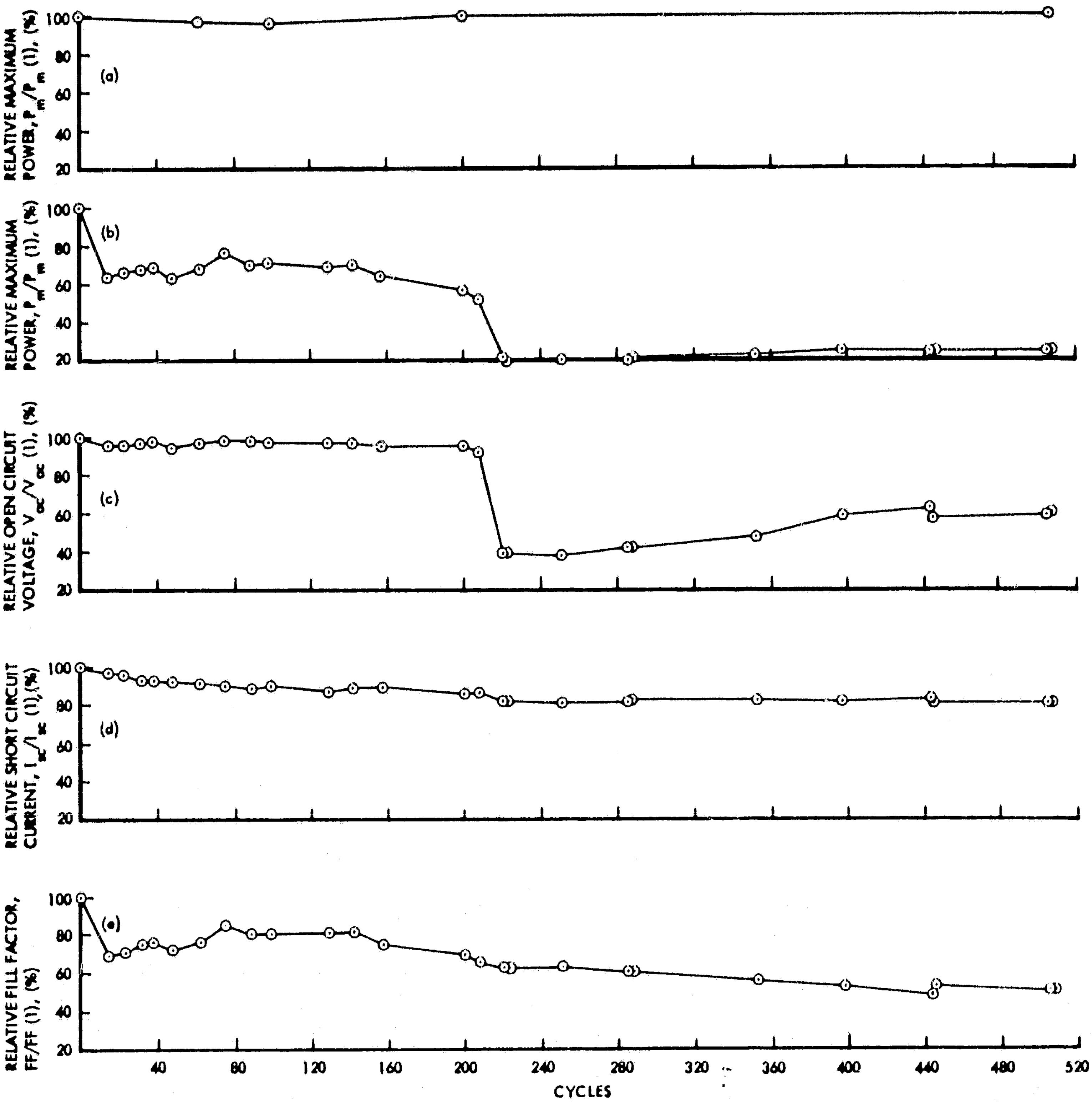

Note the reduced scales in all performance parameters.

Graph:	(a)	(b), (c), (d), (e)
Test Environment:	Double Desiccated Storage	Space Environment Thermal Cycling
Measurement Condition:	In Air	In Vacuum
Cell Temperature:	25°C	60°C
Light Intensity:	140 mW/cm^2	140 mW/cm^2
Cell Number:	A970A	A969D

Figure 33 ELECTRICAL PERFORMANCE VS CYCLES FOR CdS SOLAR CELLS MANUFACTURED IN NOVEMBER, 1967

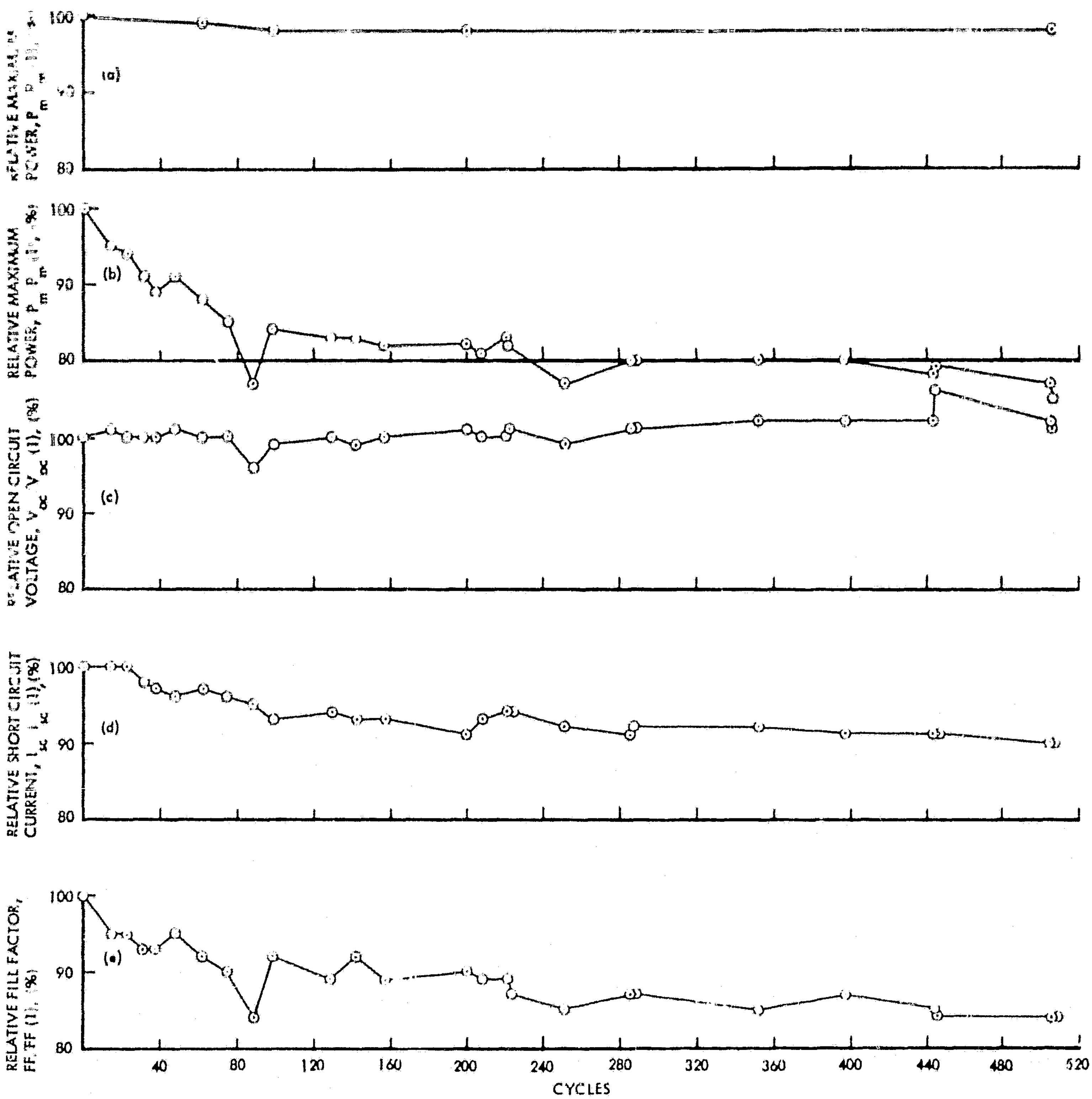

Graph,	(a)	(b), (c), (d), (e)
Test Environment;	Double Desiccated Storage	Space Environment Thermal Cycling
Measurement Condition;	In Air	In Vacuum
Cell Temperature;	25°C	60°C
Light Intensity;	140 mW/cm^2	140 mW/cm^2
Cell Number;	A89BK5	NH188AK2

Figure 34 ELECTRICAL PERFORMANCE VS CYCLES FOR CdS SOLAR CELLS MANUFACTURED IN NOVEMBER, 1967

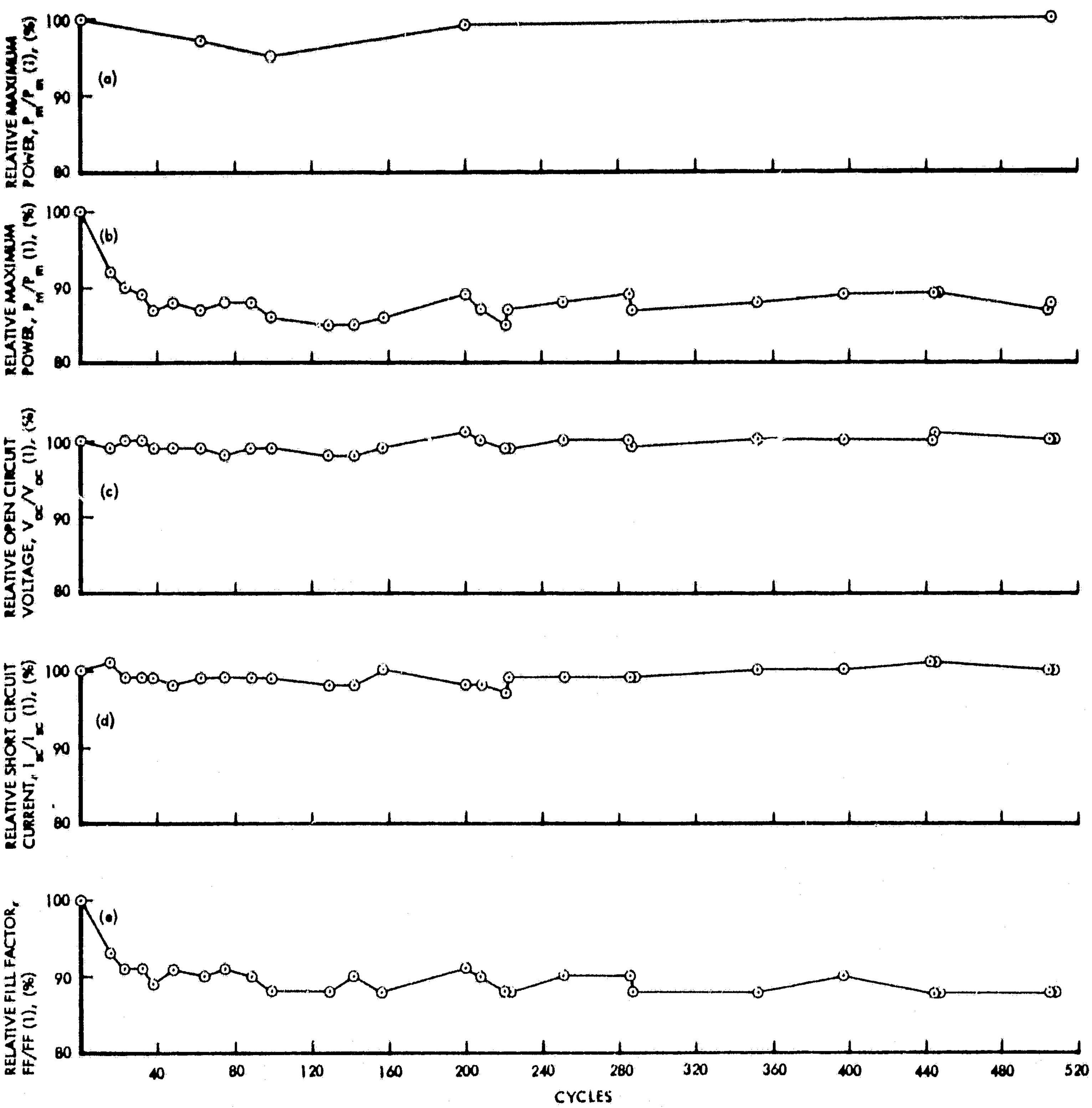

Graph:	(a)	(b), (c), (d), (e)
Test Environment:	Double Desiccated Storage	Space Environment Thermal Cycling
Measurement Condition:	In Air	In Vacuum
Cell Temperature:	25°C	60°C
Light Intensity:	140 mW/cm^2	140 mW/cm^2
Cell Number:	N90BK1	NH200AK3

Figure 35 ELECTRICAL PERFORMANCE VS CYCLES FOR CdS SOLAR CELLS MANUFACTURED IN NOVEMBER, 1967

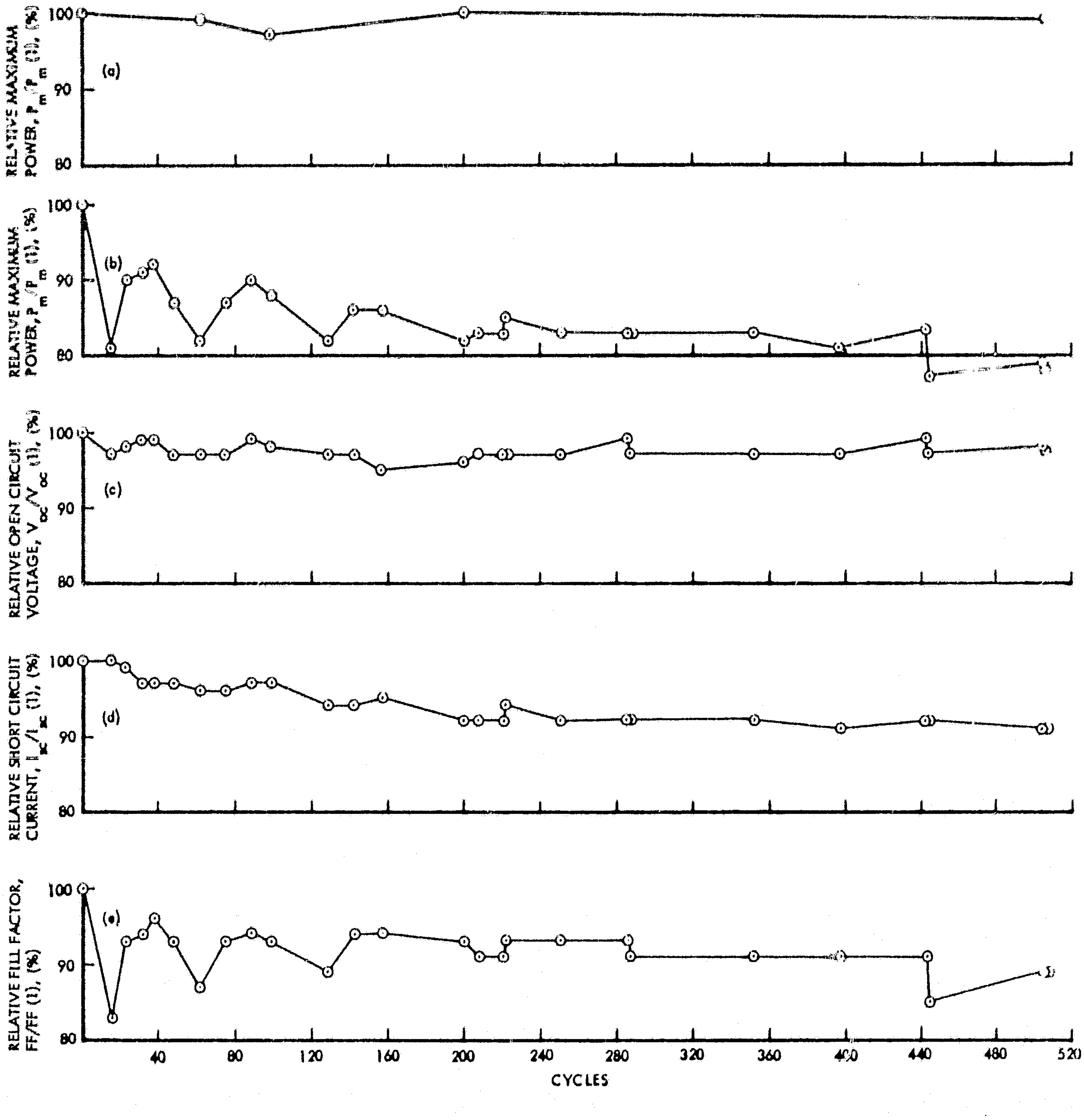

Graph:	(a)	(b), (c), (d), (e)
Test Environment:	Double Desiccated Storage	Space Environment Thermal Cycling
Measurement Condition:	In Air	In Vacuum
Cell Temperature:	25°C	60°C
Light Intensity:	140 mW/cm^2	140 mW/cm^2
Cell Number:	N90AK6	N89CK7

Figure 36 ELECTRICAL PERFORMANCE VS CYCLES FOR CdS SOLAR CELLS MANUFACTURED IN NOVEMBER, 1967

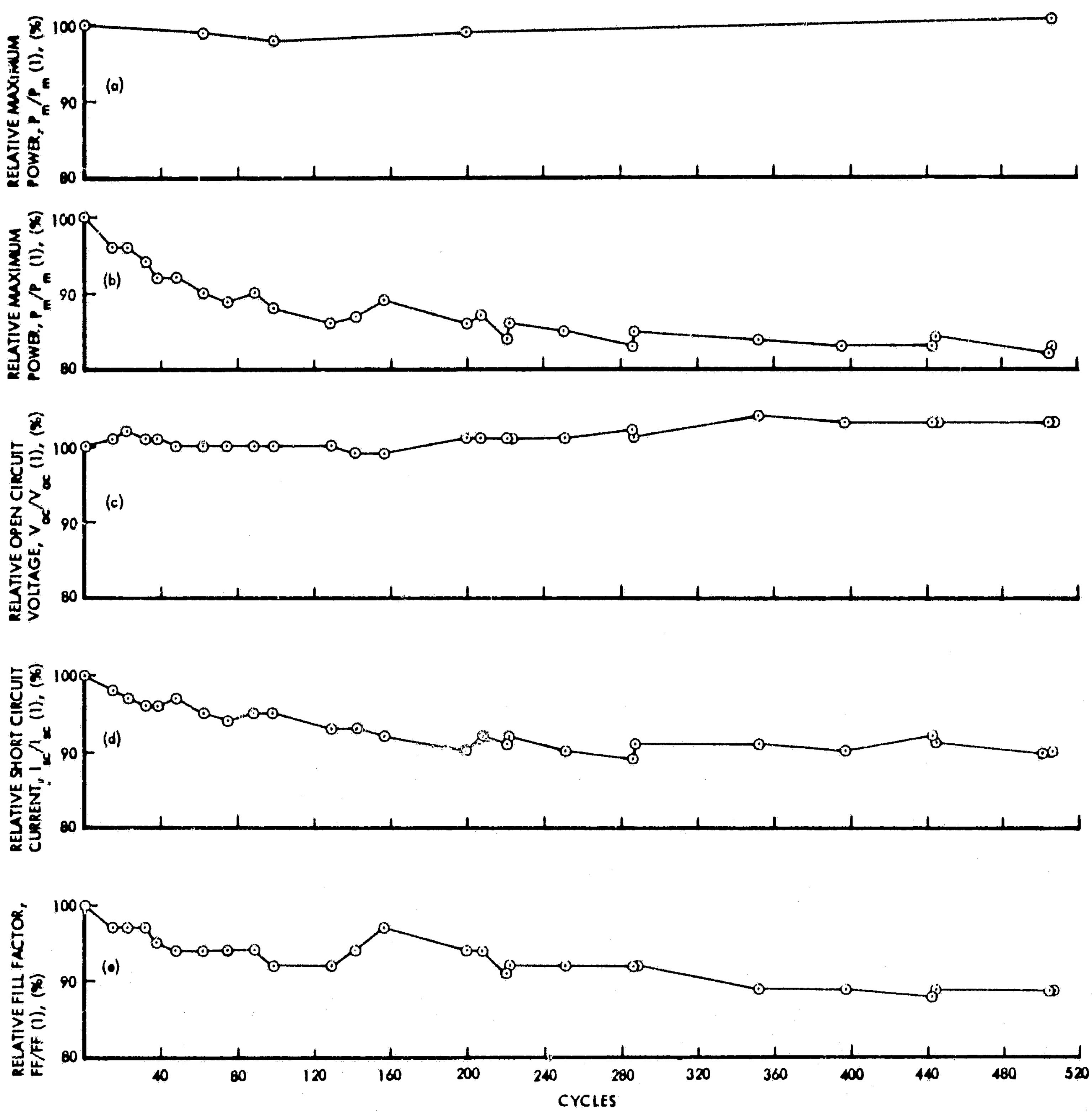

Graph:	(a)	(b), (c), (d), (e)
Test Environment:	Double Desiccated Storage	Space Environment Thermal Cycling
Measurement Condition:	In Air	In Vacuum
Cell Temperature:	25°C	60°C
Light Intensity:	140 mW/cm^2	140 mW/cm^2
Cell Number:	NH186CK6	N90AK5

Figure 37 ELECTRICAL PERFORMANCE VS CYCLES FOR CdS SOLAR CELLS MANUFACTURED IN NOVEMBER, 1967

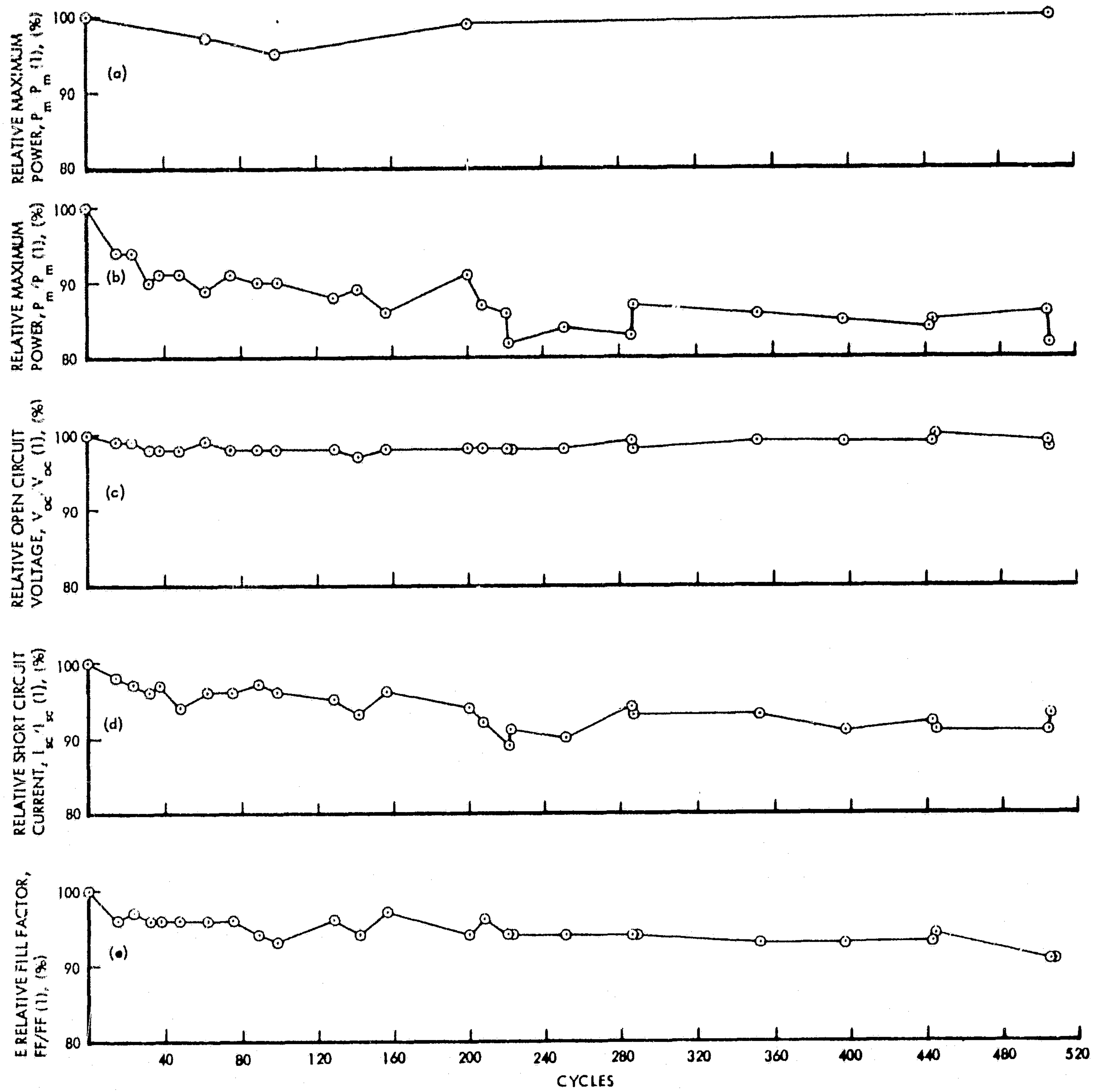

Graph:	(a)	(b), (c), (d), (e)
Test Environment:	Double Desiccated Storage	Space Environment Thermal Cycling
Measurement Condition:	In Air	In Vacuum
Cell Temperature:	25°C	60°C
Light Intensity:	140 mW/cm^2	140 mW/cm^2
Cell Number:	N89CK2	N90BK4

Figure 38 ELECTRICAL PERFORMANCE VS CYCLES FOR CdS SOLAR CELLS MANUFACTURED IN NOVEMBER, 1967

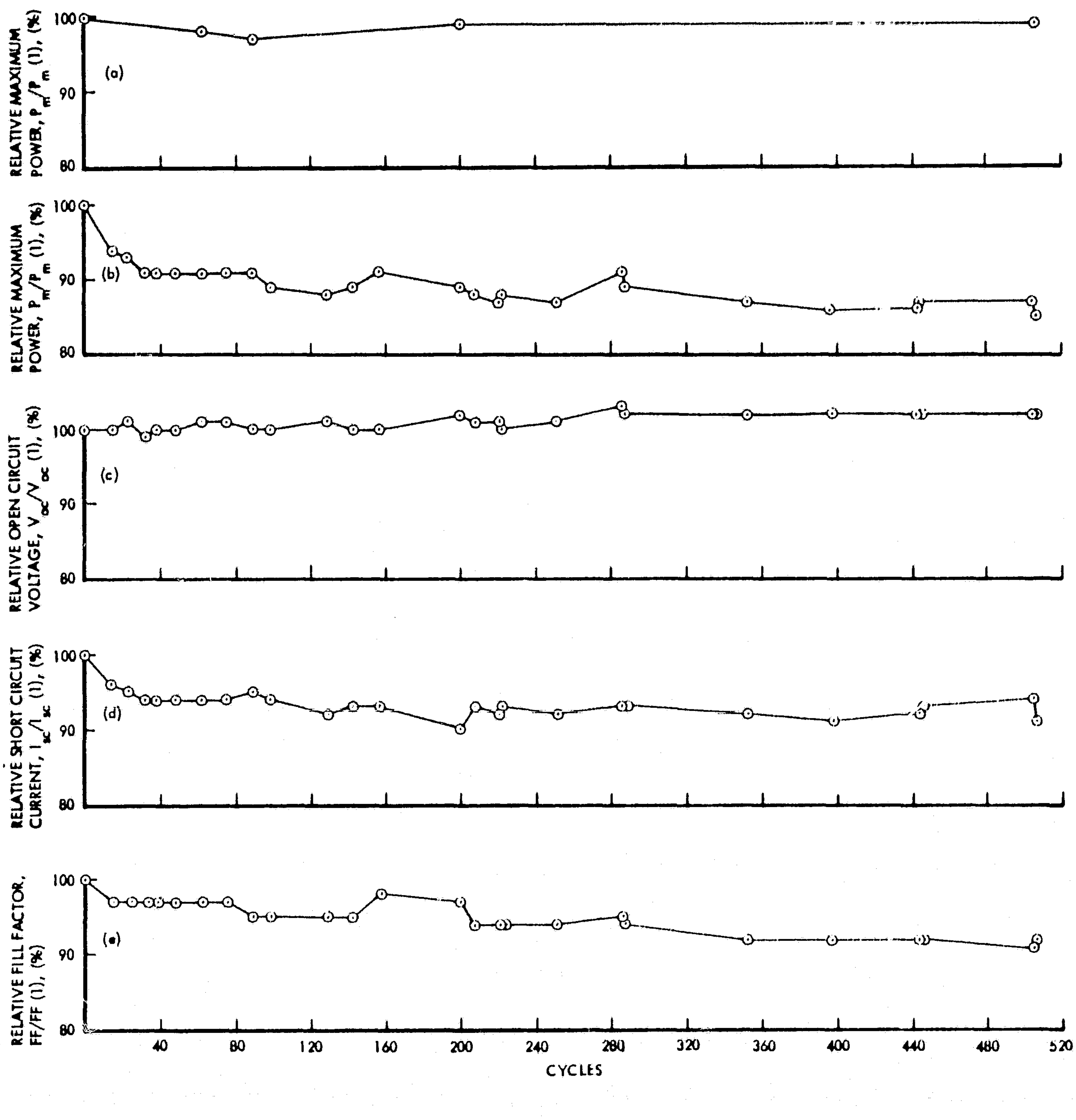

Graph: Test Environment: Measurement Condition: Cell Temperature: Light Intensity: Cell Number:	(a) Double Desiccated Storage In Air 25°C 140 mW/cm^2 N89CK6	(b), (c), (d), (e) Space Environment Thermal Cycling In Vacuum 60°C 140 mW/cm^2 N90AK1

Figure 39 ELECTRICAL PERFORMANCE VS CYCLES FOR CdS SOLAR CELLS MANUFACTURED IN NOVEMBER, 1967

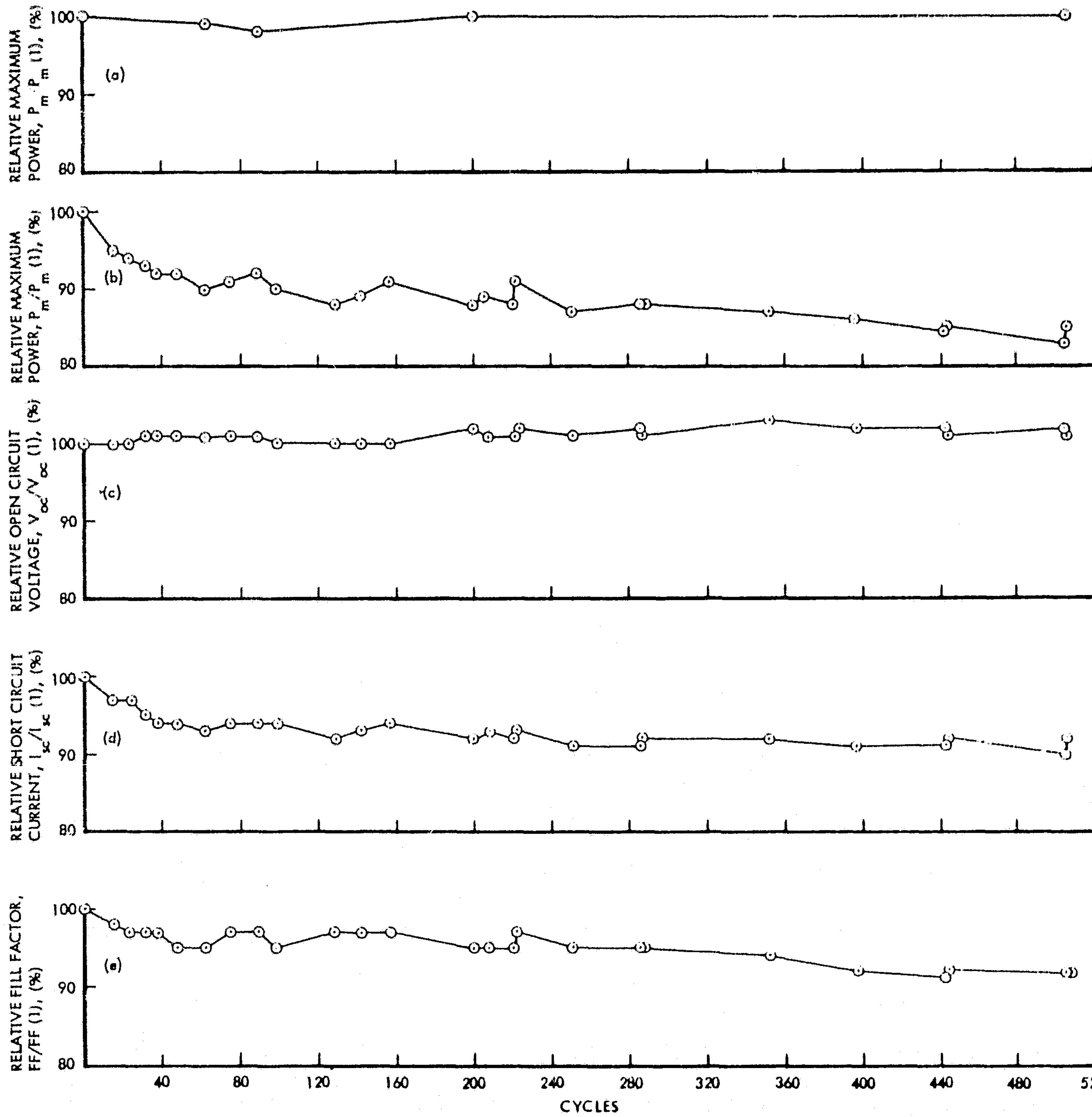

Graph:	(a)	(b), (c), (d), (e)
Test Environment:	Double Desiccated Storage	Space Environment Thermal Cycling
Measurement Condition:	In Air	In Vacuum
Cell Temperature:	25°C	60°C
Light Intensity:	140 mW/cm^2	140 mW/cm^2
Cell Number:	N89CK1	N90AK9

Figure 40 ELECTRICAL PERFORMANCE VS CYCLES FOR CdS SOLAR CELLS MANUFACTURED IN NOVEMBER, 1967

MANUFACTURE DATE	CELL TYPE	CELL NUMBER	EFFICIENCY $\eta(1)$ BEFORE (%)	η AFTER (%)	$\eta/\eta(1)$ RELATIVE (%)	MAXIMUM POWER $P_M(1)$ BEFORE (mW)	P_M AFTER (mW)	$P_M/P_M(1)$ RELATIVE (%)	OPEN CIRCUIT VOLTAGE $V_{oc}(1)$ BEFORE (V)	V_{oc} AFTER (V)	$V_{oc}/V_{oc}(1)$ RELATIVE (%)	SHORT CIRCUIT CURRENT $I_{sc}(1)$ BEFORE (mA)	I_{sc} AFTER (mA)	$I_{sc}/I_{sc}(1)$ RELATIVE (%)	FILL FACTOR FF(1) BEFORE (%)	FF AFTER (%)	FF/FF(1) RELATIVE (%)
NOVEMBER, 1967	2	A970B	4.56	4.06	89	351	312	89	0.439	0.454	103	1158	1062	92	69	65	94
		A969D	4.55	0.85	19	350	65	19	0.442	0.255	58	1158	1090	94	68	23	34
	3	NH188AK2	2.74	2.33	85	211	179	85	0.428	0.437	102	793	776	98	62	53	35
		NB200AK3	2.81	2.64	94	216	203	94	0.417	0.422	101	790	792	100	66	61	92
		N89CK7	2.68	2.13	80	206	164	80	0.427	0.434	102	796	755	95	61	50	82
		N90AK5	3.26	2.94	90	251	226	90	0.416	0.426	102	940	914	97	64	58	91
		N90BK4	3.04	2.93	96	234	225	96	0.413	0.418	101	860	867	101	66	62	94
		N90AK1	3.07	2.89	94	236	222	94	0.419	0.425	101	896	883	99	63	59	94
		N90AK9	2.89	2.63	91	222	202	91	0.418	0.423	101	817	800	98	65	60	92
MARCH, 1968	4	N154BK6	3.04	2.74	90	234	211	90	0.412	0.437	106	850	810	95	67	60	90
		N153AK8	2.96	2.47	83	228	190	83	0.415	0.425	102	860	773	90	64	58	91
		N154CK1	2.77	2.64	95	213	203	95	0.418	0.432	103	755	723	96	67	65	97
		N157BK2	3.17	2.78	88	244	214	88	0.409	0.418	102	893	842	94	67	61	91
	5	N156AK4	2.87	2.55	89	221	196	89	0.420	0.440	105	804	739	92	66	60	91
		N156CK2	2.70	2.48	92	208	191	92	0.422	0.435	103	750	700	93	66	63	95
		N156AK5	3.07	2.57	84	236	198	84	0.418	0.427	102	886	805	91	64	58	91
	6	N151CK4	2.67	1.96	74	205	151	74	0.413	0.418	101	760	693	91	65	52	80
		N150BK6	2.16	2.11	98	166	162	98	0.422	0.437	104	568	543	96	69	68	99

Measurement Condition: In air, with cell mounted on a temperature-controlled block
Light Intensity: 140 mW/cm^2, AMO
Cell Temperature: 60°C

TABLE 8: ELECTRICAL PERFORMANCE OF CdS SOLAR CELLS BEFORE AND AFTER THERMAL CYCLING

One of the cells in this group exhibited a delamination between the CdS layer and the metal coating on the substrate. Such a delamination may have increased the series resistance during thermal cycling, causing subsequent loss of power. When the cell was mounted on the temperature-controlled block after removal from the vacuum chamber, it was constrained to lie flat while its I-V curve was being obtained. This constraint may have temporarily closed delaminations, resulting in decreased series resistance and apparent recovery in maximum power.

Cell Number NH188AK2

Cell number NH188AK2 is typical of the remaining six cells in this group. After 506 cycles its P_M', V_{oc}', I_{sc}', and FF' values were 75, 101, 90 and 84 percent, respectively. A degraded I-V curve of this cell is shown in Figure 41.

Decrease in Light Generated Current

Based on the calculated effects of R_s, R_{sh}, I_g, I_o, and A on the performance of a typical CdS solar cell (Figures 16 to 20), the observed loss in I_{sc}' was most likely the result of about a 10 percent decrease in I_g. These are the reasons:

(1) A 10 percent decrease in I_g resulted in an I_{sc}' of 90 percent, which is the same as the experimental value, without causing a degraded V_{oc}'.

(2) Changes in R_s, R_{sh}, I_o, and A which resulted in a P_M less than the 75-percent experimental value resulted in an I_{sc}' greater than 98 percent, and therefore could not explain the observed 90-percent I_{sc}'.

Much evidence shows that this loss was not the result of low light intensity:

(1) The I_{sc}' of one cell (No. NH200AK3) did not degrade at all during the entire test.

(2) The I_{sc} of one of the silicon reference cells in the vacuum chamber varied by less than one percent between cycle 1 and cycle 506.

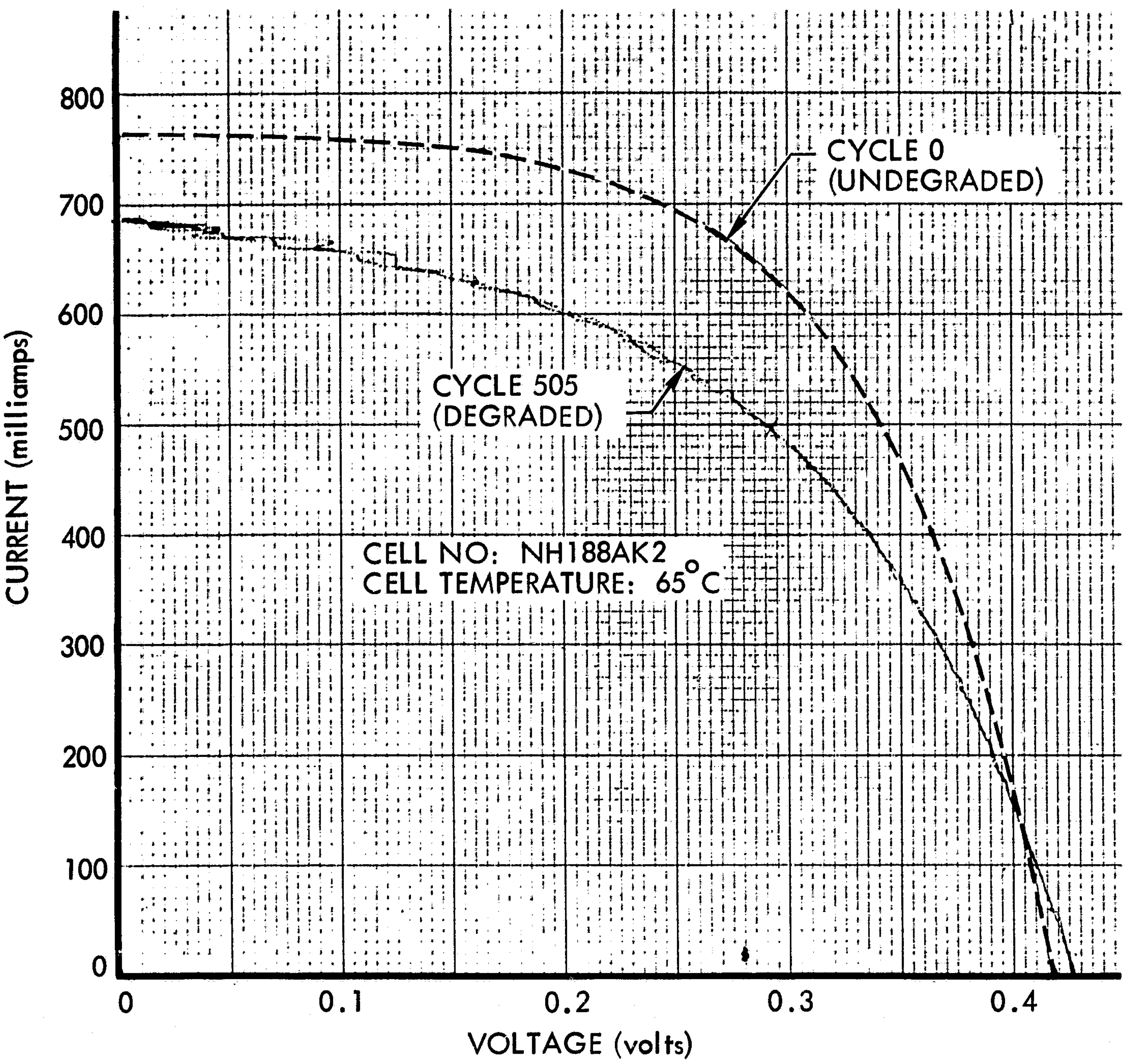

Figure 41: DEGRADED I-V CURVE OF A NOVEMBER 1967 CdS SOLAR CELL

(3) The transmission of the quartz window degraded less than one percent, based on measurements made with the CdS standard cell before and after the test.

(4) The I_{sc} of all the Kapton-substrate control cells at cycle 506 were within one percent of their cycle-1 values.

Since all these cells had the same type of covers (Kapton), and the I_{sc}' of one of these cells did not degrade at all, it appears that the loss in light-generated current cannot be attributed to a decrease in cover transmission. Furthermore, other investigations (ref. 8) have shown that Kapton does not degrade under UV in vacuum. Thus we are unable to explain why the light generated current of this one cell decreased. Data obtained in air on a temperature controlled block before and after the test (Table 8, NH188AK2) indicate only a two percent degradation in I_{sc}'.

This perplexing question of why I_g degraded during thermal cycling, and then recovered after the test has not yet been resolved. With only one exception, the other cells also exhibited a decrease in light-generated current during thermal cycling, and then recovered, at least partially, after the test was completed. Post-cycling tests (Table 9) conducted before the cells were removed from the chamber indicated that the addition of gaseous nitrogen or air seemed to have no significant effect on I_{sc}' (and hence I_g). The I_{sc}' of the cells did increase slightly in the first post cycling test, but this increase probably resulted from the below-normal temperature (50°C instead of 70°C) of the cells in this test, rather than from a recovery in light generated current.

Increase in Series Resistance

Based on the calculated effects of R_s, R_{sh}, I_g, I_o and A on the performance of a typical CdS solar cell (Figures 16 to 20), the observed decrease in FF of cell NH188AK2 was most likely caused by a change in R_s rather than a change in the other parameters. The reasons are:

Table 9: POST-CYCLING PERFORMANCE OF CdS SOLAR CELLS MANUFACTURED DURING NOVEMBER 1967

CELL TYPE	CELL NUMBER	TEST AT CYCLE-1	7 MONTHS	TEST AT CYCLE 2031	69 HOURS	FIRST POST-CYCLING TEST	24 HOURS	3 HOURS	SECOND POST-CYCLING TEST	24 HOURS	THIRD POST CYCLING TEST	4½ HOURS	FOURTH POST CYCLING TEST	7 HOURS	FIFTH POST CYCLING TEST	2 HOURS	SIXTH POST-CYCLING TEST
	PERFORMANCE – MEASUREMENT SEQUENCE	CYCLING	CYCLING	CYCLING	POST CYCLING	POST CYCLING	POST CYCLING	POST CYCLING	POST CYCLING	POST CYCLING	POST CYCLING	POST CYCLING	POST CYCLING	POST CYCLING	POST CYCLING	POST CYCLING	POST CYCLING
	ENVIRONMENTAL CONDITIONS DURING AND BETWEEN PERFORMANCE TESTS																
	TYPE OF GAS IN VACUUM CHAMBER	VACUUM	VACUUM	VACUUM	VACUUM	VACUUM	VACUUM	NITROGEN	NITROGEN	NITROGEN	NITROGEN	VACUUM	VACUUM	AIR	AIR	AIR	AIR
	PRESSURE IN VACUUM CHAMBER (torr)	10^{-8}	10^{-8}	10^{-8}	10^{-8}	10^{-8}	10^{-8}	AMBIENT	AMBIENT	AMBIENT	AMBIENT	10^{-6}	10^{-6}	AMBIENT	AMBIENT	AMBIENT	AMBIENT
	AVERAGE CELL TEMPERATURE (^{o}C)	65	ALTERNATING FROM -100 TO +65	64	65	66	ARISING FROM -100 TO +25	APPROX. 25	77	APPROX. 25	77	APPROX. 25	66	APPROX. 25	71	APPROX. 25	72
	LIGHT MODE	ON	½ HOUR ON ½ HOUR OFF	ON	ON	ON	OFF	OFF	ON	OFF	ON	OFF	ON	OFF	ON	OFF	ON
	PERFORMANCE DATA MEASURED UNDER THE ENVIRONMENTAL CONDITIONS INDICATED ABOVE (1)																
	RELATIVE MAXIMUM POWER, $P_M/P_M(1)$, %	(2) (mW)															
4	N154BK6	228		87		86			86		83		88		85		88
4	N153AK8	217		84		73			76		74		71		78		80
4	N154CK1	208		92		92			90		90		94		93		94
4	N157BK2	232		83		81			81		81		83		85		88
5	N156AK4	206		86		88			87		87		86		89		91
5	N156CK2	198		90		88			90		90		91		94		93
5	N156AK5	225		84		84			79		80		85		83		85
6	N151CK4	190		49		57			77		77		56		79		76
6	N150BK6	156		96		97			98		97		99		101		104
	RELATIVE OPEN CIRCUIT VOLTAGE, $V_M/V_M(1)$, %	(2) (V)															
4	N154BK6	0.412		103		103			100		100		103		100		101
4	N153AK8	0.415		103		100			96		99		99		100		100
4	N154CK1	0.41[illegible]		104		104			101		101		104		102		102
4	N157BK2	0.40[illegible]		103		102			100		100		103		101		102
5	N156AK4	0.413		105		104			103		102		104		103		103
5	N156CK2	0.421		102		101			99		99		101		100		100
5	N156AK5	0.413		104		105			99		100		104		100		100
6	N151CK4	0.406		97		100			101		101		100		101		101
6	N150BK6	0.420		102		102			100		100		102		101		102
	RELATIVE SHORT CIRCUIT CURRENT, $I_{SC}/I_{SC}(1)$, %	(2) (mA)															
4	N154BK6	831		97		96			96		96		96		97		96
4	N153AK8	808		92		88			90		89		90		91		92
4	N154CK1	741		96		97			98		96		96		98		97
4	N157BK2	873		94		91			92		92		90		94		93
5	N156AK4	773		94		96			93		94		94		95		96
5	N156CK2	726		95		96			96		95		95		98		96
5	N156AK5	867		89		89			88		88		91		91		90
6	N151CK4	727		91		89			91		92		92		93		94
6	N150BK6	549		100		99			101		101		101		102		102
	RELATIVE FILL FACTOR, FF/FF(1), %	(2) (%)															
4	N154BK6	67		87		87			90		87		88		88		90
4	N153AK8	65		88		82			88		83		78		85		86
4	N154CK1	67		93		91			91		93		94		94		94
4	N157BK2	65		86		88			88		88		89		91		93
5	N156AK4	65		92		91			94		95		94		95		91
5	N156CK2	62		90		90			90		92		90		91		96
5	N156AK5	62		90		90			90		92		90		91		94
6	N151CK4	64		56		[illegible]			84		83		61		84		81
6	N150BK6	68		94		96			96		96		96		98		100

(1) All data is corrected to $60^{o}C$. Light intensity was 140 mW/cm^2, AMO, during the entire test program.
(2) All cycle-1 data are actual, not relative, values given in the indicated units.

(1) A 0.076-ohm increase in R_s resulted in a FF' equal to the 84-percent experimental value, without degrading V_{oc}'.

(2) Changes in I_g do not appreciably affect FF'.

(3) Changes in R_{sh}, I_o and A which result in the experimental FF' also result in a V_{oc}' which is significantly lower than the experimental value.

Furthermore, the I-V curves at cycle-1 and cycle-506 showed that R_{oc} increased from 0.10 to 0.16 ohms. Figure 21 shows that this corresponds to a 0.046-ohm increase in R_s, in fair agreement with the preceding observations.

6.3.2.2 Copper-Substrate Cells

Cell Number A970B

After 506 cycles, the P_M', V_{oc}', I_{sc}', and FF' values of this cell were 77, 102, 81, and 93 percent respectively. The before and after measurements made in air resulted in P_M, V_{oc}, I_{sc}, and FF values of 89, 103, 98, and 94 percent respectively, indicating a significant recovery in P_M' and I_{sc}', but not in V_{oc}' and FF' during the post-test period. The fact that the I_{sc}' did not recover completely, as did the I_{sc}' of all the cells with Kapton covers, suggests that a permanent degradation in the transmission of the Mylar cover was responsible for part of the in situ degradation of I_{sc}'.

Based on the calculated effect of R_s, R_{sh}, I_g, I_o, and A on the performance of a typical CdS solar cell (Figures 16 to 20), the observed loss in FF' was due to either an increase in series resitance or a decrease in shunt resistance. These are the reasons:

(1) A 0.024-ohm increase in R_s resulted in a FF' equal to the experimental value without being accompanied by a significant decrease in V_{oc}'.

(2) A 15-ohm decrease in R_{sh} resulted in a FF' equal to the experimental value without being accompanied by a significant decrease in V_{oc}'.

(3) Changes in I_g or A which result in a FF' equal to the experimental value are accompanied by large losses in V_{oc}', which were not observed experimentally.

The values of R_{oc} obtained from the I-V curves at cycle-1 and cyle-506 did not differ significantly, indicating no change in resistance. This suggests that an increase in shunt resistance was responsible for the degradation in FF, and hence part of the power loss.

Cell Number A969D

After 506 cycles, the P_M', V_{oc}', I_{sc}', and FF' values of this cell were 25, 60, 81 and 51 percent, respectively. The drastic degradations in this cell appear to be caused by a decrease in R_{sh} resulting from a short in the cell. However a decrease in I_g may have been responsible for the decrease in I_{sc}'. Just as in cell A970B, discussed in the preceding paragraph, the I_{sc}' recovered partially after the test was completed. The permanent decrease in I_{sc}' was probably due to a decrease in the transmission of the Mylar cover.

Summary or Testing of November, 1967 Cells

In general, the cells manufactured in November, 1967 did not lose as much power as did the April, 1967 cells. Lower losses in the Kapton-substrate cells resulted from losses in light generated current and from increases in series resistance. Something other than a decrease in transmission of the Kapton covers is responsible for the observed decrease in I_g.

The loss in light-generated current seemed to recover completely after the cells were removed from the vacuum chamber. No explanation is available for this phenomenon. A few Kapton-substrate cells also exhibited occasional drops in shunt resistance resulting from shorts in the cell.

The copper-substrate cells degraded in power output because of losses in I_g and decreases in R_{sh}, but not R_s. Part of the loss in I_g was due to a degradation of the Mylar covers. This part of the loss did not vanish after the test. The fact that the R_s increased in the Kapton-substrate cells but not the copper-substrate cells suggests that the cause of increasing R_s in the Kapton-substrate cells is from either:

(1) A delamination between the CdS layer and the substrate metal layer which doesn't occur in the copper-substrate cells

(2) An increase in resistivity in the substrate metal layer.

6.3.3 March, 1968 Cells

The test cells manufactured in March, 1968 were subjected to 2031 cycles. The average P_M' of eight of the nine test cells had degraded, by cycle 2031, to 88 percent. The actual values ranged from 83 to 96 percent. The ninth degraded in P_M' to 49 percent in 2031 cycles. The P_M', V_{oc}', I_{sc}', and FF' of each of the nine test cells is plotted as a function of cycles in Figures 42 to 50. The P_M' of a matching control cell is also plotted on these graphs. These test data are also presented in Tables 10 to 14. The data have been corrected for temperature variations to correspond to 60°C. All of these data were obtained with the test-cells mounted in the vacuum chamber, under vacuum.

After completion of cycling, cell performance was measured at ambient pressure, first with gaseous nitrogen, and then with air in the chamber. The results of these tests are given in Table 15.

The performance of the cells was also measured in air before and after cycling, with the cells mounted, on a temperature-controlled block maintained at 60°C. These data are presented in Table 8.

Cell No. \ Cycle	1	2	9	16	33	34	44	48	59	62	73	76	77	80	92	95	108	142	143	162
M151CK4	2.47	2.52	2.48	2.54	2.52	2.48	2.44	2.48	2.47	2.43	2.46	2.39	2.48	2.47	2.44	2.47	2.44	2.34	2.47	2.50
M150BK6	2.03	2.02	2.07	2.09	2.05	2.05	2.02	1.94	2.02	2.07	2.07	2.08	2.08	2.07	2.05	2.04	2.09	2.05	2.07	2.07
M156AK4	2.68	2.67	2.68	2.67	2.68	2.64	2.64	2.67	2.63	2.67	2.65	2.70	2.68	2.65	2.67	2.65	2.64	2.60	2.64	2.64
M156CK2	2.57	2.56	2.59	2.60	2.57	2.57	2.57	2.56	2.52	2.56	2.57	2.59	2.59	2.57	2.59	2.60	2.63	2.50	2.57	2.55
M156AK5	2.93	.295	2.91	2.94	2.91	2.87	2.90	2.93	2.89	2.87	2.86	2.85	2.87	2.89	2.81	2.90	2.88	2.32	2.95	2.88
M154BK6	2.96	2.91	3.02	3.00	2.93	2.89	2.93	2.98	2.94	2.90	2.96	2.90	2.87	2.90	2.83	2.91	2.89	2.81	2.87	2.95
M153AK8	2.82	2.87	2.82	2.80	2.85	2.85	2.94	2.82	2.85	2.85	2.83	2.82	2.87	2.82	2.85	2.83	2.80	2.74	2.77	2.80
M154CK1	2.70	2.77	2.73	2.80	2.74	2.78	2.77	2.77	2.77	2.96	2.78	2.76	2.83	2.78	2.77	2.81	2.80	2.73	2.81	2.78
M157BK2	3.02	3.06	3.02	3.03	3.02	3.06	3.04	3.06	3.03	3.25	3.03	3.03	3.07	3.04	3.02	2.99	3.04	2.98	3.03	3.06

Cell No. \ Cycle		193	208	209	244	245	320	369	370	433	464	498	499	533	534	553	554	620	652	738
M151CK4		2.39	2.42	2.41	2.42	2.34	2.39	2.37	2.38	2.47	2.37	2.31	2.30	2.29	2.30	2.30	2.29	2.31	2.25	2.30
M150BK6		2.04	2.04	2.02	2.02	2.00	2.08	2.07	2.08	2.07	2.03	2.13	2.00	2.08	1.99	2.00	1.96	2.00	1.99	1.99
M156AK4		2.56	2.56	2.54	2.57	2.48	2.50	2.51	2.47	2.50	2.51	2.50	2.50	2.44	2.46	2.46	2.34	2.47	2.46	2.44
M156CK2		2.47	2.44	2.51	2.46	2.43	2.43	2.41	2.48	2.30	2.37	2.34	2.43	2.25	2.41	2.31	2.13	2.13	2.43	2.37
M156AK5		2.85	2.76	2.80	2.77	2.69	2.70	2.68	2.73	2.68	2.70	2.64	2.61	2.61	2.69	2.67	2.72	2.63	2.68	2.55
M154BK6		2.85	2.89	2.85	2.87	2.77	2.81	2.80	2.78	2.72	2.76	2.74	2.70	2.68	2.76	2.74	2.78	2.70	2.68	2.70
M153AK8		2.78	2.69	2.74	2.70	2.64	2.64	1.31	1.46	2.20	2.31	2.30	2.29	2.29	2.26	2.38	2.38	2.33	2.30	2.33
M154CK1		2.74	2.72	2.74	2.69	2.67	2.63	2.65	2.69	2.64	2.61	2.63	2.64	2.63	2.65	2.64	2.63	2.57	2.61	2.61
M157BK2		2.95	2.94	2.95		3.07	2.63	2.60	2.64	2.57	2.55	2.57	2.30	2.63	2.63	2.57	2.59	2.59	2.56	2.52

Cell No. \ Cycle		786	887	997	1204	1209	1301	1404	1510	1626	1764	1804	1905	1906	2031
M151CK4		2.28	2.22	2.28	1.30	1.52	1.29	1.05	1.34	1.30	1.20	1.31	1.17	1.62	1.22
M150BK6		1.94	1.99	1.94	1.98	1.87	1.90	1.96	1.95	2.03	1.99	1.92	1.99	2.02	1.95
M156AK4		2.41	2.46	2.43	2.46	2.38	2.39	2.38	2.37	2.33	2.33	2.28	2.30	2.38	2.30
M156CK2		2.34	2.39	2.38	2.44	2.39	2.37	2.37	2.37	2.33	2.35	2.25	2.33	2.37	2.31
M156AK5		2.48	2.52	2.46	2.47	2.46	2.42	2.42	2.39	2.54	2.46	2.39	2.43	2.57	2.46
M154BK6		2.64	2.56	2.61	2.61	2.54	2.46	2.54	2.52	2.64	2.61	2.52	2.59	2.69	2.57
M153AK8		2.31	2.39	2.33	2.56	2.41	2.43	2.47	2.44	2.51	2.47	2.38	2.42	2.54	2.37
M154CK1		2.52	2.51	2.48	2.51	2.48	2.46	2.50	2.46	2.59	2.54	2.44	2.50	2.57	2.48
M157BK2		2.46	2.46	2.41	2.47	2.42	2.38	2.46	2.50	2.55	2.48	2.37	2.19	2.57	2.51

Test Environment: Space Environment Thermal Cycling
Measurement Condition: In Vacuum
Cell Temperature: 60°C
Light Intensity: 140 mW/cm², AMO

TABLE 10: CONVERSION EFFICIENCY VS. CYCLES FOR CdS SOLAR CELLS MANUFACTURED IN MARCH, 1968

Cycle / Cell No.	1	2	9	16	33	34	44	48	59	62	73	76	77	80	92	95	108	142	143	162
	The maximum powers in this column are given in milliwatts.																			
H151CK4	190	102	101	103	102	101	99	101	100	98	99	97	101	100	99	100	98	95	100	101
H150BK6	156	99	102	103	101	101	99	98	99	102	102	103	103	102	101	101	103	100	102	102
H156AK4	206	100	100	100	100	99	99	100	98	100	99	101	100	99	100	99	99	97	99	98
H156CK2	198	99	101	101	100	100	100	99	98	99	100	101	101	100	101	101	102	97	99	99
H156AK5	225	101	100	100	100	98	99	100	99	98	98	97	98	99	96	99	96	96	97	96
H154BK6	228	98	102	101	99	97	99	100	99	98	100	98	97	98	96	98	97	95	97	100
H153AK8	217	102	100	99	101	101	104	100	101	101	100	100	102	100	101	100	99	97	98	99
H154CK1	208	102	101	103	101	103	102	102	102	110	103	102	105	103	102	103	103	101	104	103
H157BK2	232	101	107	100	100	101	101	101	100	108	100	100	102	101	100	99	101	99	100	101
Cycle / Cell No.		193	208	209	244	245	320	369	370	433	464	498	499	533	534	553	554	620	652	738
H151CK4		97	98	97	98	95	97	96	96	96	96	94	93	93	93	93	93	94	92	93
H150BK6		101	101	99	99	99	103	102	103	102	100	100	99	103	98	99	97	99	98	98
H156AK4		96	96	95	96	93	93	94	92	93	94	93	93	91	92	92	87	92	92	91
H156CK2		96	95	97	95	94	94	93	96	89	92	91	94	87	93	90	83	83	94	92
H156AK5		97	94	96	95	92	92	92	93	92	92	90	89	89	92	91	93	90	92	87
H154BK6		96	97	96	96	93	95	94	94	92	93	93	91	90	93	93	94	91	90	91
H153AK8		99	95	97	96	94	94	47	52	78	82	82	81	81	80	84	84	92	82	82
H154CK1		101	100	101	100	99	97	98	100	98	97	97	98	97	98	98	97	95	97	97
H157BK2		98	97	98		102	87	86	88	85	84	85	76	87	87	85	86	86	85	84
Cycle / Cell No.		786	887	997	1204	1209	1301	1404	1510	1626	1704	1804	1905	1906	2031					
H151CK4		92	90	92	53	63	52	42	54	53	48	53	47	66	49					
H150BK6		96	98	96	97	92	94	97	96	100	98	95	98	99	96					
H156AK4		90	92	91	92	89	89	89	88	87	87	85	86	89	86					
H156CK2		91	93	92	95	93	92	92	92	90	91	87	90	92	90					
H156AK5		85	86	84	84	84	83	83	82	87	84	82	83	88	84					
H154BK6		89	86	88	88	86	83	86	85	89	88	85	87	91	87					
H153AK8		82	85	82	91	85	86	88	87	89	88	84	86	90	84					
H154CK1		93	93	92	83	92	91	92	91	96	94	90	92	95	92					
H157BK2		81	81	80	82	80	79	81	83	84	82	78	79	85	83					

Test Environment: Space Environment Thermal Cycling
Measurement Condition: In Vacuum
Cell Temperature: 60°C
Light Intensity: 140 mW/cm^2, AM0

TABLE 11: RELATIVE MAXIMUM POWER VS. CYCLES FOR CdS SOLAR CELLS MANUFACTURED IN MARCH, 1968

Cell No. \ Cycle	1	2	9	16	33	34	44	48	59	62	73	76	77	80	92	95	108	142	143	162
H151CK4	.406	100	100	101	101	100	101	101	102	101	102	102	102	102	102	102	102	102	102	103
H150BK6	.420	100	100	100	100	100	101	101	101	101	101	102	101	101	101	101	101	102	101	101
H156AK4	.413	100	100	100	101	101	101	101	101	101	102	103	102	102	103	102	102	103	102	103
H156CK2	.421	100	100	.99	99	99	100	99	99	100	100	101	100	101	101	.100	101	101	100	101
H156AK5	.419	100	100	101	101	100	101	101	101	101	101	102	101	102	101	102	101	101	101	102
H154BK6	.412	99	99	100	100	101	100	101	101	101	103	102	101	102	101	101	102	102	101	101
H153AK8	.416	103	101	101	101	101	104	102	102	102	103	103	103	102	101	103	103	102	102	103
H154CK1	.419	101	101	101	100	101	101	101	102	105	102	102	102	102	102	102	103	102	102	102
H157BK2	.409	101	100	100	100	101	99	101	101	105	102	102	101	102	103	101	103	102	102	103

Cell No. \ Cycle		193	208	209	244	245	320	369	370	433	464	498	499	533	534	553	554	620	652	738
H151CK4		102	103	102	103	102	102	102	102	103	102	103	103	103	102	102	102	103	103	103
H150BK6		101	101	100	100	102	101	101	100	100	100	101	101	103	101	101	101	101	101	102
H156AK4		103	103	102	104	101	102	103	100	103	103	104	104	104	103	103	100	104	105	105
H156CK2		101	100	100	101	99	101	101	100	100	101	101	102	101	101	101	100	100	102	102
H156AK5		104	102	102	102	101	102	102	101	102	101	102	101	102	102	102	102	102	102	103
H154BK6		102	103	101	103	101	102	102	101	102	102	103	102	102	101	102	103	102	102	103
H153AK8		103	103	[illegible]	104	101	103	90	95	103	103	103	102	103	102	103	103	103	103	104
H154CK1		103	102	102	103	101	102	102	102	102	102	103	100	102	103	102	102	102	103	103
H157BK2		103	102	101		102	100	100	100	100	101	101	93	103	101	101	101	102	102	102

Cell No. \ Cycle		786	887	997	1204	1209	1301	1404	1510	1626	1764	1804	1905	1906	2031					
H151CK4		104	103	103	96	99	93	94	98	98	97	98	98	100	97					
H150BK6		101	101	101	101	101	101	101	101	101	101	101	101	102	102					
H156AK4		105	106	105	107	107	108	106	109	104	105	104	105	107	105					
H156CK2		102	103	102	104	105	105	103	103	100	101	101	103	102	102					
H156AK5		102	103	103	104	103	104	106	103	104	104	103	104	104	104					
H154BK6		103	103	103	103	102	102	103	103	103	104	102	104	103	103					
H153AK8		105	105	104	102	101	103	104	103	103	103	103	104	103	103					
H154CK1		103	104	103	104	102	103	104	104	104	103	103	104	103	104					
H157BK2		102	101	102	102	101	102	103	102	103	103	100	102	102	103					

The open-circuit voltages in this column (cycle 1) are given in volts.

Test Environment: Space Environment Thermal Cycling
Measurement Condition: In Vacuum
Cell Temperature: 60°C
Light Intensity: 140 mW/cm^2, AMO

TABLE 12: RELATIVE OPEN CIRCUIT VOLTAGE VS. CYCLES FOR CdS SOLAR CELLS MANUFACTURED IN MARCH, 1968

The short-circuit currents in this column are given in milliamperes. (column 1)

Cycle / Cell No.	1	2	9	16	33	34	44	48	59	62	73	76	77	80	92	95	108	142	143	162
M151CK4	727	100	100	100	101	99	99	99	99	99	99	100	99	99	99	99	100	95	100	97
M150BK6	549	99	101	101	101	100	99	100	101	101	101	100	99	102	100	101	100	97	101	99
M156AK4	773	101	101	101	100	100	99	99	100	99	98	99	99	99	98	99	98	93	99	95
M156CK2	726	100	101	102	101	100	100	100	101	102	100	100	100	100	99	103	100	102	101	101
M156AK5	867	99	100	101	100	99	99	99	99	99	98	98	99	98	98	99	98	94	98	95
M154BK6	831	100	100	102	101	100	100	100	101	101	102	101	101	101	99	102	99	95	101	96
M153AK8	808	101	99	100	101	99	99	99	100	100	98	98	100	98	101	100	98	94	99	96
M154CK1	741	100	98	99	101	100	102	101	101	105	101	101	102	100	101	101	100	96	102	99
M157BK2	873	100	100	101	101	101	101	101	101	104	101	101	103	101	100	103	101	96	101	99
Cycle / Cell No.		193	208	209	244	245	320	369	370	433	464	498	499	533	534	553	554	620	652	738
M151CK4		96	96	98	95	94	99	98	100	97	96	95	96	96	94	95	96	96	94	94
M150BK6		99	99	98	98	97	101	102	102	100	100	100	99	99	97	101	99	99	99	98
M156AK4		94	95	95	94	96	98	98	99	96	95	95	95	93	93	95	95	94	94	92
M156CK2		101	102	103	102	98	98	98	99	98	97	98	97	95	95	96	96	95	96	96
M156AK5		94	95	95	94	93	96	95	95	95	94	93	93	92	92	95	95	94	91	89
M154BK6		95	96	97	95	96	99	98	99	95	95	95	95	94	96	98	98	97	95	94
M153AK8		96	95	94	93	95	94	91	89	87	87	86	87	86	84	87	87	87	87	84
M154CK1		98	98	98	97	98	102	98	102	99	96	97	95	95	95	98	97	97	96	94
M157BK2		97	96	98		98	97	95	98	95	93	95	93	93	95	95	95	95	96	94
Cycle / Cell No.		786	887	997	1204	1209	1301	1404	1510	1626	1764	1804	1905	1906	2031					
M151CK4		92	93	91	88	89	87	88	89	90	89	88	87	91	91					
M150BK6		97	99	95	101	97	97	99	100	102	101	99	100	102	100					
M157AK4		91	92	88	93	92	90	92	92	94	93	93	93	96	94					
M156CK2		94	95	97	96	94	94	96	94	98	97	96	95	95	95					
M156AK5		88	89	84	90	90	88	89	89	90	90	89	90	93	89					
M154BK6		94	90	89	96	94	92	95	94	98	97	96	96	100	97					
M153AK8		82	87	87	96	94	92	93	92	95	94	92	90	95	92					
M154CK1		94	93	90	96	95	94	96	94	99	98	96	96	98	96					
M157BK2		92	93	91	92	93	90	92	90	95	95	91	91	95	94					

Test Environment: Space Environment Thermal Cycling
Measurement Condition: In Vacuum
Cell Temperature: 60°C
Light Intensity: 140 mW/cm^2, AMO

TABLE 13: RELATIVE SHORT CIRCUIT CURRENT VS. CYCLES FOR CdS SOLAR CELLS MANUFACTURED IN MARCH, 1968

Cycle / Cell No.	1	2	9	16	33	34	44	48	59	62	73	76	77	80	92	95	108	142	143	162
M151CK4	64	102	102	102	102	102	100	102	100	98	98	95	100	98	98	98	97	98	100	102
M150BK6	68	100	100	102	100	101	99	97	97	100	100	100	103	97	100	99	101	100	97	101
M156AK4	65	99	99	97	99	97	98	98	97	99	99	98	98	98	97	97	97	100	97	100
M156CK2	65	99	100	99	100	100	100	100	97	99	100	100	100	98	100	97	100	94	97	97
M156AK5	62	102	100	99	98	100	100	100	98	99	99	97	98	98	97	98	97	102	98	100
M154BK6	67	99	102	99	97	96	97	99	96	96	99	96	94	97	96	94	96	97	94	101
M153AK8	65	97	100	105	99	100	100	98	98	99	99	98	98	98	97	97	98	100	97	100
M154CK1	67	102	103	103	100	101	100	100	100	99	100	99	101	101	100	100	100	103	101	101
M157BK2	65	100	100	100	99	100	100	98	97	99	97	97	97	98	98	95	97	100	97	100
Cycle / Cell No.		193	208	209	244	245	320	369	370	433	464	498	499	533	534	553	554	620	652	738
M151CK4		100	100	98	102	98	97	97	95	97	98	95	95	94	98	95	95	95	94	97
M150BK6		100	100	101	101	100	100	99	100	101	99	99	99	100	99	97	97	97	97	99
M156AK4		97	97	97	98	95	92	92	92	94	95	94	94	94	95	92	91	92	92	94
M156CK2		94	92	94	92	97	95	94	97	91	94	92	95	91	97	92	86	85	95	94
M156AK5		100	97	98	98	98	95	95	97	95	97	95	94	95	97	94	97	94	98	95
M154BK6		99	99	97	99	97	94	93	93	94	96	94	93	94	94	93	93	91	93	93
M153AK8		98	97	100	98	97	95	66	60	86	91	92	91	91	92	94	94	92	91	94
M154CK1		101	100	101	100	99	94	97	96	97	99	97	101	100	100	99	97	96	97	100
M157BK2		97	98	98		102	89	91	89	89	89	89	88	91	91	89	89	88	86	88
Cycle / Cell No.		786	837	997	1204	1209	1301	1404	1510	1596	1764	[illegible]	1905	[illegible]	2031					
M151CK4		97	94	100	63	70	64	52	63	[illegible]	57	[illegible]	56	[illegible]	56					
M150BK6		97	99	100	96	94	94	96	96	96	[illegible]	[illegible]	96	[illegible]	94					
M156AK4		94	94	97	91	91	91	89	83	88	[illegible]	[illegible]	88	[illegible]	86					
M156CK2		94	95	94	95	95	94	94	94	91	92	89	92	[illegible]	92					
M156AK5		94	94	97	90	90	90	87	89	[illegible]	89	[illegible]	89	[illegible]	90					
M154BK6		93	93	96	88	88	88	87	88	87	87	85	87	[illegible]	87					
M153AK8		94	94	92	92	89	91	89	91	91	89	89	91	91	83					
M154CK1		96	96	99	94	94	94	93	93	93	93	91	[illegible]	94	93					
M157BK2		86	86	86	88	86	86	86	89	86	85	86	85	[illegible]	86					

The fill factors in this column (cycle 1) are the actual fill factors, in percent.

Test Environment: Space Environment Thermal Cycling
Measurement Condition: In Vacuum
Cell Temperature: 60°C
Light Intensity: 140 mW/cm^2, AM0

TABLE 14: RELATIVE FILL FACTOR VS. CYCLES FOR CdS SOLAR CELLS MANUFACTURED IN MARCH, 1968

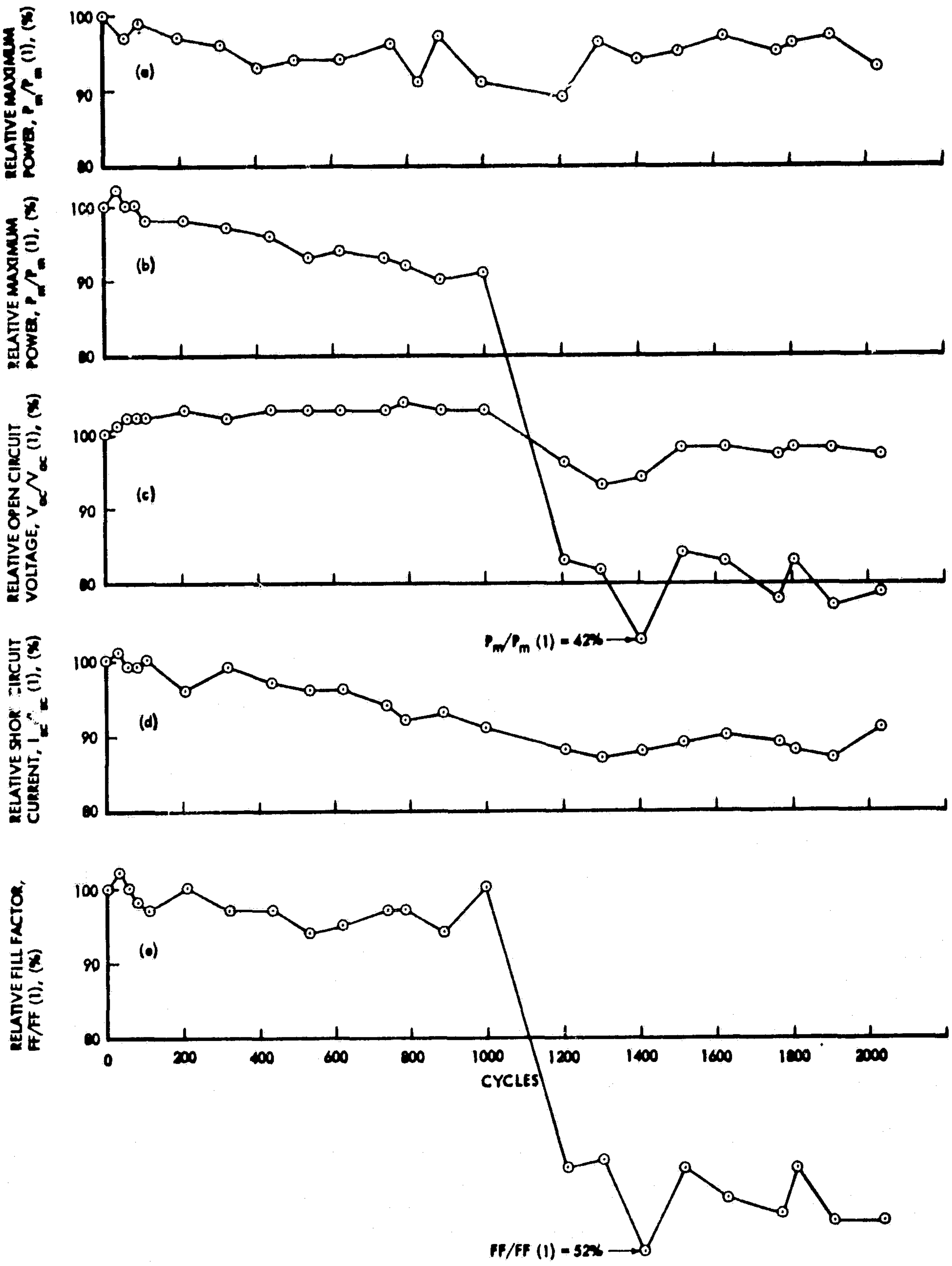

Graph:	(a)	(b), (c), (d), (e)
Test Environment:	Double Desiccated Storage	Space Environment Thermal Cycling
Measurement Condition:	In Air	In Vacuum
Cell Temperature:	25°C	60°C
Light Intensity:	140 mW/cm^2	140 mW/cm^2
Cell Number:	N150BK4	N151CK4

Figure 42 ELECTRICAL PERFORMANCE VS CYCLES FOR CdS SOLAR CELLS MANUFACTURED IN MARCH, 1968

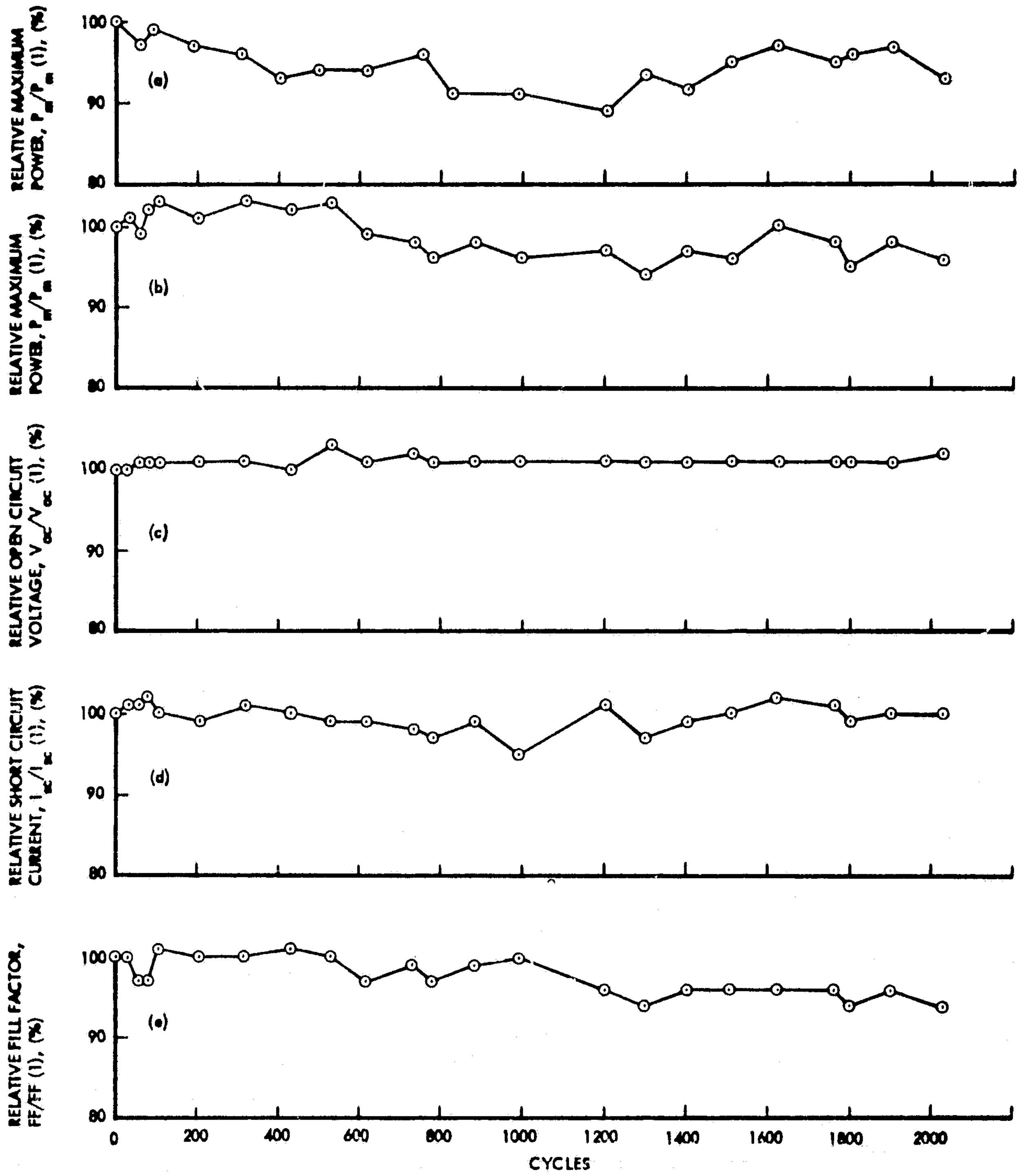

Graph:	(a)	(b), (c), (d), (e)
Test Environment:	Double Desiccated Storage	Space Environment Thermal Cycling
Measurement Condition:	In Air	In Vacuum
Cell Temperature:	25°C	60°C
Light Intensity:	140 mW/cm^2	140 mW/cm^2
Cell Number:	N150BK4	N150BK6

Figure 43 ELECTRICAL PERFORMANCE VS CYCLES FOR CdS SOLAR CELLS MANUFACTURED IN MARCH, 1968

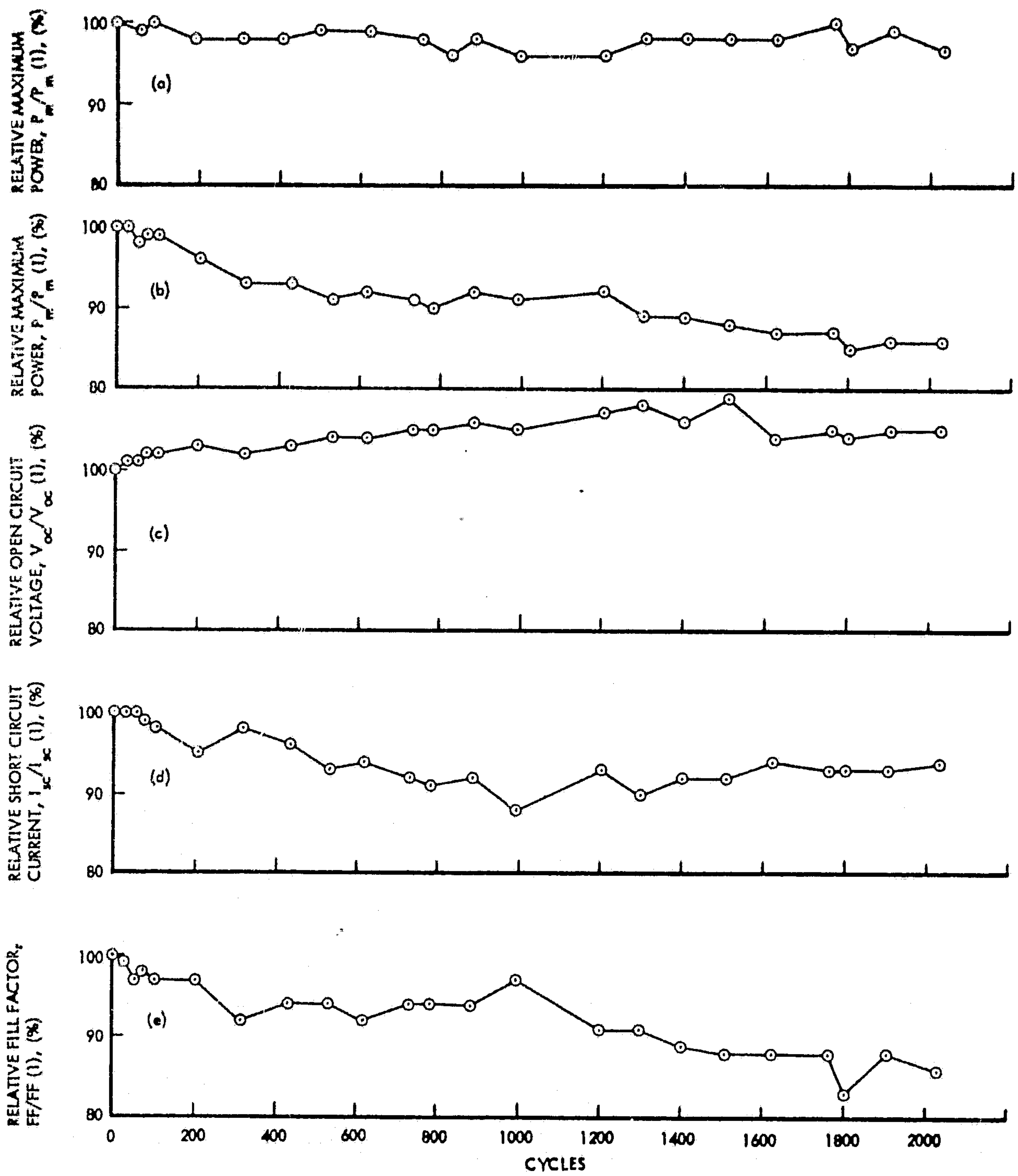

Graph:	(a)	(b), (c), (d), (e)
Test Environment:	Double Desiccated Storage	Space Environment Thermal Cycling
Measurement Condition:	In Air	In Vacuum
Cell Temperature:	25°C	60°C
Light Intensity:	140 mW/cm^2	140 mW/cm^2
Cell Number:	N156CK3	N156AK4

Figure 44 ELECTRICAL PERFORMANCE VS CYCLES FOR CdS SOLAR CELLS MANUFACTURED IN MARCH, 1968

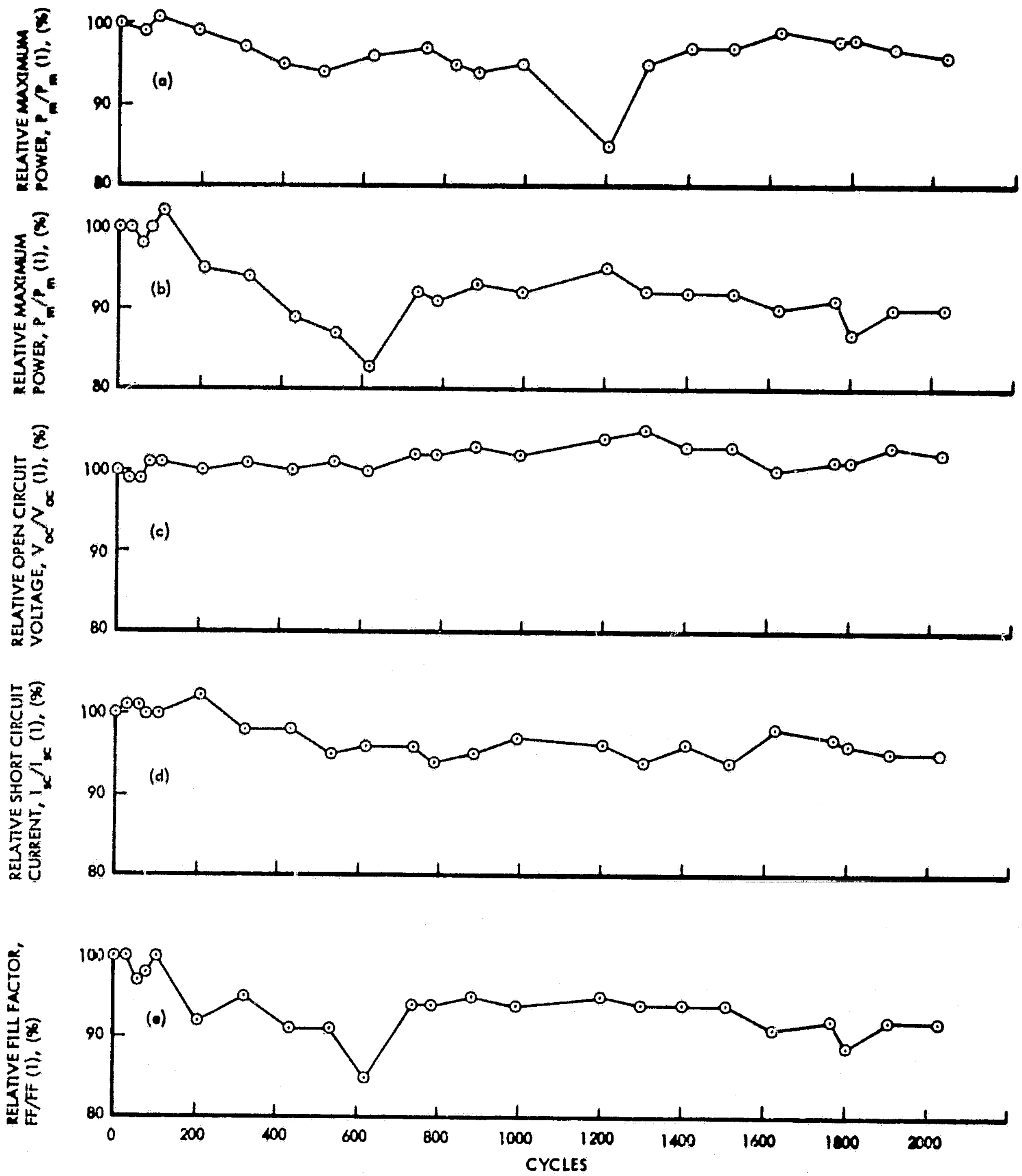

Graph:	(a)	(b), (c), (d), (e)
Test Environment:	Double Desiccated Storage	Space Environment Thermal Cycling
Measurement Condition:	In Air	In Vacuum
Cell Temperature:	25°C	60°C
Light Intensity:	140 mW/cm^2	140 mW/cm^2
Cell Number:	N155BK9	N156CK2

Figure 45 ELECTRICAL PERFORMANCE VS CYCLES FOR CdS SOLAR CELLS MANUFACTURED IN MARCH, 1968

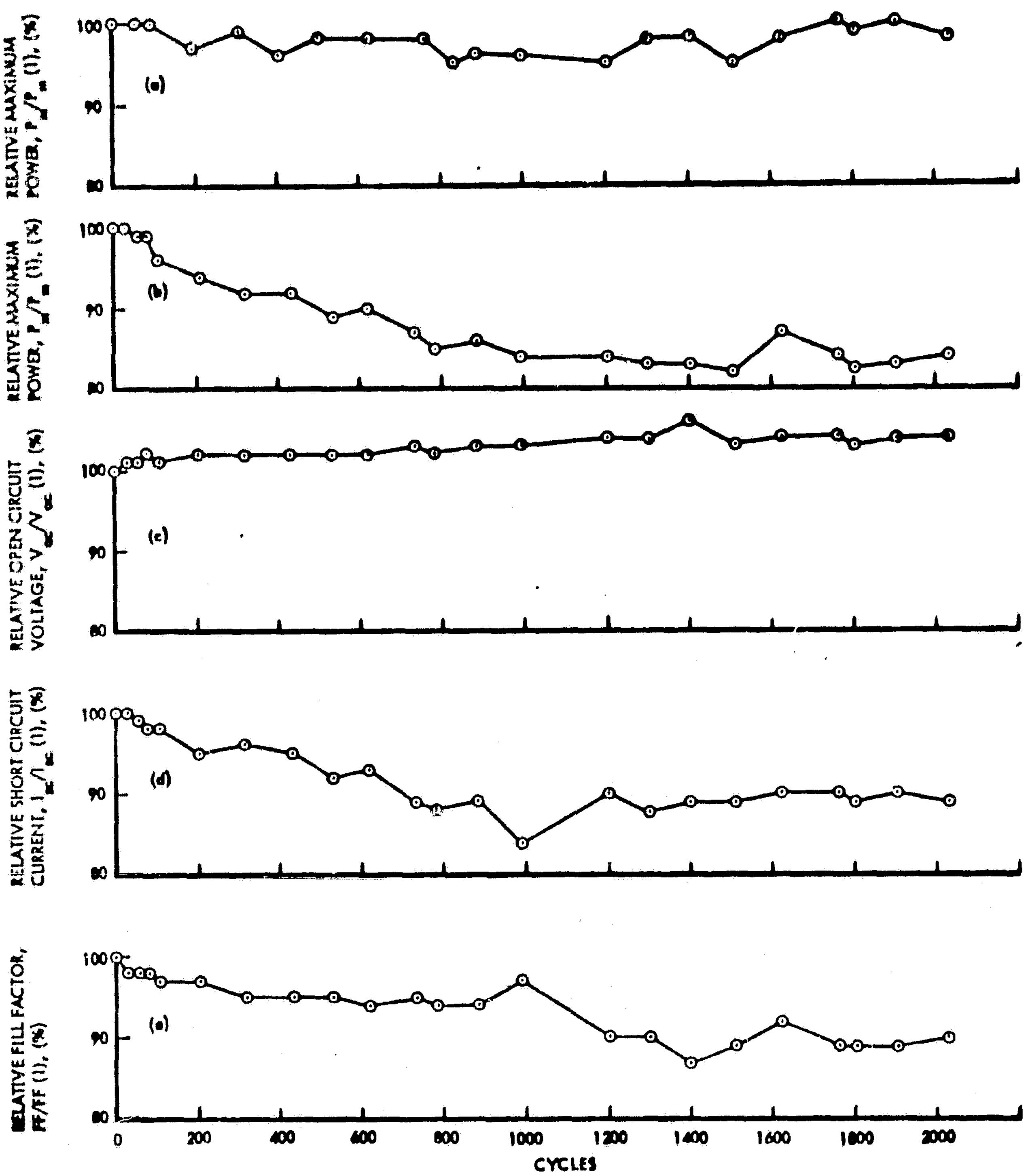

Graph:	(a)	(b), (c), (d), (e)
Test Environment:	Double Desiccated Storage	Space Environment Thermal Cycling
Measurement Condition:	In Air	In Vacuum
Cell Temperature:	25°C	60°C
Light Intensity:	140 mW/cm^2	140 mW/cm^2
Cell Number:	N156AK6	N156AK5

Figure 46 ELECTRICAL PERFORMANCE VS CYCLES FOR CdS SOLAR CELLS MANUFACTURED IN MARCH, 1968

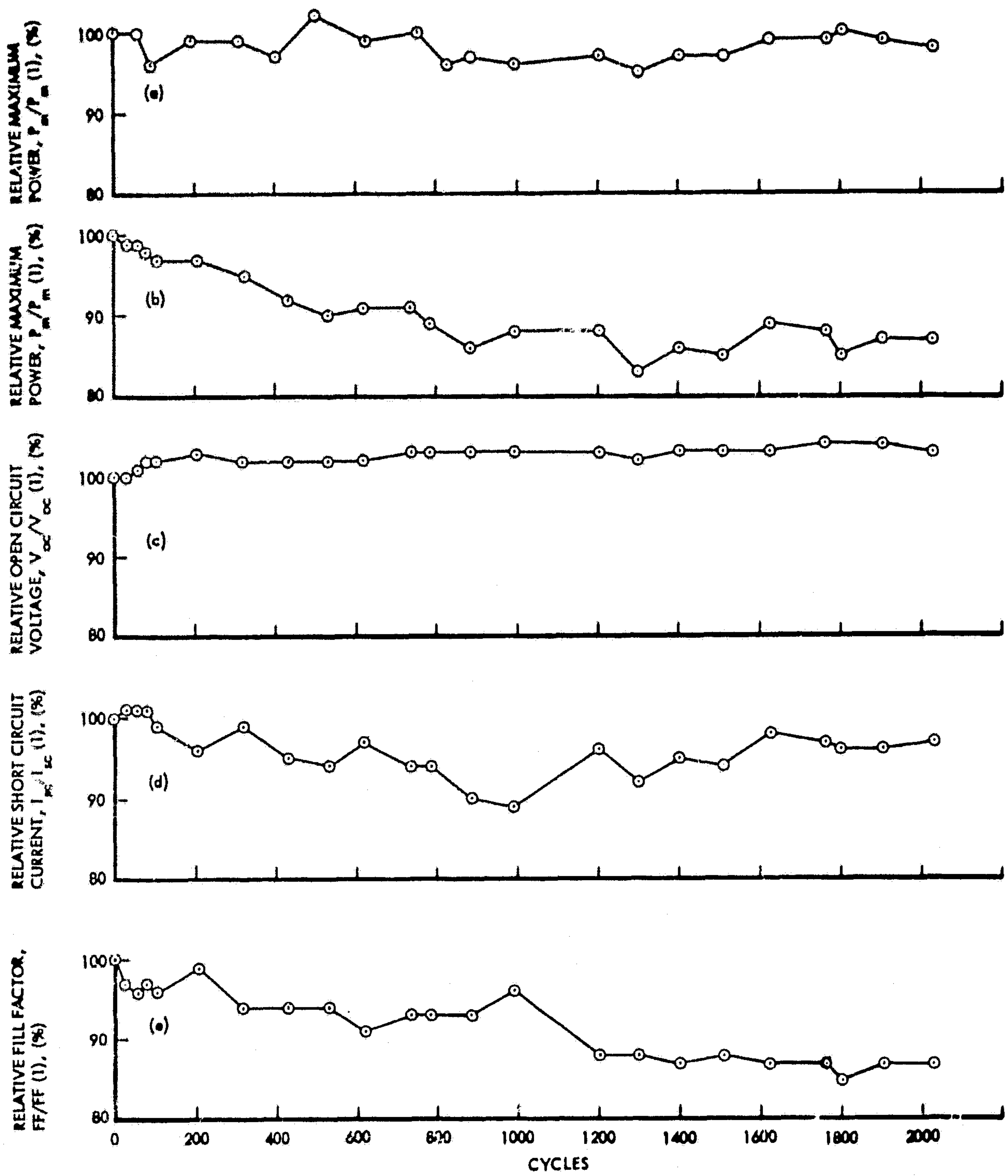

Graph:	(a)	(b), (c), (d), (e),
Test Environment:	Double Desiccated Storage	Space Environment Thermal Cycling
Measurement Condition:	In Air	In Vacuum
Cell Temperature:	25°C	60°C
Light Intensity:	140 mW/cm^2	140 mW/cm^2
Cell Number:	N153BK6	N154BK6

Figure 47 ELECTRICAL PERFORMANCE VS CYCLES FOR CdS SOLAR CELLS MANUFACTURED IN MARCH, 1968

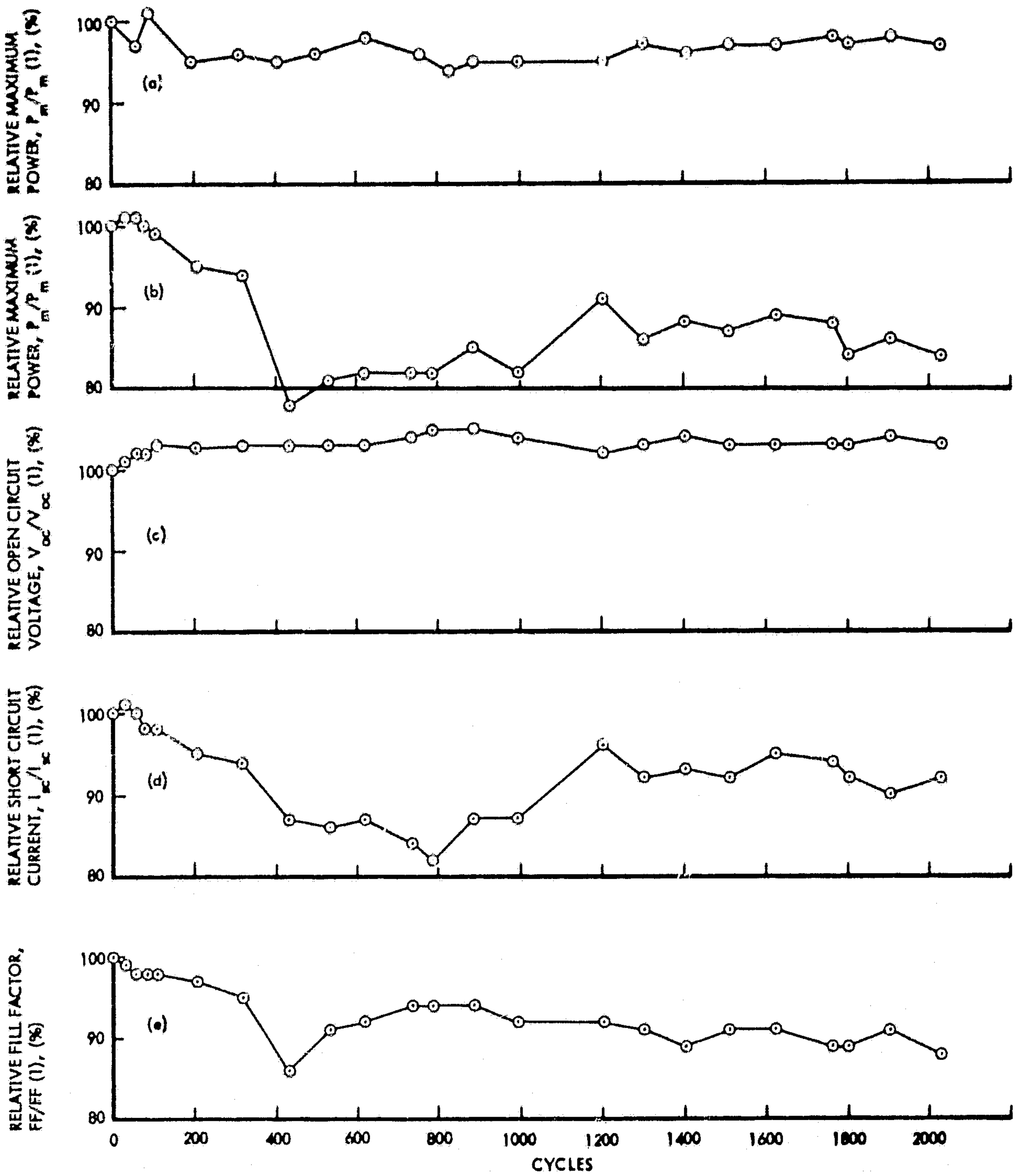

Graph:	(a)	(b), (c), (d), (e)
Test Environment:	Double Desiccated Storage In Air	Space Environment Thermal Cycling In Vacuum
Measurement Condition:		
Cell Temperature:	25°C	60°C
Light Intensity:	140 mW/cm^2	140 mW/cm^2
Cell Number:	N157CK2	N153AK8

Figure 48 ELECTRICAL PERFORMANCE VS CYCLES FOR CdS SOLAR CELLS MANUFACTURED IN MARCH, 1968

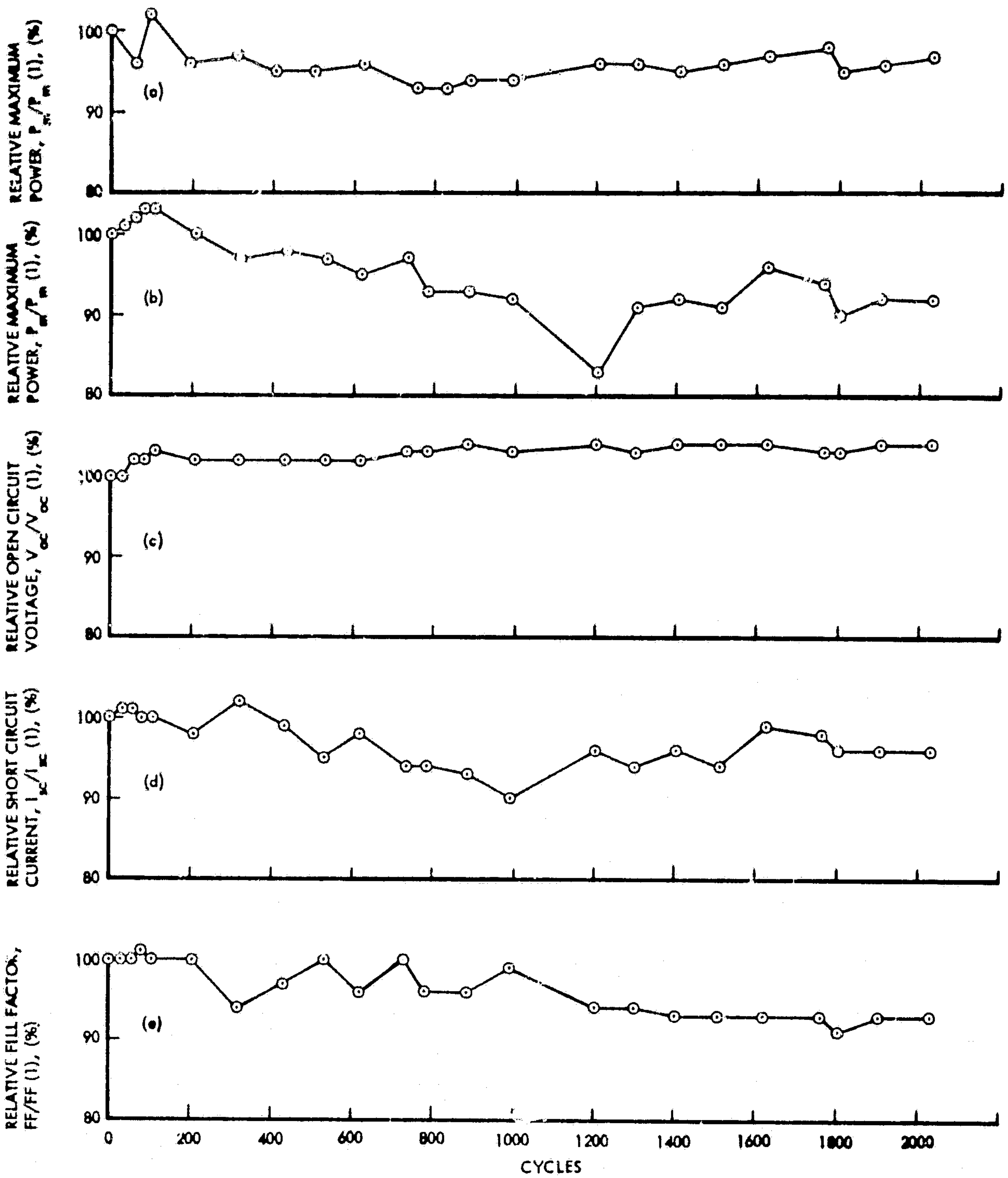

Graph:	(a)	(b), (c), (d), (e)
Test Environment:	Double Desiccated Storage	Space Environment Thermal Cycling
Measurement Condition:	In Air	In Vacuum
Cell Temperature:	25°C	68°C
Light Intensity:	140 mW/cm^2	140 mW/cm^2
Cell Number:	N153AK7	N154CK1

Figure 49 ELECTRICAL PERFORMANCE VS CYCLES FOR CdS SOLAR CELLS MANUFACTURED IN MARCH, 1968

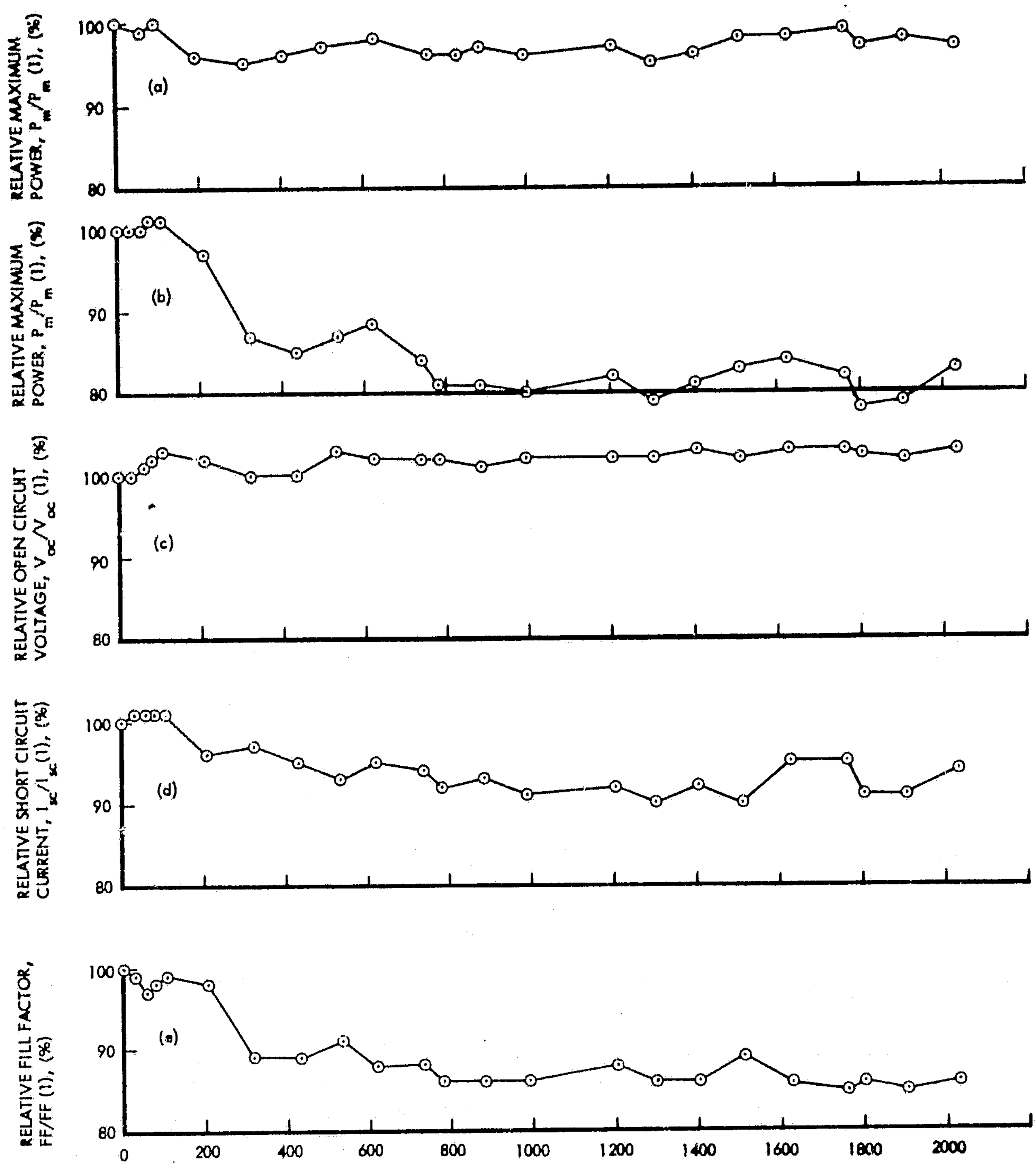

Graph:	(a)	(b), (c), (d), (e)
Test Environment:	Double Desiccated Storage	Space Environment Thermal Cycling
Measurement Condition:	In Air	In Vacuum
Cell Temperature:	25°C	60°C
Light Intensity:	140 mW/cm^2	140 mW/cm^2
Cell Number:	N152BK7	N157BK2

Figure 50 ELECTRICAL PERFORMANCE VS CYCLES FOR CdS SOLAR CELLS MANUFACTURED IN MARCH, 1968

Table 15: POST-CYCLING PERFORMANCE OF CdS SOLAR CELLS MANUFACTURED DURING MARCH 1968

CELL TYPE	CELL NUMBER	TEST AT CYCLE 1	2 MONTHS	TEST AT CYCLE 506	3 HOURS	1 HOUR	FIRST POST-CYCLING TEST	24 HOURS	SECOND POST-CYCLING TEST	2 HOURS	1 HOUR	THIRD POST-CYCLING TEST	20 HOURS	FOURTH POST-CYCLING TEST	18 HOURS	FIFTH POST-CYCLING TEST
		PERFORMANCE - MEASUREMENT SEQUENCE														
		CYCLING			POST-CYCLING											
		ENVIRONMENT CONDITIONS DURING AND BETWEEN PERFORMANCE TESTS														
		TYPE OF GAS IN VACUUM CHAMBER														
		VACUUM	VACUUM	VACUUM	VACUUM	NITROGEN	NITROGEN	NITROGEN	NITROGEN	NITROGEN	AIR	AIR	AIR	AIR	AIR	AIR
		PRESSURE IN VACUUM CHAMBER (torr)														
		10^{-8}	10^{-8}	10^{-8}	10^{-8}	AMBIENT	AMBIENT	AMBIENT	AMBIENT	AMBIENT	AMBIENT	AMBIENT	AMBIENT	AMBIENT	AMBIENT	AMBIENT
		AVERAGE CELL TEMPERATURE (°C)														
		75	69	68	RISING FROM -100 TO + 10	10	50	25	70	25	25	69	25	68	25	69
		LIGHT MODE														
		ON	1/2 HOUR ON 1/2 HOUR OFF	ON	OFF	OFF	ON	OFF	ON	OFF	OFF	ON	OFF	ON	OFF	ON
		PERFORMANCE DATA MEASURED UNDER THE ENVIRONMENTAL CONDITIONS INDICATED ABOVE (1)														
		RELATIVE MAXIMUM POWER, $P_M/P_M(1)$, percent														
		(2) (mW)														
2	A970B	330		77			80		79			91		84		84
2	A969D	329		25			13		24			22		25		24
3	NH188AK2	199		75			79		75			75		76		75
3	NH200AK3	210		88			90		90			90		90		90
3	N89CK7	175		78			89		81			82		81		80
3	N90AK5	251		83			85		84			85		84		82
3	N90BK4	234		82			84		83			85		82		82
3	N90AK1	247		85			83		85			83		83		83
3	N90AK9	224		85			83		86			84		84		86
		RELATIVE OPEN CIRCUIT VOLTAGE, $V_{OC}/V_{OC}(1)$, percent														
		(2) (V)														
2	A970B	0.443		102			101		102			101		101		101
2	A969D	0.453		60			53		58			54		61		59
3	NH188AK2	0.426		101			101		100			99		99		99
3	NH200AK3	0.415		100			100		100			99		99		99
3	N89CK7	0.424		97			99		93			98		98		98
3	N90AK5	0.416		103			102		101			100		101		100
3	N90BK4	0.419		98			97		98			97		97		97
3	N90AK1	0.421		102			100		99			98		99		99
3	N90AK9	0.420		101			95		103			99		99		99
		RELATIVE SHORT CIRCUIT CURRENT, $I_{SC}/I_{SC}(1)$, percent														
		(2) (mA)														
2	A970B	1095		81			85		85			87		90		90
2	A969D	1075		81			88		86			88		92		93
3	NH188AK2	760		90			96		91			92		91		91
3	NH200AK3	750		100			103		103			103		102		101
3	N89CK7	760		91			98		93			94		93		91
3	N90AK5	945		90			94		92			94		92		92
3	N90BK4	838		93			92		92			95		92		92
3	N90AK1	909		91			96		95			95		94		94
3	N90AK9	817		92			95		93			94		93		94
		RELATIVE FILL FACTOR, FF/FF (1), percent														
		(2) (%)														
2	A970B	68		93			93		93			93		93		93
2	A969D	68		51			28		47			46		44		44
3	NH188AK2	62		84			82		84			84		85		84
3	NH200AK3	68		88			87		87			88		88		90
3	N89CK7	64		89			93		87			91		89		91
3	N90AK5	67		89			88		89			91		91		89
3	N90BK4	65		91			93		91			91		93		91
3	N90AK1	65		92			88		91			89		91		89
3	N90AK9	65		92			89		94			91		92		92

(1) All data is corrected to 60°C. Light intensity was 140 mW/cm^2, AM0, during the entire test program. Cells were mounted in the vacuum chamber

(2) All cycle-1 data are actual, not relative, values given in the indicated units

Cell Number N150BK6

This cell was the most stable cell thus far tested. After 2031 cycles, its P_M', V_{oc}', I_{sc}' and FF' values were 96, 102, 100 and 94 percent.

This cell was different from the others in that it had an evaporated grid beneath the standard preformed grid. It is significant that the I_{sc}' of this cell did not degrade.

Cell Number N156CK2

The behavior of this cell is fairly representative of the eight cells whose P_M' ranged between 83 and 96 percent after 2031 cycles. After 2031 cycles, the P_M', V_{oc}', I_{sc}', and FF' of this cell were 90, 102, 95, and 92 percent, respectively. A degraded I-V curve of this cell is shown in Figure 51.

Increase in Series Resistance

Based on the calculated effects of R_s, R_{sh}, I_g, I_o, and A on the performance of a typical CdS solar cell (Figures 16 to 20), the observed loss in FF' of cell N156CK2 was due to a change in either series resistance or shunt resistance. The reasons are:

(1) A 0.03-ohm increase in R_s would produce the experimental 92-percent FF' without changing V_{oc}'.

(2) A 15.2-ohm decrease in R_{sh} would also produce the experimental 92-percent FF' without changing V_{oc}'.

(3) Changes in I_g do not significantly affect FF'.

(4) Changes in I_o and A which result in experimental FF' drastically reduce V_{oc}', an effect which did not occur.

The R_{oc} measured from the I-V curve increased from 0.09-ohms to 0.13-ohms between cycle-1 and cycle 2031. This corresponds to a 0.027-ohm increase in series resistance (Figure 21). This suggests that series resistance was responsible for the degradation in FF' and hence part of the power loss.

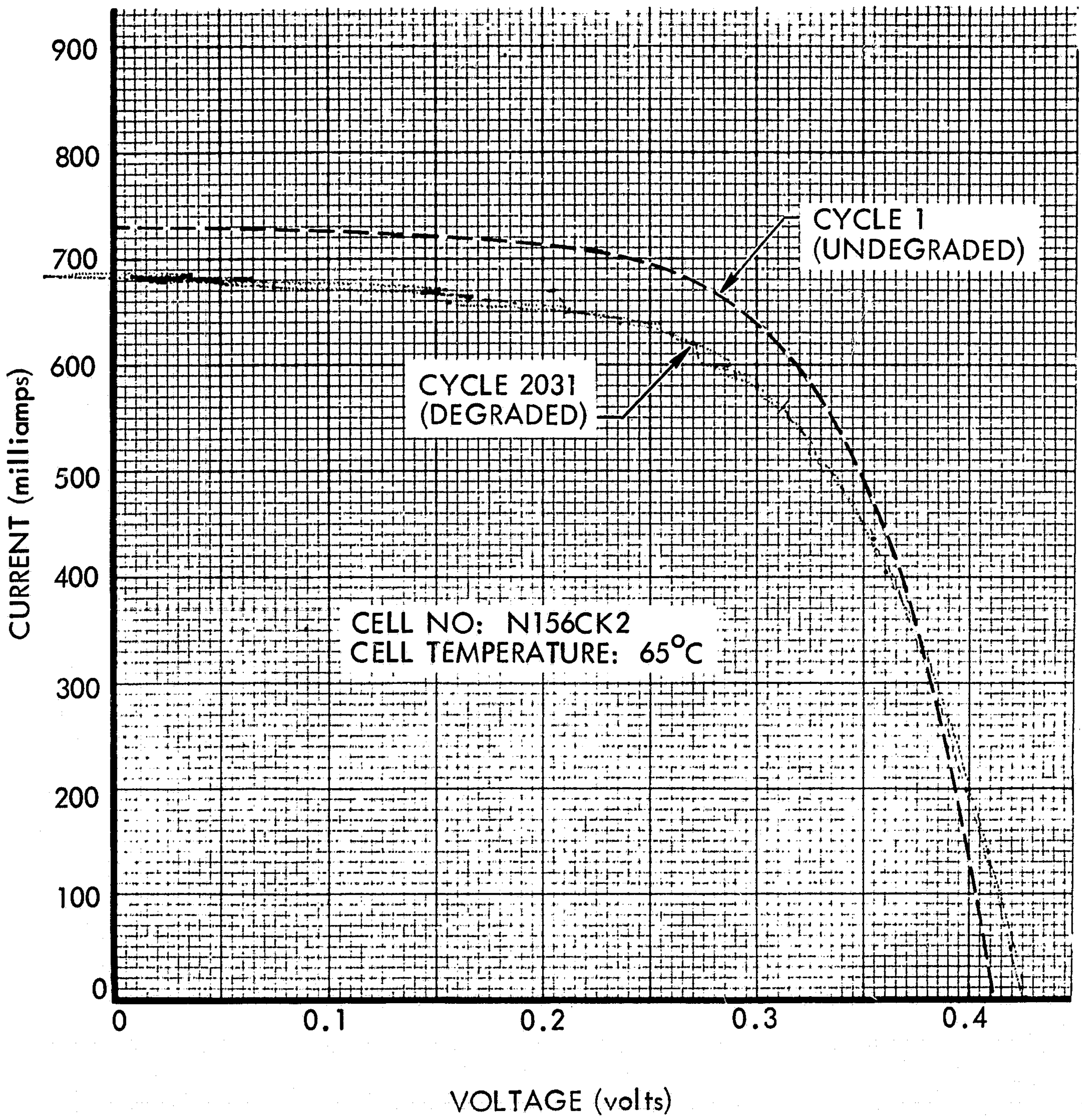

Figure 51: DEGRADED I-V CURVE OF A MARCH 1968 SOLAR CELL

Decrease in Light Generated Current

Based on the calculated effects of R_s, R_{sh}, I_g, I_o, and A on the performance of a typical CdS solar cell (Figures 16 to 20), the observed loss in I_{sc}' of cell N156CK2 was due to a loss in light generated current. Here are the reasons:

(1) A five-percent decrease in I_g produced the experimental 95-percent I_{sc}' without an accompanying loss in V_{oc}'.

(2) Changes in R_s, R_{sh}, I_g, or A which could produce the observed I_{sc}' are accompanied by a drastic loss in V_{oc}' which did not occur.

Low light intensity could explain the five-percent decrease in I_g. However, this evidence indicates that the light intensity was not too low:

(1) The I_{sc}' of one CdS test-cell (No. NH150BK6) was still 100 percent after 2031 cycles.

(2) The I_{sc} of one of the silicon reference cells varied less than 2.5 percent between cycle-1 and cycle-2031.

(3) The transmission of the quartz window degraded less than one percent, according to measurements made with the CdS standard cell before and after the test.

(4) The I_{sc} of all the control cells at cycle 2031 were within two percent of their initial values.

Gaseous nitrogen, and then air, were admitted to the vacuum chamber after completion of cycling. No significant recovery in the I_{sc}' of cell N156CK2 was observed (Table 15). Measurements made in air on the temperature controlled block produced an I_{sc}' of 93 percent, a value not significantly different from the 95 percent value obtained <u>in situ</u> at cycle 2031. In general, this group of cells did not exhibit a significant recovery in I_{sc}'. The average <u>in situ</u> I_{sc}' of these eight cells was 95 percent, at cycle 2031, and 93 percent in air after removal from the chamber. Apparently the losses in I_{sc}' were permanent.

It seems significant that the losses in I_{sc}' cannot be explained by changes in R_s, R_{sh}, I_g, or A; only a decrease in I_g can explain the observed permanent loss in I_{sc}'. Since Kapton covers have been demonstrated to be unaffected by UV in vacuum, the cause of the decrease in I_g cannot be explained at this time.

Cell Number N151CK4

After 2031 cycles, the P_M', V_{oc}', I_{sc}', and FF' values of this cell were 49, 97, 91 and 56 percent respectively. The fact that both FF' and V_{oc}' degraded suggests that much of this degradation was caused by a decrease in shunt resistance. The degraded I-V curves exhibited an erratic form of hysteresis and approximated a straight line between I_{sc} and V_{oc}.

Summary of Testing of March, 1968 Cells

The March, 1968 cells were the most stable yet tested, the maximum powers degrading, on the average, to 88 percent of initial. Two of these cells had evaporated grids. One evaporated-grid cell lasted over 2000 cycles with only a 4 percent power loss. The second evaporated-grid cell degraded slowly to 92 percent at 997 cycles after which it degraded suddenly to 53 percent. Power losses in other cells resulted from increased series resistance and decreased light-generated current. The loss in light-generated current could not have been caused by a loss of illumination or by degradation of the Kapton covers, nor did it disappear after the cells were removed from the chamber. No satisfactory explanation is available.

Several of these newest cells exhibited the effects of internal short circuits, a common problem with every cell design tested in this program.

7.0 CONCLUSIONS

As a result of the testing conducted in this program, the following conclusions have been reached:

1. Most CdS solar cells exhibit a loss in power when exposed to a simulated space environment involving thermal cycling. It is not clear what aspects of the environment contribute to the observed losses.

2. Some CdS solar cells can withstand over 2000 thermal cycles in a simulated space environment without significant loss in power. One cell degraded by only four percent in maximum power in 2031 cycles.

3. The most recently manufactured cells degraded less than earlier cells. A more favorable electrical loading during exposure to the simulated space environment could have contributed to the better performance. Improved quality of the cells could be another contributor.

4. Use of an evaporated gold grid results in a solar cell that is potentially more stable than one having a grid bonded with epoxy.

5. Internal short circuits in CdS solar cells result in large and unpredictable decreases in power output. Eliminating these short-circuits would enhance the usefulness of CdS solar cells for space power applications. Shorts occurred in some cells in each of the three manufacturing batches tested.

6. A more subtle but significant cause of degradation in the recent cells (November, 1967 and March, 1968) is an increase in the series resistance of the cells.

7. Another significant cause of degradation in all the cells is a decrease in their light-generated currents. Sometimes the degraded light-generated current recovers after the test.

No satisfactory explanation for this loss in light-generated current is available at this time.

8. A CdS-cell mathematical model is a useful tool for analyzing I-V curves tc establish the causes of cell degradation.

8.0 REFERENCES

1. Shirland, Fred A.: The History, Design, Fabrication and Performance of CdS Thin Film Solar Cells. Advanced Energy Conversion, vol. 6, 1966, pp. 201-222.

2. Ewashinka, John G.; and Stephenson, George K.,Jr.: Thermal Cycling and Heat Damage Tests of Thin-Film Cadmium Sulfide Solar Cells. NASA TN D-3038, 1965.

3. Spakowski, Adolph E., and Ewashinka, John G.: Thermal Cycling of Thin-Film Cadmium Sulfide Solar Cells. NASA TN D-3556, 1966.

4. Kennerud, K. L.: Space Environment Tests on Thin-Film Solar Cells. Contract NAS3-6008 Topical Report, A Summary of Work Completed in Phases I and II, 1967.

5. Spakowski, A. E.; and Kennerud, K.L.: Environmental Testing of Thin-Film Solar Cells. Sixth Photovoltaic Specialists Conference, Vol. 1, IEEE, 1967, pp. 201-209.

6. Shirland, F. A.; Bower, W. K.; and Green, J.R.: CdS Solar Cell Development. Contract NAS3-9434, Interim Technical Report, NASA CR-72382, 1968.

7. Spakowski, A.E.: Acampora, F. L.; and Hart, R. E.Jr.: Effect of Moisture on Cadmium Sulfide Solar Cells. NASA TND-3663, 1966.

8. Anagnostou, Evelyn: Effect of Ultraviolet Irradiation on Selected Plastic Films In Vacuum. NASA TM X-1124, 1965.

9. Handbook of Geophysics, Chapter 16.3, Solar Radiation Tables, pp. 16-16 and 16-17, McMillan Company, 1960.

10. Scarborough, J. B., Numerical Mathematical Analysis, pp 192-194, Johns Hopkins Press, 1958.

11. Spakowski, A. E.; and Forestieri, A.F.: Observations on CdS Solar Cell Stability. NASA TMX-52485, 1968.

9.0 APPENDIX

SUMMARY OF EQUATIONS AND SYMBOL LIST

Equations

$$\eta = \frac{P_M}{(S)(\alpha)} \times 100 = (.013)\ P_M$$

$$P_M = P_{MU} + K_{MP}\ (T_R - T)$$

$$V_{oc} = V_{ocU} + K_{ocv}\ (T_R - T)$$

$$FF = \frac{P_M}{(V_{oc})(I_{sc})} \times 100$$

$$P_M' = P_M/P_M(1)$$

$$V_{oc}' = V_{oc}/V_{oc}(1)$$

$$I_{sc}' = I_{sc}/I_{sc}(1)$$

$$FF' = FF/FF(1)$$

$$R_{oc} = -\left[\frac{\Delta V}{\Delta I}\right]_{I=0}$$

$$I = I_o\left\{\exp\left[\frac{q}{AkT}(V - IR_s)\right] - 1\right\} - I_g + \frac{V - IR_s}{R_{sh}}$$

Symbols

α = active cell area = 54.75 cm^2

A = empirical fitting constant (equal to 1 for an ideal junction)

FF = fill factor (percent)

FF(1) = initial fill factor (percent)

FF' = relative fill factor (percent)

I = current output of cell (amperes)

I_s = light generated current (amperes)

I_o = reverse saturation current (amperes)

I_{sc} = short circuit current (milliamperes)

$I_{sc}(1)$ = initial short circuit current (milliampere)

I_{sc}' = relative short circuit current (percent)

k = Boltzmann constant

K_{MP} = temperature coefficient of maximum power (mW/°C)

K_{ocv} = temperature coefficient of open circuit voltage (volts/°C)

η = conversion efficiency (percent)

P_M = corrected maximum power (milliwatts)

$P_M(1)$ = initial corrected maximum power (milliwatts)

P_M' = relative maximum power (percent)

P_{MU} = uncorrected maximum power (milliwatts)

q = electronic charge

R_{oc} = equivalent series resistance (ohms)

R_s = series resistance (ohms)

R_{sh} = shunt resistance (ohms)

S = light intensity = 140 mW/cm^2

σ_s = standard deviation

σ_M = maximum deviation

T = actual cell temperature (°C)

T_R = reference cell temperature (°C)

V = voltage appearing at cell terminals (volts)

V_{oc} = corrected open circuit voltage (volts)

$V_{oc}(1)$ = initial corrected open circuit voltage (volts)

9.0 APPENDIX (Cont.)

V_{oc}' = relative open circuit voltage (percent)

V_{ocu} = uncorrected open circuit voltage (volts)

$\bar{X}$ = average

10.0 NEW TECHNOLOGY

A new technique for identifying the cause of performance degradation in CdS thin-film solar cells was developed in this contract. This technique uses a digital computer to calculate the changes in internal cell parameters that can satisfactorily explain the I-V curve being analyzed. A complete description of the technique appears in Section 6.1, and a summary is provided below.

The computer program generates the I-V curve of a CdS solar cell from a set of 5 physically meaningful parameters. Each of these five parameters is varied individually, and its effect on the I-V curve of a typical CdS solar cell is determined. The maximum power (P_M) open circuit voltage, (V_{oc}) short circuit current, (I_{sc}) and fill factor (FF) are then plotted as functions of each parameter. The resulting curves are then compared with the experimental values of P_M, V_{oc}, I_{sc}, FF obtained from CdS test-cells which degraded during thermal cycling. The parameter which changed to cause the degradation then becomes apparent.